ARL 72-0035
FEBRUARY 1972

Aerospace Research Laboratories

PERFORMANCE TRIALS OF THE EIGHT-INCH DIAMETER UTIAS IMPLOSION-DRIVEN HYPERVELOCITY LAUNCHERS MK II AND MK III

S. K. CHAN
G. CAPPELLI
W. O. GRAF

UNIVERSITY OF TORONTO
TORONTO, CANADA

CONTRACT NO. AF33(615)-5313
PROJECT NO. 7065

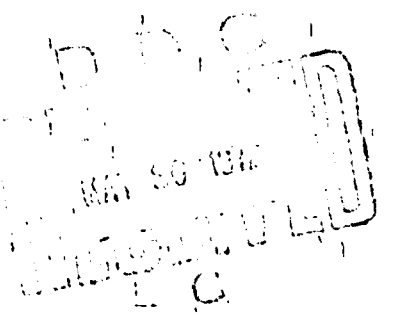

AIR FORCE SYSTEMS COMMAND
United States Air Force

Reproduced by
NATIONAL TECHNICAL
INFORMATION SERVICE

NOTICES

When Government drawings, specifications, or other data are used for any purpose other than in connection with a definitely related Government procurement operation, the United States Government thereby incurs no responsibility nor any obligation whatsoever; and the fact that the Government may have formulated, furnished, or in any way supplied the said drawings, specifications, or other data, is not to be regarded by implication or otherwise as in any manner licensing the holder or any other person or corporation, or conveying any rights or permission to manufacture, use, or sell any patented invention that may in any way be related thereto.

Agencies of the Department of Defense, qualified contractors and other government agencies may obtain copies from the

Defense Documentation Center
Cameron Station
Alexandria, Virginia 22314

This document has been released to the

CLEARINGHOUSE
U. S. Department of Commerce
Springfield, Virginia 22151

for sale to the public.

Copies of ARL Technical Documentary Reports should not be returned to Aerospace Research Laboratories unless return is required by security considerations, contractual obligations or notices on a specified document.

AIR FORCE: 225-72/200

UNCLASSIFIED
Security Classification

DOCUMENT CONTROL DATA - R & D

(Security classification of title, body of abstract and indexing annotation must be entered when the overall report is classified)

1. ORIGINATING ACTIVITY (Corporate author)	2a. REPORT SECURITY CLASSIFICATION
Institute for Aerospace Studies University of Toronto Toronto, Canada	Unclassified 2b. GROUP

3. REPORT TITLE

PERFORMANCE TRIALS OF THE EIGHT-INCH DIAMETER UTIAS IMPLOSION-DRIVEN HYPERVELOCITY LAUNCHERS MK II AND MK III

4. DESCRIPTIVE NOTES (Type of report and inclusive dates)

Scientific Interim

5. AUTHOR(S) (First name, middle initial, last name)

S. K. Chan, G. Cappelli and W. O. Graf

6. REPORT DATE	7a. TOTAL NO. OF PAGES	7b. NO. OF REFS
February 1972	117	49

8a. CONTRACT OR GRANT NO.	9a. ORIGINATOR'S REPORT NUMBER(S)
AF 33(615)-5313 b. PROJECT NO. 7065-00-22 c. DoD Element 61102F d. DoD Subelement 681307	UTIAS Technical Note No. 161 9b. OTHER REPORT NO(S) (Any other numbers that may be assigned this report) ARL 72-0035

10. DISTRIBUTION STATEMENT

Approved for public release; distribution unlimited.

11. SUPPLEMENTARY NOTES	12. SPONSORING MILITARY ACTIVITY
TECH OTHER	Aerospace Rsch Laboratories/LF Air Force Systems Command Wright-Patterson AFB, OH 45433

13. ABSTRACT

An experimental investigation of the performance of the 8-inch diameter MK-II and MK-III UTIAS Implosion-Driven Hypervelocity Launchers was carried out. Many problems were encountered in the operation of this unique device such as off-centre implosions, projectile integrity, preparation of the hemispherical explosive-liner package and the erratic operation of the velocity measuring system. Detailed descriptions of the solutions were presented. Measured velocities of the 0.22-inch diameter projectile (a maximum of 13,500 fps was obtained) were found to be 30-50% lower than computed values. Heavy erosion and expansion of the gun barrel was noted that could possibly account for the low measured velocities. An investigation of a technique of initiating the PETN liner by light sensitive explosive was carried and is presented in Appendix A. The possibility of measuring the velocity and acceleration of the projectile in the launcher barrel using a laser interferometer technique was investigated and is reported in Appendix B. Appendix C is a summary of the work carried out on the MK I launcher including the evaluations of the impact craters, projectile materials, pre-launched projectile locations, projectile integrity and dynamic stress calculations.

DD FORM 1 NOV 68 1473

UNCLASSIFIED
Security Classification

A

14. KEY WORDS	LINK A		LINK B		LINK C	
	ROLE	WT	ROLE	WT	ROLE	WT
implosion-driven launchers						
implosions						
detonations						

U.S.Government Printing Office: 1972 — 759-085/554

B

ARL 72-0035

PERFORMANCE TRIALS OF THE EIGHT-INCH DIAMETER UTIAS IMPLOSION-DRIVEN HYPERVELOCITY LAUNCHERS MK II AND MK III

S. K. CHAN, G. CAPPELLI AND W. O. GRAF

INSTITUTE FOR AEROSPACE STUDIES
UNIVERSITY OF TORONTO
TORONTO, CANADA

FEBRUARY 1972

CONTRACT AF 33(615)-5313
PROJECT NO. 7065

AEROSPACE RESEARCH LABORATORIES
AIR FORCE SYSTEMS COMMAND
UNITED STATES AIR FORCE
WRIGHT-PATTERSON AIR FORCE BASE, OHIO

FOREWORD

This interim report was prepared at the Institute for Aerospace Studies, University of Toronto, Toronto, Canada under Contract No. 33(615)-5313 for the Aerospace Research Laboratories, Air Force Systems Command, United States Air Force. This research was accomplished under the technical cognizance of Mr. Kenneth F. Stetson, Fluid Dynamics Facilities Research Laboratory.

The authors wish to express their appreciation to Dr. G. N. Patterson for making possible the opportunity to conduct this work at the Institute for Aerospace Studies. We should also like to thank Dr. I. I. Glass for his continuous advice and guidance throughout the entire project. Thanks are also due to Prof. G. F. Wright and Mr. T. Huber of the Department of Chemistry for their suggestions and assistance on the development of the explosive liners.

The authors wish to acknowledge the assistance of Mr. W. Czerwinski for his unending interest in the design of the launchers; the staff of the Machine Shop, particularly Mr. R. MacKay, for technical assistance; Mr. A. Perrin for the design and construction of the electronic equipment; and the members of the launcher laboratory, Mr. W. C. Burgess, Mr. P. Crouse, Mr. A. Elsenaar, Dr. S. Lin and Dr. I. Wada for many constructive suggestions and considerable assistance.

The initial effort put into the development of the explosive liners by Mr. David Welsh, of the Canadian Safety Fuse Co. Ltd., Brownsburg, Quebec, is acknowledged with thanks.

This research was partially supported by the National Research Council of Canada.

ABSTRACT

An experimental investigation of the performance of the 8-inch diameter MK II and MK III Implosion-Driven Hypervelocity Launchers was carried out. Many problems were encountered in operating the launchers. They include off-centre implosions, projectile integrity, preparation of the hemispherical, explosive-liner package and the erratic operation of the velocity detecting units. The performance of the velocity measuring system was perfected by using a sequential hold-off programmer. The damage from extreme off-centre implosion problem was prevented by the addition of a conical-liner plate. Progress was made in the direction of obtaining a very uniform, explosive-liner package.

In order to launch a half caliber 0.22-inch diameter titanium projectile intact, it had to be placed 3 inches downstream of the origin. Measured velocities of the projectile (a maximum of 13,500 fps was obtained as a result), were found to be 30-50% lower than the computed values. Heavy erosion and expansion of the gun barrel were noted which could possibly account for the low measured velocities.

An investigation of a technique of initiating the PETN liner by light sensitive explosive was also carried out, and is presented in Appendix A. The results were insufficient to draw a conclusive evaluation of the technique, although the PETN was successfully initiated by this technique at initial gas pressure of less than 6 psi.

The possibility of measuring in detail the velocity and acceleration of the projectile in the launcher barrel using a laser interferometer technique was investigated and is reported in Appendix B. A 12-gauge shot gun was used to accelerate plastic projectiles to a final velocity of approximately 3500 ft/sec to test the technique. The expected signals were found to be masked by signals due to the vibrations of the projectile.

Appendix C is a summary of the work carried out on the MK I launcher including the evaluation of the impact craters on lead targets by projectiles, testing of the various projectile materials, effect of projectile locations in the barrel on performance and projectile integrity, flash X-ray observation of the moving projectile inside the barrel and dynamic stresses in the wall of the implosion chamber. Some theoretical and experimental results on the projectile integrity problem are also presented.

TABLE OF CONTENTS

LIST OF ILLUSTRATIONS

(Illustrations, cont'd)

(Illustrations, cont'd)

NOTATION

A	Area
a	Acceleration
c_L	Longitudinal speed of sound
c	Speed of sound, speed of light
D_c	Implosion chamber diameter
d_p	Barrel or projectile diameter
E	Young's modulus
e	Specific internal energy
f_m	Laser modulation frequency
H	Height of a spherical sector defined in Fig. 19
L	Delay leg length in the laser interferometer (Appendix B)
L_r	Projectile recess distance from the origin
m	Mass, decay rate constant
P, p	Pressure
P_i	Initial chamber loading pressure
R	Radius or particle position relative to the origin
R_c	Implosion chamber radius
r_b	Radius of the base of the spherical sector (Fig. 19)
r_p	Projectile radius
t	Time
T	Time for light to travel a distance L (Eqn. B.2.4)
u	Velocity
v	Specific volume
w_e	Explosive weight
x	Distance from spherical wall of the implosion chamber
Y^o	Yield strength
α	Angle of the conical entrance geometry (Fig. 19)

ϵ	A fraction as defined in section B. 4.5 in Appendix B
λ	Wavelength
θ	Angle of the conical liner plate (Fig. 18)
μ	Shear modulus
ν	Poisson's ratio
ρ	Density
σ_1	Incident normal stress
σ_t	Transmitted normal stress

1. INTRODUCTION

Up to now the most successful and widely used hypervelocity launchers are still the conventional light-gas guns. However, projectile velocities produced by them have long been realized to have reached a plateau despite the various modifications introduced into the basic system. The maximum velocity of 11.3 km/sec (37,000 ft/sec) for a 45 mg polyethylene projectile has been attained at NASA, Ames (Ref. 1). In order to overcome this limit, researchers have been trying a number of new ideas such as the explosively driven linear accelerator (Refs. 2,3,4) and the magnetohydrodynamic hypervelocity gun (Ref. 5). Recently, a velocity of 12.2 km/sec (40,000 ft/sec) has been reported for a 2g projectile in Ref. 46. The UTIAS Implosion-Driven Hypervelocity Launcher suggested in 1959 by Prof. I. I. Glass of the Institute for Aerospace Studies (Ref. 6) was another direction of research toward overcoming the hypervelocity limit by making use of the extremely high-pressure and high-temperature gas generated by explosive-driven, spherical implosion waves.

The principle of operation of the UTIAS Implosion-Driven Hypervelocity Launcher is shown in Fig. 1 (a detailed description can be found in Refs. 7 and 8). The hemispherical cavity is filled with a mixture of stoichiometric H_2-O_2 which is ignited at the geometric centre of the hemisphere by an exploding wire creating a hemispherical detonation wave (Fig. 1A). This outgoing detonation wave hits an explosive liner placed against the wall of the hemispherical cavity and simultaneously and uniformly initiates it, thus generating an implosion (Fig. 1B). The strength of the implosion wave increases as it travels towards the centre at which presumably infinite pressure and temperature can be generated ideally. As the implosion wave reflects from the origin it leaves behind a region of high pressure and temperature gas which can be used to propel the projectile along the barrel (Fig. 1C).

While the basic concept is rather simple, to bring it into practical reality nevertheless involves quite a number of problems never before encountered. A considerable amount of research and development had been expended in the past decade at UTIAS (Ref. 6-33) in the various stages of development of the project. These include the study of the properties of hydrogen-oxygen-helium reactions (Refs. 14, 18, 19, 22), the initiation of the hemispherical explosive liners (Refs. 8, 13, 17), the study of the implosion and explosion wave systems (Refs. 12, 26, 27, 30, 31), the theoretical performance calculations of the launchers (Refs. 15, 20, 21, 23, 27), the measurement of the projectile velocity inside the barrel (Ref.28), the projectile integrity problem (Ref. 33) and the design and construction of the various models of the implosion-driven launcher (Refs. 9, 10, 29, 32). Without these significant efforts in development, the present calibration runs would have been impossible. However, as will be shown later, considerable difficulties were still encountered in the experiments, some of which still have to be overcome.

In the following section a description of the experimental equipment and set-up will be given. In Chapter 3 the numerical computer program used to calculate the performance corresponding to the runs carried out and described in the present report will be discussed. Chapter 4 is devoted to the presentation and discussion of the experimental results including the off-centre implosions and gun barrel expansion and erosion. In the last chapter some general conclusions will be made.

2. EXPERIMENTAL EQUIPMENT AND PROCEDURE

For the investigations in earlier reports, the UTIAS MK I Implosion-Driven Hypervelocity Launcher was used. For details see Refs. 8 and 20. For the results in the present report, only the newer models MK II and MK III were used. Figure 2 shows the MK III launcher in the firing position. The outside appearance of MK II is quite similar to MK III. While some of the electronic equipment was built especially for the present calibration runs, most of the other equipment such as the ignition unit, the plumbing system, the range, etc., were the same as those used in Ref. 8 and 20. They will be described here briefly and the details can be found in the above cited references.

2.1 The UTIAS Implosion-Driven Hypervelocity Launchers

2.1.1 The MK II Launcher

Figure 3 shows the construction of the 24-inch diameter MK II launcher. The 8-inch diameter or 1/3-scale model was used in some of the calibration runs for the present report. The design of the 1/3-scale model is basically the same as for the full scale, with slight differences mainly in the construction of the barrel and its holder. Detailed descriptions of the design and calculations can be found in Refs. 29 and 32.

The launcher consists of two halves, namely, the Front Plate and the Explosion Chamber Block. A hemispherical cavity was machined in the explosion chamber block and it holds the explosive liner assembly which will be discussed in Section 2.1.4. The front plate consists of a segmented cone which supports the barrel assembly and the liner plate. In the later runs a conical liner plate was added on top of the regular liner plate. This addition was to guard against any possible extreme off-centre implosions directed towards the rim of the hemispherical cavity causing serious damage to the chamber. Depending on the angle of the conical liner plate (10°, 15° and 20° liners have been used), there are a number of different cavity geometries produced. An exploded view of the launcher top-half is shown in Fig. 4, where the barrel and half of the segmented cone are shown in their respective seating positions in the front plate. In front of the top-plate are the liner plate and the conical liner plate, which is normally screwed on top of the liner plate. On the lefthand side of the picture is the explosive liner package and on the right is another half of the segmented cone.

Gas is let in through the gas fill-line which is made of high pressure tubing and can be seen on the upper part of the front plate in Fig. 4. The positive electrode for ignition is provided by the ignition line which consists mainly of a steel rod insulated from the chamber block by a teflon sleeve. It can be seen on the lower part of the front plate in Fig. 4. The chamber block acts also as the electrical ground for the exploding wire.

2.1.2 Shortcomings of the MK II Design and the MK III Model

The pressure experienced by the parts close to the origin during a run with an explosive-driven implosion was tremendous. After each run the top liner plate, the segmented cone and the barrel assembly were usually distorted, the amount of distortion was generally dependent on the amount of explosive used and the symmetry of implosion. Even if the implosion was well centered, the amount of distortion after a few runs was found to be too large to allow the

parts to be reassembled inside the launcher, the design of which called for close tolerances on all mating parts. Hence, when this happened either re-machining and/or replacement was necessary. The liner plate was relatively easy to manufacture and was generally replaced after a few runs. However, the segmented cone require more serious considerations. The MK II has a double truncated-cone design for the segmented cone, with a large diameter, relatively short, truncated conical base and a slender conical end (see Figs. 3 and 4). It was found that the amount of machining involved was comparable to that required for machining the front plate. Also, the expansion of the external diameter of the barrel, which becomes practically nil 3-4 inches from the origin, shows that the ultra high pressure region for the present loadings must be concentrated within this region. Thus not the entire length of the slender cone was fully made use of. Based on these and other reasons (Ref. 32), the top plate of the launcher was redesigned. A new version of the launcher called MK III was manufactured and used in the later series of runs.

A schematic drawing of the MK III Launcher is shown in Fig. 5 and a photograph of the top half of the launcher in exploded view is shown in Fig. 6. In the MK III model, the idea of a segmented cone was retained; however, the shape of it was much simplified and the length reduced. One-half of it lies on the left hand side in front of the front plate in Fig. 6. Special stainless steel (17-4 PH precipitation-hardened type) with a very high tensile strength (210 K psi) was used. Manufacture of the segmented cone has thus been simplified significantly. It was hoped that the combined improvements in design and strength of material would reduce the amount of distortion experienced by the segmented cone. Despite these changes after four runs with explosive weighing from 113 gm to 176 gm, the cone was again distorted and re-working was required to rectify it. Although the amount of work involved in re-working was much less than the MK II cone, it was still disappointing. However, the range of pressure involved was an order of magnitude higher than the yield strength of any high-strength material. The distortion was probably unavoidable and replacement must be taken as part of the running cost of the equipment.

Notice also that the MK III liner plate was slightly modified for simplicity and strength. The thickness was increased to 1/2" and the outer O-ring groove was replaced by a simple "V". The use of a 15° conical liner plate became standard practice for all explosive runs in this model. The use of these combinations did result in much less distortion on the liner plate, hence, less frequent replacement was necessary.

2.1.3 Barrel Entrance Geometries and Gun Barrels

While it is possible to place the projectile flush with the top liner of the hemispherical cavity, it is undesirable and, in fact, detrimental from the point of view of production of stress in the projectile. A collapsing hemispherical implosion wave would subject the projectile to non-planar loading even if the implosion is symmetrical about the geometric centre. At the magnitude of pressure we are concerned with here (over 5 million psi for a 0.22 in. projectile) any significant degree of unevenness on loading would certainly disintegrate the projectile instantly. To allow the imploding hemispherical shock wave to become more planar when it hits the projectile, it is necessary to recess the projectile from the origin. Also, recessing the projectile would remove it away from the wall disturbances close to the origin.

Four types of entrance geometries were used for the recessed

projectile mode of operation. They are shown in Fig. 7.

Type A was used with the 5/16 in. barrel which was made of 5/16 in. I.D. stainless steel high pressure tubing with 1/8 in. wall thickness (Aminco* type No. 45-11220). The barrel was held in place by an entrance plug as shown. The projectile was recessed 3/4 in. from the origin, 0. The barrels used were 3 ft. long.

Type B was used with the old type of 0.22 in. barrel which was also held in position by an entrance plug as shown. The projectile was recessed 1/2 in. from the origin. The barrel used was the same type as described in Ref. 8. It has a 0.22 in. nominal bore diameter, 1 in. O.D. and 2 ft. long machined to dimensions shown in Fig. 7, to fit into the barrel holder. Outside the chamber block the original O.D. was retained to obtain maximum rigidity.

Type C was an improved version of the barrel and entrance design. The entrance plug and the barrel holder are all dispensed with and substituted by a new type of barrel and a shoulder piece. The barrels used were 0.22 in. nominal bore, 1-1/4 in. O.D. and 2 ft. in length, supplied by Canadian Arsenals Ltd., Small Arms Division** The projectile recessed distance could easily be changed for the investigation of projectile integrity problems. The barrel assembly could only be used once, since erosion and barrel bore expansion were found to be too serious to allow the barrel to be reused.

Types A, B and C were used with the MK II launcher. For the MK III launcher type D was used which was basically the same as type C except a change in the diameter of the shoulder piece and the bore diameter upstream of the recessed projectile. The projectile recess distance was fixed at 3 in. for the present series of runs. For this configuration the projectile flange thickness was reduced from .006 to 0.002 in. so that it would be released right after the gaseous detonation reaches it instead of by the impact of the imploding shock had the 0.006 in. flange thickness been used. This change was thought to reduce the chance of projectile disintegration by the imploding shock impact. Results did show that the projectile came out intact (some retained the original cylindrical shape) for all runs. All barrels used were honed and polished to obtain a smooth bore.

2.1.4 Explosive Shell Liners

With the present way of preparing the explosive liners, a detachable carrier of the explosive shell is desirable not only from the point of view of efficiency of operation and ease of manufacture. Another major consideration is the fact that the detonation pressure of the explosive (3.9×10^5 psia for "superfine" PETN with a relatively low loading density of 0.588 gm/cc) exceeds the yield strength of the chamber material by almost an order of magnitude. Plastic flow and distortion of the chamber wall can be expected if the explosive is in direct contact with the cavity wall. The metal liner is therefore used to protect the cavity wall and take up at least part of the plastic deformation due to the explosive loading, although in the original design calculations (Ref.29) the liner effect was not taken into consideration. In addition, the metal liner protects the accurately machined cavity surface from imprints generated by interacting waves in the detonating PETN.

---

* American Instrument Co, Inc., Silver Spring, Maryland, U.S.A.
**Canadian Arsenals Ltd.,Small Arms Div,Long Branch,Port Credit,Ont.Canada.

Aluminum was originally chosen for the full scale 30-inch model (Ref. 29) mainly for its light weight, in handling, and for its relative ease in manufacture. For the 8-inch MK II model 1/8 in. thick aluminum, laminated steel-aluminum and laminated aluminum shells were used for the first few runs with explosive and in some of the gas runs. In the case of the laminated liners, the inner liner was invariably buckled probably due to the expansion under heat of the gas trapped between the liners. Solid shells spun from 3/16 in. thick aluminum plate with the outside machined to final dimensions were then used. Aluminum has a fairly low melting point and being a very chemically reactive metal, it was reasonable to find that in all runs, including the gas runs, part of the inner surface was corroded. Reaction between aluminum and oxygen is a highly exothermic phenomena. This is a very undesirable feature as far as protecting the steel cavity is concerned. (This may have been partly responsible for the accident we once had in which a hole was burnt through the chamber wall). Subsequently, all explosive runs were carried out with copper liners. Although copper shells are far more difficult (and hence more expensive) to manufacture, it has many advantages over aluminum. Copper is fairly inert to chemical reaction with oxygen compared with aluminum and has a higher melting point (1481°F vs. 1220°F). No appreciable corrosion was ever observed in the shell after the runs. Consequently, a liner under normal conditions could be used over a few times. (In fact, one liner has been used for five runs). In addition, the acoustic impedance of copper as shown in Table 1 is quite closely matched with that of steel; consequently the ratio of transmitted to initial wave strength is only 1.072 compared with 1.315 for aluminum. Using copper thus reduces the magnitude of stress on the steel cavity. Also shown in the table is lead which was used in the runs carried out in the MK I implosion-driven launcher (Ref. 8). The ratio of transmitted to incident stresses σ_t/σ_I for the lead-steel combination is the highest amongst the three combinations. This, plus the fact that lead is too soft for handling and has too low a melting point, make it a very undesirable material for use as an explosive container shell.

2.2 Projectile Design and Material

The projectiles used in all runs have a simple cylindrical shape with a shear flange machined on the rear end of the projectile (Fig. 8) (both types 1 and 2 have been used) eliminating the need of a metal diaphragm. The flange acts as a seal against the high pressure loading gas used in the chamber and to keep the projectile in place prior to ignition. Different lengths (1 to 1/3 calibre) have been tried. The diameter of the projectile was machined to a push fit for each barrel. The front and the rear ends were polished.

Materials such as titanium, magnesium and Lexan have been used for manufacture of projectiles. Laminated materials composed of titanium and Lexan, and titanium and magnesium were also tried. As a compromise between strength and weight of the projectile, in the later series of runs half calibre titanium was generally used. The titanium used (MST 6 Al-4V annealed alloy) was obtained from Atlas Alloys Co., Toronto. This MST 6 Al-4V has a density of 4.43 gm/cm^3, tensile strength of 130,000 psi and yield strength of 120,000 psi.

The choice of material and the shape of the projectile depends on a few factors. First, in order to achieve high velocity, the weight of the projectile must be low. Second, the shape of the projectile should be such that minimum tensile stress should be kept throughout the entire launch cycle in order to keep the projectile intact throughout the acceleration period. Thirdly, the projectile should have a good gas seal, such that the driving gas should not leak around it causing a loss of driving pressure. All these

imply the use of materials with a high strength/weight ratio and a one-dimensional shape to avoid reinforced stress due to two or three-dimensional effects. (For further discussion see Appendix C).

2.3 Range, Plumbing and Control Room

The range (Figs. 9, 10) measures 2 ft. in diameter by 15 ft. long. It has three viewing stations; each consists of 4 windows allowing optical observations, recordings and velocity measurements by the light beam detectors of the projectile in flight. Upstream of the range is a blast tank (Fig. 9) which is 2 ft. in diameter by 6 ft. long with 18.8 cu.ft. volume, intended to contain the bulk of the driving gas. At the end of the range is a target station which consists of a replaceable lead target and an impact accelerometer. Figure 9 shows the overall dimensions and relative positions of the implosion chamber, blast tank, range, observation stations and the target station. Figure 10 shows two views of the range and instrumentation.

The control room has 12 in. concrete block walls, sand-filled and reinforced with rods. After assembly of the launcher, the operation of the entire range including monitoring pressures, vacuum pumps and filling up of gas can be remotely controlled at the control panel (Fig. 11) in the control room. The control panel is "human engineered" (Ref.8) for ease of operation and to guard against any accidental damage to the instruments caused by following a wrong sequence of operation. The gases used were all direct from commercial compressed gas bottles. They are placed inside the blast room. A sketch of the pressure and vacuum manifolds associated with the launcher driver chamber is shown in Fig. 12.

2.4 Velocity Measurements and Photographs

2.4.1 Light Screen Detectors and Associated Electronics

The velocity measuring system consists of a photomultiplier-light screen detector unit at each of the three measuring stations. These detector units (Fig. 10a) were designed and manufactured by the Aerophysics Branch of Computing Devices of Canada Ltd*. They have the capability of detecting 1/32-inch diameter particles up to velocities of 30,000 fps and 0.22 in.dia. particles well in excess of this. It was found that the intense magnetic radiations from the discharge of the ignition unit to the exploding wire in the chamber and that from the shadowgraph spark source and the X-ray unit strongly interfere with the proper operation of the detectors. Many ways of shielding were tried but none was found to be satisfactory. Finally it was felt that the only solution to this was to build a Sequential Hold-Off Programmer (SHOP).

The SHOP was designed to prevent spurious triggering of the electronic counters or the oscilloscopes by the light screen detectors. This was done by ensuring that the detectors were prevented from operating the counters for a period long enough to allow for sufficient damping of the magnetic and other radiations. The system consists of a series of lock-out astable and one-shot multivibrators (Fig. 13). The delay for each detector has been set to allow maximum velocity measurement and yet long enough to stop any unwanted pulses to reach the counters through gates controlled by the delaying system. Before firing of the gun, all gates are closed by a single pushbutton. A lamp

* Computing Devices of Canada Ltd., Ottawa 4, Ontario, Canada.

for each time interval section indicates that the gate is locked. The triggering pulse from the firing unit is applied to a light-emitting diode which turns on a photo-diode, triggering the first delay multivibrator. (The purpose of the combination of photo diode-light emitting diode is to isolate the system electrically from the ignition unit which may interfere with the proper functioning of the system). After 300 μ sec, the multivibrator resets and opens the gate connected to the first light screen detector. When the projectile passes through the first light screen, the detector sends a pulse through the now open gate and triggers the counter and/or spark and/or X-ray generator. At the same time the same trigger signal starts the second delay multivibrator. After 100 μ s, the second gate opens for the next light screen detector signal, and so on.

The system can only operate in sequence; that is, the first gate must be energized before the second gate can be operated and then the third. A manual pushbutton test system is built-in allowing a slow check of the operation of the detectors, the sequential lock-out circuit and counters This is paralleled by a high-speed, sequential, test system that sends a train of three pulses with time intervals of the order of 160 μsec (the same order of the maximum expected performance of the experiment). This gives a general test to the whole measuring system. The Sequential Hold-Off Programmer can be seen in Fig. 10a above the three electronic counters in the instrument cabinet.

The electronic counters used were Hewlett Packard 3734A which normally have a resolution of 10 μsec. The accuracy was improved to 1 μsec by using a 1 M Hz crystal as an external time base. The accuracy of the average velocity calculated from the time counted is 0.5% for a projected velocity of 20,000 fps.

An Endevco 2218 accelerometer mounted at the end of the target station (Fig. 10a) was used to monitor the impact of the projectile on the target at the end of the range. This was primarily used as a back-up system for velocity measurement. The output of the impact accelerometer together with the three triggering pulses from the sequentail programmer were displayed in a Tektronix 555 oscilloscope, a typical output is shown in Fig. 14.

2.4.2 Flash X-Ray Units

A Flexitron Model 730-1,2710 300 Kv flash X-ray unit (Fig. 10b) was used in the first measuring station (to take an X-ray radiograph of the projectile). It has a 20 nanosecond exposure time. The units are operated at approximately 150 Kv. The X-ray head can be seen on the top part of Fig. 10b while the triggering system is on the righthand side of the same picture.

2.4.3 Shadowgraph System

The shadowgraph system is a folded beam arrangement (Ref. 8 and 20). The projectile was photographed on polaroid film using a spark light source with an effective pulse width of approximately 400 nanosec. The light source is triggered by the same electrical pulse from the sequential programmer that triggers the electronic counter.

Figure 15 is a schematic diagram of the range of instrumentation circuitry showing the various instruments used in the experiment as described above.

2.5 Ignition System

In order to produce a spherically symmetric detonation essentially a point source of ignition with large energy output is necessary. The ignition is accomplished by discharging a 7.0 μf capacitor through a hydrogen thyratron into an 0.1-inch long 4 mil copper wire. The capacitor is normally charged to 6 Kv, thus giving a stored energy of approximately 130 joules. Comparing the discharge current wave forms between the discharge through a short circuit, it was found (Refs. 13,20) that the resistance of the exploding wire was only about 10% of the total resistance of the discharge circuit. Hence the energy release in the exploding wire must be only a small portion of the stored energy. No rigorous studies had been carried out to determine the exact amount of energy dumped in the exploding wire to date. (The stored energy was always quoted as a parameter in determining ignition characteristics). However, this setup was found to be quite sufficient to initiate detonation in the stoichiometric hydrogen-oxygen mixture used in the present series of experiments.

2.6 PETN-Explosive and the Preparation of Explosive Liners

In all experiments, superfine PETN was used as the explosive to generate implosions. Extensive work has been carried out by Flagg and Makomaski (Refs. 8 and 13) in search of suitable explosives which can be initiated by the detonation wave of a stoichiometric oxygen and hydrogen mixture. PETN is one of these and it was chosen on the grounds of handling safety, uniformity of initiation, and explosive yield. PETN also has an added advantage that its initiation properties can be changed by using different loading densities which can be varied over a wide range (0.59-1. gm/cc). Superfine PETN has a relatively low loading density (0.588 gm/cc), and is correspondingly more sensitive to initiation (Ref.8) and has a lower detonation pressure (Ref.35) compared with the higher density PETN formulations. Despite all these advantages, PETN crystals have no mechanical binding strength by themselves and manufacture of homogeneous hemispherical explosive liners with close dimensional tolerances was found to be a very challenging problem.

Considerable effort has been put into developing a manufacturing process by Canadian Safety Fuse Ltd., Brownsburg, Quebec. Four basic methods of making liners were tried in each of which a thin slurry of Superfine PETN mixed with water and binder (Cellosize) was used. The final dimension was obtained by machining, which gave very close tolerances and smooth surface finish. However, in all cases, it was found that the binder material generally floated to the surface on drying causing the liner to shrink and cracks developed as a consequence . Also, because of the thin slurry used the finish liner thickness could only be obtained by building up layer by layer with drying in between. Cohesions between layers were found to be poor. In view of these difficulties and the amount of labour involved, the development was terminated for economic reasons.

At UTIAS, Flagg (Ref.8) used a shell made of open core plastic foam sheet* to provide the dry PETN with a support matrix. Four orange peel segments of open core foam plastic were cemented to the metal liner then the PETN slurry (PETN mixed with 50% water) was forced into the cores of the foam until the PETN was flush with the foam surface. The assembly was dried slowly by warm air. Figure 16 shows the steps in manufacture. This type of liner was

* Scott Paper Company, Chester, Pennsylvania, U.S.A.

used quite extensively in the early runs of the launcher. However, it was felt that the homogeneity of this type of liner was doubtful since the presence of air pockets inside the liner were unavoidable. Also, the dry PETN was quite fragile, a few times when the launcher had to be opened up after assembly it was found that some explosive was blown away by the high velocity gas jet from the gas inlet. Other ways of manufacture had to be tried.

A new technique was developed by Professor G. F. Wright and Mr. T. Huber of the Chemistry Department, University of Toronto. In this method cotton linters was used as a binder. No detailed studies were carried out to determine the degree to which the initiation properties of the Superfine PETN might have been affected. However, it was found that the liner always initiated under 400 psi initial gas pressure. Details of preparation are reported in Ref. 32. The procedure of preparation can be briefly described in the following. A thick slurry of Superfine PETN with 0.5 to 1.5% of cotton linters was prepared with approximately 50% of water. The slurry was put into the metal liner which was placed in a mould-press (Fig. 17) and the final hemispherical shape of the explosive liner was formed by pushing the hemispherical plunger into the slurry. The assembly was then dried slowly in warm air. Most of the explosive launcher runs were carried out with this type of liner. However, the results were not particularly good. (See Chapter 4 on Results and Discussion). Slight off-centre implosions were still experienced in most of the runs. A check on the density of a finished liner showed variations up to 50%. This was thought to be caused by the uneven pressure exerted by the plunger on the explosive surface. Hence considerable effort still has to be spent in order to perfect this technique.

Each of the above two techniques has its own advantages and shortcomings. To date a satisfactory technique is still unavailable in that the homogeneity of the liner before ignition was still not certain. Cotton linters as a binder is quite promising; it gives the fragile PETN a very positive support as a closely interwoven matrix. A combination of the cotton linters as a binder and the plastic foam as a matrix for support while drying the slurry is presently being tried. Results (see Chapter 4) on two runs were quite promising. However, further development is still needed.

3. PERFORMANCE CALCULATIONS

3.1 Description of the Computer Program

The computer program used in the present study was developed from a one-dimensional numerical code used by Piacesi et al (Ref. 36) using the von Neumann-Richtmyer (Ref.37) technique of artificial viscosity to deal with the shock discontinuities numerically the original code was used to predict the performance of a two-stage light gas gun. This code was adapted and modified by Sevray (Ref.21) and Flagg (Ref.8) to study the performance of the UTIAS implosion-driven hypervelocity launcher. For the case of the detonating gas, Wilkin's technique (Ref. 38) was used to spread the detonation front over a number of zones.

The process in the hemispherical chamber and in the barrel can be described by a set of one-dimensional equations in Lagrangian form.

Conservation of Mass $$\frac{1}{\rho} = A \frac{\partial R}{\partial m} \qquad (1)$$

Conservation of Momentum $$\frac{\partial u}{\partial t} = A \frac{\partial P}{\partial m} \qquad (2)$$

Conservation of Energy $$\frac{\partial e}{\partial t} = -P \frac{\partial v}{\partial t} \qquad (3)$$

This set of equations is essentially one-dimensional and theoretically should be sufficiently described by a one-dimensional numerical code. However, many difficulties were encountered in practice in dealing with flows in the hemispherical cavity and in the entrance region into the gun barrel as discussed extensively by Sevray (Ref. 21), Flagg and Mitchell (Ref.23), Poinssot (Ref. 25), and more recently by Brode (Ref. 39). The first difficulty stems mainly from the large change in surface area A(R) in the hemispherical cavity. It is thus very difficult to have a proper division of zones to keep the difference in mass in the adjacent zones small in order to avoid spurious shocks if the total number of zones have to be limited to keep the expensive computer time short. The second difficulty is in the transition region joining the hemispherical flow region to the planar barrel flow region. The flow in this region is basically two-dimensional and can only be rigorously represented by a two-dimensional code. Any results obtained from a one-dimensional code can at best be approximate.

All of the work done so far (Refs. 8, 21, 25) considered a simple hemispherical cavity joining the barrel at the origin (Fig. 18a). This was the first configuration used in the UTIAS MK I Launcher. In some of the runs in the MK II and all runs in the MK III launchers, some slightly different configurations were tried. These involved the use of conical liner plates of various angles θ, on top of the hemispherical cavity and recessing the projectile from the geometric centre by a distance L_r as shown in Fig. 18b and described in the previous chapter. Flagg and Mitchell's scheme of zoning and their continuous treatment at the transition region can be easily adapted to this configuration and is physically more meaningful with a minimum of disturbance generated. A modified version of their program (Ref. 23) was used in the present computations for the configurations shown in Fig 18. The entrance geometry is shown in Fig. 19. Also shown in Fig. 19 is the zoning scheme. Upstream of the plane AB (Fig. 19) the zone boundaries are defined in a way identical to that used by Flagg (Ref. 8). The zone boundaries are defined by sectors of spheres with the respective radii from origin O until the radius is smaller than or equal to OA. Then the zone boundary surfaces are defined by sectors of an expanding sphere with base radius r_b. Downstream of the plane AB and upstream of the projectile, the boundary surfaces are circular planes with radius depending on the position of the plane in the conical entrance. According to the above, the following relations are used for defining the boundary areas:

$$A = 2\pi(R_c - x)^2 (1-\sin\theta) \qquad 0 \le x \le (R_c - \overline{OA}) \qquad (3.1)$$

$$A = \pi(H^2 + r_b^2) \qquad (R_c - \overline{OA}) < x < (R_c - \overline{OC}) \qquad (3.2)$$

$$A = \pi(r_p + (R_c - x)\tan\alpha)^2 \qquad (R_c - \overline{OC}) \le x < (R_c + L_r) \qquad (3.3)$$

$$A = \pi r_p^2 \qquad x \ge (R_c + L_r) \qquad (3.4)$$

The volume is calculated based on the areas found above. A total number of 65 zones were used with 25 for the explosive liner and 40 zones for the gas region assuming a vacuum ahead of the projectile. Flagg's scheme of zoning divisions was again used here. Since the final velocity and the appearance of the projectile base pressure history were quite similar, whichever scheme was used (Fig. B-1, and B-2 in Ref. 23), and since the present program was not meant to be extremely rigorous without considering loss mechanisms, it was therefore considered satisfactory for the present purpose. In order to compare the present numerical code with the more rigorous one used by Brode (Ref. 39) a calculation was performed using the present code with the same boundary conditions. The results are plotted in Fig. 20. It can be seen that the numerical code presently used gives a velocity which is lower than that obtained by Brode "without loss" using an "old" equations of state. While both are lower than the result obtained by using an "improved" equations of state including losses for the first 3 meters.

3.2 Results and Discussions

For the MK III launcher runs the projectile is recessed 3 inches from the origin with $\theta = 15^{\circ}$ and $\alpha = 5^{\circ}$. This configuration is slightly different from that shown in Fig. 7D. However, it was thought that with the volumes of gas in the transition region approximately the same, the results for the two configurations would not differ significantly. Therefore, no effort was spent on reproducing the entrance geometry exactly as many changes in the program would be required to represent all the different configurations used in the experiments.

It is interesting to compare the intermediate cases as the hemispherical configuration is gradually changed to that finally shown in Fig. 18b. In Fig. 21, four pressure history curves as a function of projectile travel distance are shown. Figure 22 shows the velocity versus distance curves. The curves represent the following cases: (1) a hemispherical configuration with 100 gm PETN and zero projectile recess; (2) a $15^{\circ}(\theta)$ conical liner plate with 74.12 gm PETN (which has the same thickness of PETN as in case (1); and (3) and (4) have 15° conical liner plates with projectiles recessed 3 inches (L_r) from the origin and barrel entrance angles (α) of 10° and 5° respectively. Both the projectile base pressure and the projectile velocity curves for the first two cases are quite similar. The final projectile velocity for case (1) is 8.79 Km/sec (at the barrel exit 72 cm downstream of the original projectile position), compared with 8.37 Km/sec for case (2) which is approximately 95% of the former although the amount of explosive used is only 74%. This justifies the use of a conical protective liner plate in the hemispherical cavity. In fact, experiments showed that the performance of the two configurations were similar. Projectile velocities for cases (3) and (4) showed marked increases from cases (1) and (2). The base pressures also remain higher for longer periods compared with cases (1) and (2). Thus, recessing the projectile with the two entrance geometries considered should theoretically increase the projectile velocity besides the other obvious reasons which will be considered in the next chapter.

It should be noted that the above runs were not meant to optimize the muzzle velocities. As Sevray has shown (Ref. 21) this requires an explosive thickness of about 1/10 the initial radius, or about 400 gm PETN, in this case.

4. EXPERIMENTAL RESULTS AND DISCUSSIONS

4.1 Raw Data

Table 2 shows the initial conditions and results of all projectile

runs carried out in the 8-inch diameter MK II and MK III launchers. In this table, the dimensions, material and weight of the projectile, explosive weight and the binding agent used, the initial gas loading pressure, the measured projectile velocity, the number of craters on the lead target, the off-centre-implosion distance from the origin, and the conical liner plate angle θ are given. The integrity of the projectile as quoted in the following are judged from the X-ray, shadowgraph photographs of the projectile, and also from the number of craters formed on the lead target. The latter is usually quite sufficient to determine the integrity of the projectile except when the projectile hit the wall of the range and disintegrated, such as in the last run 3.7 in which the X-ray picture showed that the projectile was intact while the cratering on the target was completely scattered.

Tables 3(a) and 3(b) show the initial conditions and results of all contained gas and explosive runs in which a copper witness plug was placed in the position where the projectile normally sat. Listed in the tables are also the conditions of the imprint left by the implosion. The contained runs were carried out mainly to test the various techniques and improvements in the chamber configurations before they were used in launching a projectile.

4.2 Off-Centre Implosions

4.2.1 Observations

In the case of gas runs only, all implosions were well-focussed and centered. Of the 41 explosive runs carried out, 20 of them show well-focussed, centred implosions. The rest exhibit various degrees of being off-centre from 1/4 inch from the origin (Fig. 23) to the worst cases of side implosions where the imploding waves focussed at the rim of the hemispherical cavity (Fig. 24).

The positions of implosion are shown in Figs. 26 and 27(a) and (b) for the cases of hemisphere cavities without the conical liner plate, with 10^{o} liner plate and with 15^{o} liner plate respectively. In the figures, the circles indicate the position of the imprint left by the off-centre implosion while the number(s) accompanying the circle are the run number of that run(s). The orientation of the off-centre implosion imprints varies rather randomly although about half of them are in the vertical direction (the direction joining the ignition inlet to the gas inlet. In the normal launching condition this direction is vertical with respect to the ground level). The imprints due to off-centre implosion were mostly fairly well defined and had roughly circular shape (e.g., See Figs. 23 and 25). However, in Fig. 25 we see that the secondary imprint(s) appears to be an elongated trough which is much shallower than the accompanying primary imprint (p). The size of the various imprints varies also from 2 inches (Fig. 24) to a fraction of an inch (Fig. 23).

In general, off-centre implosions occurring within approximately 2-1/2 inches diameter were tolerable in that they would hit on the disposable barrel assembly only and no other parts were affected. However, when the implosion occurred outside the barrel assembly, it would hit the liner plate, rendering it unusable again. The worst cases were when the implosion hit the wall of the hemispherical cavity directly. This invariably damaged the cavity wall which occurred in runs 7, 10, 33 and 36. (Run 36 is shown in Fig. 24).

4.2.2 Possible Causes of and Ways to Improve the Off-Centre Implosions

One of the most important parameters for a successful operation of the implosion-driven launcher is to have stable and symmetrical imploding shock waves focussing at the geometric centre of the implosion cavity. Due to the extreme pressure generated by the imploding shock at the point of focus, any implosion which is not centered would definitely cause damage to the chamber parts. If the implosion offset is more severe, it may even damage the whole chamber rendering it unworkable until repaired. This was a costly and time-consuming operation when it occurred. Hence it is extremely important to achieve a high degree of reproducibility of centered implosions if the operation of the launcher is to be carried out smoothly.

Up to now there has been very little theoretical and hardly any experimental work done on the stability and behaviour of the imploding shock waves in the range of shock Mach numbers we are interested in. Huni (Ref. 40) and Lee et al (Ref. 41) observed that converging cylindrical detonation waves were stable. The stabilizing mechanism was suggested by Huni to be the supposed increase in detonation wave velocity at the regions lagging behind the circular wave front which have higher curvature and a reverse effect at those regions ahead of the circular wave which have lower curvature. However, his argument was based on the Chester-Chisnell-Whitman model developed by Lee and Lee (Ref. 42). This model is essentially one-dimensional and could not possibly account for the effect of a change in wave curvature on the wave front velocity. In fact, any region lagging behind the circular wave front has an increase in surface area which according to the C-C-W model would result in a reduced wave velocity rather than an increase as suggested by Huni. Likewise, regions ahead of the circular wave front have smaller surface area and would result in an increase in wave velocity. To this effect then, both regions anead of and lagging behind a converging cylindrical wave are unstable. In other words, a converging cylindrical (or spherical) wave is unstable by itself. A similar argument would show that a diverging cylindrical (or spherical) wave is intrinsically stable. Therefore the observed stabilizing effect in the cylindrical imploding detonations must be due to some external mechanisms other than the wave front itself. A stabilizing mechanism was suggested by Lee et al (Ref. 41) to be the rotating transverse waves following the contracting detonation front. These transverse waves are distinctive features of a detonation front and are lacking in a converging shock wave. Therefore their findings are not contradictory to the argument above or to the theoretical predictions by Butler (Ref. 43) and Zaidel and Lebedev (Ref.44).

Butler (Ref. 43) and Zaidel and Lebedev (Ref. 44) considered the stability of spherical and cylindrical self-similar converging strong shock waves perturbed by small disturbances. While Zaidel and Lebedev considered only the $\gamma = 7$ case, Butler proved that all imploding shock waves, spherical and cylindrical, are unstable to disturbances in that the shape of the disturbed wave will not regain the original shape. This agrees qualitatively with the argument above based on the C.C.W. model. However, it was noted that the convergence of the shock wave to a point may still be quite sharp. This is only a first order perturbation solution for the Guderley (Ref. 45) type of strong imploding shock and cannot account for any possible offset in the final focus position which was observed in experiment. For large disturbances, it is quite logical to expect that the final focus position would be perturbed also and the amount of displacement should depend on the degree of the perturbation. This was, in fact, observed in the beautiful schlieren photographs obtained by Perry and Kantrowitz (Ref. 46) who perturbed the converging cylindrical shock

wave by a small obstacle in the path and the final focus was observed to have shifted towards the disturbed side. In most of our experiments where there was an off-centre implosion the convergence was still quite sharp. This agrees with Butler's conclusion even though our average imploding shock Mach number was only of the order 4.5 which cannot strictly speaking be compared with the Guderley type of intense implosion except near the origin. However, the theory does give the right trend.

Although the exact causes of the off-centre implosions are yet unknown, according to the above they must have been due to some disturbances to the imploding shock causing the focus point to shift from the origin. A number of possible sources of disturbances and the methods to eliminate or to try at least to reduce their effects will be described.

4.2.2.1 Asymmetry in the Initiating Hemispherical Gaseous Detonation Wave

The PETN liner should be initiated ideally by a perfect hemispherical detonation wave in the stoichiometric H_2-O_2 mixture. However, since the hydrogen and oxygen mixture is initiated by dumping a finite amount of energy to explode an elongated copper wire in the gas, the initial stage of the detonation wave was highly unsymmetrical (Ref. 30). The asymmetries could probably smooth out as the wave propagates outward because an expanding spherical wave is stable compared with a converging wave (Ref. 40) provided the gas mixture is homogeneous and does not introduce any more disturbances after the initial stage. In a number of gas runs by Elsenaar (Ref. 28) in studying the focussing of the implosion wave due to the reflection from the wall of the gaseous detonation wave alone, he found that the implosion was offset by 0.03 to about 0.6 inches, always along the vertical axis to the bottom side no matter in which direction the ignition wire was. He suggested that gravitational effect must have played an important role in bringing about this type of offset. It was thought that if the gases were allowed to go in the chamber slowly as it was done in his runs, the much heavier oxygen gas would stay at the bottom, thus introducing gradients in the proportion of the mixture along the vertical direction. This gradient introduces continuous disturbances to the detonation velocity (Ref. 19) and hence to the symmetry of the wave. These disturbances are reflected into the imploding shock wave causing its focus to be off-centre.

Because of safety reasons, we could not pre-mix the gases, since a large amount of hydrogen and oxygen mixture at high pressure is very dangerous. The diffusion process of the gas mixture seemed to be very slow. In four runs (Run 14, 15, 16, 17) the hydrogen gas was pumped in before the oxygen and the final mixture was allowed to settle by 0, 3, 5 and 30 minutes, the mixture failed to detonate in the first three runs and only partially detonated in the last run. Since the sonic velocity of oxygen is about 1/4 of that of hydrogen, even assuming oxygen choked flow in the gas inlet ports, the final mixing jet velocity is at most only 1/4 that of hydrogen. These results show that there is insufficient mixing with this order of filling while diffusion up to 1/2 an hour was not sufficient in bringing about a uniform mixture.

Finally, the hydrogen was allowed to pump in after the oxygen in a few fast strokes, deliberately introducing turbulent mixing to the gas mixture. The mixture was allowed to settle for a few minutes before ignition. The results were very good in that all implosion imprints on the copper witness plug were found to be almost exactly centered and the imprints were very sharp

(Fig. 28, runs 13, and 3.1). To ensure that the gas mixture would detonate properly (Ref. 30) all runs were carried out with an initial gas pressure of 400 psi. Judging from the well-centered implosion imprints, the outgoing detonation wave when reaching the chamber wall must have been very symmetrical, otherwise any asymmetries would have affected the implosion focus. The slight asymmetries in Fig. 3c in Ref. 30 which used the fast pumping technique at gas pressure of 400 psi, could probably be due to optical effects and the fact that the chamber conditions were not exactly duplicated.

Instead of initiating the PETN by the hemispherical detonation wave, a light initiation technique has also been investigated as reported in Appendix A. This method would insure an instantaneous initiation of the explosive liner thus getting rid of any uncertainties in the irregularities in the detonation wave. Unfortunately, the results were not very conclusive.

4.2.2.2 Nonuniformities in the PETN Liners

To date two basic methods were used to produce PETN liners as described in Section 2.6. The open-core, plastic-foam technique allows the PETN slurry to dry by slow evaporation, the density of the explosive should be fairly uniform. However, air bubbles can be trapped inside the plastic-foam cores making its uniformity uncertain. Also the surface finish of the liner was not very smooth and the dry PETN although supported by the foam cores can still crumble by shaking and by the high-velocity gas jets from the gas inlet of the implosion chamber. In this sense, the cotton linters PETN mixture worked with the liner preparation-mould press was far superior. The latter technique produces liners with very smooth surface and the cotton linters provides the liner surface with a tough texture. However, one setback of this technique so far is that pressure applied on the press to dry the wet PETN slurry can be quite nonuniform over the entire hemispherical surface and the final product was obtained by patching the air pockets left on the liner surface by the press. Thus the density of the finished liner can be quite nonuniform. In fact, one typical 0.1" thick explosive liner was tested in which 10 samples were taken equidistant on a circle approximately 1-1/2 inches from the edge of the explosive liner. It was found that the densities measured from these samples differed by up to 20%. (Admittedly this depended a lot on the skill of production). However, the nonuniform density could have accounted for at least some of the offset implosions shown in Figs. 26 and 27, and also the same could also have been the reason for the irregular shapes of the implosion imprint on the witness copper plug shown in Fig. 28 (runs 26 and 56). The centre copper witness plug in Fig. 28 was from run 24 where a plastic foam type of liner was used and the imprint is very well focussed and symmetrical. This shows that the plastic foam type of liner in general detonates more uniformly and introduces fewer disturbances into the implosion than the cotton linters type of liner. In fact, the size of the nonuniformity caused by the air pockets could at most be of the order of the size of a single core in the plastic foam which has approximately 10 cores per lineal inch. Comparing the relative number of off-centre implosions, the foam-type liners have 31% compared with 76% for the cotton linter type.

Until a more reliable technique of drying the cotton linters liners is found, it seems that by combining the cotton-linters technique with the plastic-foam would be a compromise. Thus, we can pre-mix the PETN with cotton linters and force this wet slurry into the plastic foam in the same way as described in Section 2.6 in preparing a plastic-foam type of liner. The finished liner should have a fairly uniform density and the texture of the explosive

should be improved, making it less susceptible to shaking and blowing away by the incoming gas. Although this concept has still to be proved by many experiments, runs 3.6 and 3.7 used this type of liner and the results were very good.

As far as explosive liner manufacture is concerned, it is still far from being perfect. Further development will be necessary before we can come up with a more reliable and practical technique which would produce the type of liners which are homogeneous, geometrically uniform and with high mechanical strength.

4.2.2.3 Other Causes and Extreme Off-Centre Implosions

Besides these potential disturbances described above, there can still be some other causes. In the MK II model the positive electrode inlet is only 1/2 inch from the explosive liner. If there is electrical breakdown here, then the gas could detonate locally and prematurely, initiating the part of the explosive liner close to the electrode. This type of offset initiation can produce the worst type of off-set implosion focussing on the edge at the opposite side of the hemispherical cavity causing a tremendous amount of damage to the launcher chamber. Although this may be possible, it is not suggested here that this was the cause of this type of offset implosion.

Out of the three more serious off-centre implosions of this type, runs 7, 10 and 36, the first two imploded on the wall opposite to the electrode side while the third imploded in a direction at right angle to it. It is unlikely that, premature local detonation of the gas by electrical breakdown at the electrode could have accounted for the last one. To avoid this type of devastating side implosion a conical liner plate was added on top of the regular liner plate. The idea is that even if there is side initiation of the explosive liner, the presence of the conical liner plate makes the imploding wave physically impossible to focus at the other side of the wall. Instead the imploding wave would hit on the surface of the conical plate. (Note: No abrupt changes should be allowed in the geometry of the conical liner plate. This could have accounted for the results of some contained gas runs (e.g. Runs 39, 40, 41 and 42) which had either deflagration of the gas or extremely diffused implosion without imprint on the copper witness plug).

Figure 29 shows a postulated developing wave patterns in the implosion chamber with and without a conical liner plate due to side initiation of the explosive liner. If we assume a constant detonation velocity in the explosive liner, a side initiation of a hemispherical explosive liner (Fig. 29a) will always lead to an implosion at a point "B" in the figure, 180° from the point of initial "A" because point B is equidistance from A in all directions along the surface of a hemisphere on which the explosive liner lies. However, if we add to the hemispherical cavity a conical plate as shown in Fig. 29b), the situation will be changed. Since now a point C opposite to point A on the rim of the conical plate will have different spherical distances along different directions on the spherical explosive liner, with the minimum distance along the great circle containing these two points. Thus it would be physically impossible for the detonation to collapse to a point at point C from all directions and the implosion will be away from the rim of the cavity.

In the old type of explosive liners the liner had a square edge. It was thought that around this region where the detonation wave could diffract around the corner thus forming a locally higher pressure region compared with the

rest of the explosive surface. Since the initiation of the explosive is strongly dependent on the strength of the incident shock (Ref. 8), the explosive is more readily detonated at this region compared with the other parts of the liner. In order to minimize the chance of any premature detonation at the edge, the square edge was replaced by a chamfered edge.

4.3 Projectile Integrity and Velocity

(i) Projectile Integrity:

The projectile is photographed on both X-ray and shadowgraph pictures at the respective station along the range section. Typical shadowgraph and X-ray pictures of an intact projectile are shown in Fig. 30a and 30b. At the end of the range, a 1-3/8 in. thick, 6 in.dia. lead target is placed in the path of the projectile. Judging from the crater(s) formed on the target, we can tell whether the projectile is intact or not. When the projectile is disintegrated they normally do not show up in the shadowgraph nor the X-ray pictures. Thus the impact formation on the lead target is a more positive way of telling whether the projectile launched is intact or disintegrated. A lead target with a crater formed by the impact of an intact projectile is shown in Fig. 31. The projectile integrity for each run is shown in Table 2.

The projectile integrity depends on a number of factors such as the type of material, geometry, amount of explosive, and its distance downstream of the geometric centre of the chamber. It is further complicated by the fact that the implosion wave is not always symmetrical, hence introducing non-planar pressure profiles on the projectile thus straining the already critical environment for the projectile. In order to eliminate the effect of the off-centered implosion, the data shown in Table 1 were regrouped in Table 4, leaving out all runs with significant off-centre implosions (more than 1/2 in. off-centered). At a 1/2-inch projectile recess distance from the origin and moderate loading of explosive, 1/2 calibre Lexan, 1/2 cal. and 1 cal. Mg, 1/2 cal. titanium and a composite projectile made up of two 1/2 cal. pieces of titanium and Lexan were all disintegrated. However, a compositie projectile made up with titanium and magnesium (each of 1/2 cal. length) was found to remain intact over two runs (31 and 32) with explosive weights of 102 and 142 grams. At a 1-inch projectile recess distance from the origin, 1/2 cal. Ti projectile failed in all four runs with explosive weights from 102 to 122 grams. At 2 inches from the origin the same 1/2 cal. Ti projectile survived in one run but failed in the other with 73 and 125 gm explosive, respectively. At 3 inches from the origin 1/2 cal. titanium projectile survived in all runs. However, the Ti-Mg projectile which survived at 1/2 in. from the origin failed here. Failure of the projectile in this run was judged from the fact that the size of the projectile measured from the shadowgraph was found to be about half the original. The cause of the reduction in projectile size was not ascertained. (Further discussions on projectile integrity problems can be found in Appendix C).

4.3.2 Projectile Velocity and Barrel Expansion and Erosion

Figure 32 is a plot of the launched velocity versus explosive weight for the intact 0.22" diameter, 1/2 calibre titanium projectiles launched from both the MK II and MK III Launchers. (The condition of the implosion and the projectile recess distance from the origin are all indicated adjacent to the data points). The meximum projectile launch velocities and weights (Ref. 47, 48) are replotted in Fig. 33 with the additional data from The Physics International

Co. (Ref. 49) and the present report. This graph thus brings up-to-date the present launcher performance limit and the relative position of the UTIAS facility at the present stage of the development. Shown on the same graph are also the theoretical results obtained by Brode (Ref. 39), Sevray (Ref. 21) and from the present report. The data obtained from the MK II Launcher using 5/16" diameter, 1 calibre length titanium projectiles are shown in Fig. 34. Also shown in the same figure are the corresponding numerical solutions for the runs. Figure 35 shows the theoretical and the experimental performance of the MK III Launcher runs using 15° conical liner plate with 3 inches of projectile recess. Two theoretical performance curves were shown with 5° and 10° barrel entrance angle (α) respectively.

While the theoretical performance curves (Fig. 35 and 36) show that the projectile velocity should increase with the amount of explosive used, the experimental performance as shown in Figs. 34 and 35 show that the projectile velocity increases only very slightly with the increase in the explosive weight. For example, from Fig. 34, the numerical results show that for the 5/16 inch diameter, 1.73 - gram projectile the velocity should increase by over 30% while the measured velocity for the centered implosion runs increases by only 3% increasing the explosive weight from 80 grams to 144 grams. From Fig. 35, the numerical results indicate that for the 0.22 inch diameter, 0.28 grams projectile the velocity should increase by 21 and 17.5% for $\alpha = 10^{\circ}$ and 5° respectively, while the measured velocity increases by only 10% increasing the explosive weight from 80 to 176 grams.

Although the experimental projectile velocity depends only slightly on the explosive weight, it depends strongly on the projectile weight as shown in Fig. 33.

While theory (Chapter 3) predicts an increase in velocity by recessing the projectile downstream from the origin, the few experimental results shown in Fig. 32, however, cannot verify the prediction very positively. This is due to the fact that projectiles with recessed distance less than 3 inches always broke up. Also, due to the complication of the off-centre implosion problem, the conditions of the runs are not identical, making it difficult to compare experiments with theoretical predictions.

Finally, it can be seen in Figs. 34 and 35 that the experimental performance falls well below the theoretical performance lines. Although the same numerical program used here gave results which for the 24-inch launcher compared favourably with the results obtained by Brode (Ref. 39) whose calculation included more realistic equations of state for the PETN and for the $2H_2 + O_2$, wall loss, effects including radiation, heat conduction and wall abrasion, projectile losses and air resistance ahead of the projectile. However the relative effect of the loss effects and especially the barrel expansion problem for the 5/16 - and 0.22 -inch diameter barrels could have been more severe and could possibly account partly for the low efficiency of the experimental runs. In fact, heavy wall abrasions have been observed for all runs. A sectioned view of the first 5-1/4 inches of a typical gun barrel after a single shot is shown in Fig. 36. In this run 143 gm of PETN was used. The implosion was well centered. The original shape of the bore of the barrel is also shown in a sketch at the bottom of the photograph to the same scale. A step on the bore is allowed for the seating of the projectile which was recessed 3 inches from the end of the barrel for this run.

It can be seen that the shape of the barrel bore is completely changed after the run. The bore diameter increases considerably and very unevenly along the first four inches of the barrel. The enlargement from the original contour of the barrel must have been due to both erosion and expansion by the extremely high temperature and pressure driver gas. The bore diameters at a few places along the rest of the same gun barrel were also measured and are shown in Fig. 37. The original bore diameter was 0.214 inches. Thus there are erosion and/or barrel expansion along practically the entire length of the barrel judging from the increase in bore diameter. In fact, during this run a total amount of 45 gm of barrel material had been removed. This is 160 times the weight of the projectile and 2.3 times the weight of the driver gas. Erosion of the barrel wall would contaminate and cool the driver gas reducing the escape speed and introducing rarefaction waves into the flow thereby lowering the effective driving pressure. Barrel expansion would further reduce the driver pressure. In fact a recent calculation by Watson (Ref. 49) showed that the wall expansion effect reduces the final calculated velocity of their gun (with a peak projectile base pressure of about 66 k bars) by approximately 30%. Since the peak driver pressure is higher in our launcher, it is reasonable to expect that the effect of barrel expansion on the performance of the gun would be even more significant. In view of these effects, it is therefore hardly surprising to find the measured velocities to be less than 40% of the theoretical predictions (Figs. 34 and 35). In fact, the erosion effect and the barrel expansion problem could also have accounted for the fact that the centered implosion runs (e.g., runs 62, 64 and 3.6) give approximately the same projectile velocities compared with the off-centre implosion runs (e.g., runs 52, 55, 32, 34 and 36), which would definitely produce lower driver pressure and resulted in relatively less erosion and expansion. Furthermore, the apparent ineffectiveness on projectile velocity of the increase in explosive weight in the driver now becomes apparent in view of the effect of the barrel expansion and erosion. A higher explosive loading would increase the peak driving pressure which would increase the degree of barrel expansion and erosion which in turn reduce the original driving pressure. Therefore, the increased driving pressure due to an increase in explosive weight could be balanced by the decrease due to barrel expansion and erosion thus offsetting the predicted increase in the effective driving pressure and the final projectile velocity.

Another possible cause of concern is the gas leakage around the projectile as suggested by Elsenaar (Ref. 28). Normally the first inch of the barrel suffered the maximum amount of distortion as can be seen in Fig. 36. Therefore, if we place the projectile within this region the high pressure gas could easily open up the barrel allowing gas to leak around the projectile before the projectile could move away from this region. The leaking of high temperature and pressure gas around the projectile could be very detrimental to the projectile itself and could have contributed to the breakup of the projectile. In the runs reported by Elsenaar (Runs 4, 5, 6 and 9 in Table 2), 5/16 -inch diameter, one calibre length titanium projectiles were placed at 3/4 inch from the origin. Ionized gas was detected well ahead of the projectile suggesting that the driving gas had leaked around the projectile. The shadowgraph pictures of the projectiles also showed that the rear ends of the projectile were rounded, probably caused by the gas flow from behind. Thus this is another contribution to the severe conditions at positions close to the origin. In the later series of runs in the MK III Launcher, the projectile was recessed 3 inches from the origin. All shadowgraph pictures of the projectiles in flight (e.g., Fig. 30) showed that they retained the original shape which did not show any effect caused by leakage around the projectile. Also, the barrel expansion at the original projectile position as shown in Fig. 36 was much less compared to the first 1 inch

of the barrel. Thus the driving pressure of the projectile must have been reduced appreciably by the expansion of the first inch of the barrel. Watson's calculation (Ref. 49) also showed a similar expansion around the original position of the projectile. However, no appreciable barrel expansion was observed within a few diameters from the travelling projectile. No gas leakage was reported. Except close to the original projectile position, our calculated projectile base pressure was comparable to that of their gun. Thus gas leakage was not considered to be a serious factor reducing the efficiency of the gun for the later series of runs.

CONCLUSION

A total of 35 explosive runs (including contained runs) were carried out in the 8-inch diameter MK II launcher. Based on the experience gained from these runs, an improved version, the 8-inch diameter MK III launcher was manufactured and a total number of 6 explosive runs were carried out in this model. Despite all the improvements incorporated into the MK III launcher, significant distortions of the launcher parts were still experienced although re-working of the parts was simplified. The distortions were perhaps unavoidable in a device of this nature encountering gasdynamic pressures up to a few million psi.

The problem of edge implosion seemed to have been solved by adding a conical liner plate on top of the regular liner plate. However, the problem of the less severe off-centered implosions were still largely unsolved. In this respect the nonuniform explosive liner density seemed to be responsible for at least some of the off-centre implosions. A new technique of preparing the explosive liner package was used in the last two runs. The results were quite encouraging. However, further development and tests would still be necessary before a satisfactory technique of producing explosive liners becomes available.

With the use of the Sequential Hold-Off Programmer, the efficiency of obtaining the correct projectile velocity measurements, X-ray and shadowgraph pictures of the projectile were proved to be almost 100%.

While projectile integrity was proved to be a serious problem close to the origin, we were able to launch an 0.22-inch diameter, 1/2 calibre titanium projectile intact from the gun with the projectile initially placed at 3 inches downstream from the origin. However, the measured projectile velocities were less than 50% of the computed results and was probably due to excessive barrel expansion and erosion. About 45 gm of material was found to have been removed from the 0.22 inch bore diameter, 2-feet long barrel, after a single shot. In order to improve the efficiency of the launcher, the serious barrel expansion and erosion problems must be solved.

REFERENCES

1. Denardo, B. P. — "Penetration of the Polyethylene Into Semi-Infinite 2024-T351 Aluminum Up to Velocities of 37,000 ft/sec", NASA TN D-3369, 1966.

2. Moore, F. T.; Mumma, D.; Godfrey, C. S.; Bernstein, D. — "Implosive Gas Guns for Hypervelocity Acceleration". Proceedings of the 4th Hypervelocity Techniques Symposium, Tullohoma, Tenn. Nov, 1965. pp.457-484.

3. Crosby, J. K.; Gill, S. P. — "Feasibility Study of an Implosive Gun". NASA CR-709, 1967.

4. Crosby, J. K.; Gill, S. P.; Fowles, G. R. — "Explosive Compression and Acceleration of Helium for Hypervelocity Applications". Proceedings of 4th Hypervelocity Techniques Symposium, Tullahoma, Tenn. Nov, 1965, pp.429-456.

5. Chapman, R. L.; Harms, D. E.; Sorenson, G. P. — "The Magnetohydrodynamic Hypervelocity Gun". Proceedings of 6th Symposium on Hypervelocity Impact, Aug, 1963. Vol.1. pp.319-330.

6. Bulletin and Annual Progress Report. Institute for Aerospace Studies, University of Toronto, 1959.

7. Glass, I. I. — "Research Frontiers at Hypervelocities", Canadian Aeronautics and Space Journal, Vol.13, No's. 8 and 9. 1967, pp.347-429.

8. Flagg, R. F. — "The Application of Implosion Wave Dynamics to a Hypervelocity Launchers". UTIAS Report No.125, 1967.

9. Bremner, G. F.; Glass, I. I. — "Hypervelocity Launcher". UTIAS Progress Report, Section C-5, 1961.

10. Benoit, A.; Bremner, G. F.; Brode, A. L.; Glass, I. I. — "Implosion Driven Hypervelocity Launcher". UTIAS Progress Report, Section C-1, 1962.

11. Glass, I. I. — "Hypervelocity Launchers, Part I: Simple Launchers", UTIAS Review No. 22, 1963.

12. Benoit, A. — "An Experimental Investigation of Spherical Combustion for the UTIAS Implosion Driven Launcher". UTIAS Tech.Note No.71, 1963.

13. Makomaski, A. H. — "Preliminary One-Dimensional Investigation of the Initiation of Low Density PETN by Hydrogen-Oxygen Detonation Waves". UTIAS Tech.Note No.83. 1965.

14. Benoit, A. — "Thermodynamic and Composition Data for Constant Volume Combustion of Stoichiometric Mixtures of Hydrogen-Oxygen Diluted with Helium or Hydrogen". UTIAS Tech.Note No.85, 1964.

15. Glass, I. I. "Shock and Combustion Wave Dynamics in an Implosion-Driven Hypervelocity Launcher". UTIAS Review No.25, 1965 (also APL Report No.67-0018).

16. Glass, I. I. "Hypervelocity Launchers, Part 2: Compound Launcher-Driving Techniques". UTIAS Review No. 26, 1965.

17. Kennedy, J. E.
Glass, I. I. "Multi-Point Initiated Implosions From Hemispherical Shells of Sheet Explosive". UTIAS Tech.Note No. 99, 1966.

18. Benoit, A. "Specific Heat Ratios and Isentropic Exponents for Constant Volume Combustion of Stoichiometric Mixtures of Hydrogen-Oxygen Diluted with Helium or Hydrogen". UTIAS Tech.Note No.102, 1966.

19. Benoit, A. "Characteristics of Chapman-Jouguet Detonation Propagating in Stoichiometric Hydrogen-Oxygen Mixtures Diluted with Helium and Hydrogen". UTIAS Tech. Note No.104, 1966.

20. Watson, J. D. "Implosion-Driven Hypervelocity Launcher Performance Using Gaseous Detonation Waves". UTIAS Tech.Note No.113, 1967.

21. Sevray, P. A. "Performance Analysis of the UTIAS Implosion Driven Hypervelocity Launcher". UTIAS Tech.Note No.121, 1968.

22. Benoit, A. "Equilibrium Thermodynamic Data for the H_2-O_2-He Systems". UTIAS Tech.Note No.128, 1968.

23. Flagg, R. F.
Mitchell, G. P. "An Optimization Study of the UTIAS Implosion-Driven Hypervelocity Launcher MK II". UTIAS Tech.Note No. 130, 1968.

24. Garg, S. K. "Spherical Elastic-Plastic Waves in Solid Media". UTIAS Tech.Note No.132, 1969.

25. Poinssot, J. C. "A Preliminary Investigation of a UTIAS Implosion-Driven Shock Tube". UTIAS Tech.Note No.136, 1969.

26. Roberts, D. E. "A Spectroscopic Investigation of Combustion-Driven Spherical Implosion Waves". UTIAS Tech. Note No.140, 1969.

27. Elsenaar, A. "A Numerical Model for a Combustion-Driven Spherical Implosion Wave". UTIAS Tech.Note No. 144, 1969.

28. Elsenaar, A. "Microwave Measurements of Projectile Motion in the Barrel of the UTIAS Implosion-Driven Hypervelocity Launcher". UTIAS Tech.Note No.145, 1969.

29. Dawson, V. C. D.
Waser, R. A.
Oakes, D. O.
"The MK II UTIAS Implosion-Driven Hypervelocity Launcher Design Analysis". UTIAS Tech.Note No.147, 1970.

30. Macpherson, A. K.
"A Preliminary Study of Spherical Detonation Wave Symmetry in Stoichiometric Hydrogen-Oxygen Mixtures". UTIAS Tech.Note No.154, 1970.

31. Macpherson, A. K.
"A Preliminary Monte Carlo Analysis of the Reflection of an Imploding Hemispherical Shock Wave Similar to that Generated in the UTIAS Implosion-Driven Hypervelocity Launcher or Shock Tube". UTIAS Report No. 152, 1970.

32. Czerwinski, W.
"Structural Design and Development of UTIAS Implosion-Driven Launchers". UTIAS Report No. 153 (to be published).

33. Graf, W. O.
Work in Progress, Institute for Aerospace Studies, University of Toronto, Ph.D. Thesis.

34. Diedrich, J. H.
Stepka, F. S.
"Investigation of Damage to Brittle Materials by Impact with High-Velocity Projectiles Into Glass and Lucite". NASA TN-D-2720, March, 1965.

35. Cook, M. A.
"The Science of High Implosives". Reinhold Publishing Co. 1958.

36. Piacesi, R.
Gates, D. G.
Seigel, A.E.
"Computer Analysis of Two Stage Hypervelocity Model Launchers". U.S. Naval Ordnance Laboratory, Silver Spring, Maryland. NOL-TR-62-87, 1963.

37. von Neumann, J.
Richtmyer, R. D.
"A Method for the Numerical Calculation of Hydrodynamic Shocks". J. Appl. Phys. Vol.21, p.332, 1950.

38. Wilkins, M. L.
"Calcul de Detonations mono et Bidimensionelles". Colloques Internationaux du Centre National de la Recherche Scientifique sur les ondes de detonation, 1961.

39. Brode, H. L.
"Theoretical Description of the Performance of the UTIAS Hypervelocity Launcher". (to be published). Second International Colloquim on Gasdynamics of Explosions and Reactive Systems. Akademgorodok, Novosibirsk, Aug 24-29, 1969. Proceedings, Astronautica Acta.

40. Huni, J. P. R.
"A Study of Concentric Imploding Detonations". Ph.D. Thesis. Department of Physics, University of British Columbia, 1970.

41 Lee, J. H.
Knystautas, R.
Bach, G. G.
"Theory of Explosions". AFOSR 69-3090 TR, Nov, 1969.

42. Lee, J. H.
Lee, B. H. K. "Cylindrical Imploding Shock Waves". Physics of Fluids, Vol.8, pp.2148-2152, 1965.

43. Butler, D. S. "The Stability of Converging Spherical and Cylindrical Shock Waves". ARDE Report (B) 18/56. Aug, 1956.

44. Zaidel, R. M.
Lebedev, V. S. "The Stability of One Case of a Converging Shock Wave". Soviet Physics. Doklady, Vol.135, No.2. Nov, 1960.

45. Guderley, G. "Strong Spherical and Cylindrical Shock Waves in the Neighbourhood of the Centre of the Sphere or the Axis of the Cylinder". Luftfahrtforschung, Vol. 19, No.9, pp.302-312, 1942.

46. Perry, R. W.
Kantrowitz, A. "The Production and Stability of Converging Shock Waves". J. Appl. Phys., Vol.22, p.878, 1951.

47. Lukasiewicz, J. "Constant Acceleration Flows and Application to High Speed Guns", Arnold Engineering Development Centre, AEDC-TR-66-181, Nov, 1966.

48. Seigel, A. E. "The Theory of High Speed Guns". AGARDograph 91, May, 1965.

49. Watson, J. D. "High-Velocity Explosively Driven Guns". NASA-CR-1533, June 1970.

TABLE 1

	Density slugs/ft^3	Longitudinal Sound Speed C_L ft/sec.	Characteristic Impedence ρC_L Slugs/ft^3-sec
Steel	15.2	19,500	2.97×10^5
Lead	21.9	7,100	1.55×10^5
Aluminum	5.22	20,900	1.09×10^5
Copper	17.2	14,900	2.57×10^5

The above material properties are taken from Ref. 34

	$\frac{\text{Transmitted Wave Strength}}{\text{Incident Wave Strength}} = \sigma_t/\sigma_I$
Lead/Steel	1.46
Aluminum/Steel	1.315
Copper/Steel	1.072

where $\sigma t/\sigma_I = 2\rho_2 C_{L_2} / \rho_1 C_{L_1} + \rho_2 C_{L_2}$,

subscript 2 and 1 refer to materials on the left and right hand side of a boundary respectively when the wave is travelling from right to left.

TABLE 2. RAW DATA

	Run No.	Entrance Geometry (Fig. 7)	Projectile: Diameter (in.)	Material	Length (calibre)	Weight (gm)	Recess (in.)	Explosive: Binding Agent	Weight (gm)	Initial Gas ($2H_2 + O_2$) Pressure (psi)	Measured Proj. Velocity (fps)	Craters on Lead Target	Implosion Distance from Origin (in.) (Figs. 26, 27)	θ	Liner Material
MK II	4	A	5/16	Ti	1	1.73	3/4	foam	144	300	6100	1	0	0°	1/8" lam.alum.
	5	A	5/16	Ti	1	1.73	3/4	foam	94	200	4800	2	0.3	0°	" "
	6	A	5/16	Ti	1	1.73	3/4	foam	122	200	5970	1	0	0°	lam.steel,alum.
	7	A	5/16	Ti	1	1.73	3/4	foam	134	200	5630	1	4	0°	" " "
	8	A	5/16	Ti	1	1.73	3/4	-	-	200	1400	1	0	0°	solid alum.
	9	A	5/16	Ti	1	1.73	3/4	foam	83	200	5880	1	0	0°	lam. alum.
	10	A	5/16	Ti	1	1.73	3/4	foam	80	200	4500	scattered	4	0°	alum.
	25	B	0.216	Lexan	1/3	.06	0.5	foam	109	400		0	0	0°	copper
	27	B	.216	Mg	1/2	.11	0.5	foam	88	400		scattered	0	0°	"
	28	B	.216	Mg	1	.23	0.5	foam	98	400	14500	slight scatt.	0	0°	"
	29	B	.216	Mg	1	.23	0.5	foam	82	400	13000	scattered	0	0°	"
	30	B	.216	Ti+Lex.	½½	.35	0.5	foam	83	400	14000	scattered	0	0°	"
	31	B	.216	Ti+Mg	½½	.40	0.5	foam	102	400	11000	slight scatt.	0	0°	"
	32	B	.216	Ti+Mg	½½	.40	0.5	foam	142	400	10000	2	0	0°	"
	33	C	.216	Ti+Mg	½+½	.45	1.	foam	104	400	8333	1	local deform on edge of liner plate	0°	"
	34	C	.216	Ti+Mg	½½	.40		foam	110			did not detonate		0°	"
	35	C	.216	Ti+Mg	½½	.35	3.	foam	89	400	13300	2 small	0	0°	"
	36	C	.216	Ti	½	.3	1.	cot.lint.	255	400	13800	1	4" perp.to Ign-fill line direction	0°	"
	49	C	.216	Ti	½	0.32	½	" "	89						
	50	C	.216	Ti	½	0.23	1	" "	134	400	17000	scattered	0	10°	"
	51	C	.216	Ti	½	.345	1	" "	131	400		scattered	3/4	10°	"
	52	C	.216	Ti	½	0.25	1	" "	143	400	9400	slight scatt.	3/4	10°	"
	57	C	.216	Ti	½	0.27	1	" "	102	400	12700	1	3/4	10°	"
	58	C	.213	Ti	½	0.27	1	" "	122	400	9300	scattered	1/4 secondary	10°	"
	59	C	.213	Ti	½	0.257	1	" "	129	400	7460	scattered	1/2 "	0°	"
	60	C	.213	Ti	½	0.285	1	" "	105	400	11550	1	1-1/2	0°	"
								max.23% uneven thick cot.lint.		400	10600	1+ scatt.	1/4	10°	"
	61	C	.213	Ti	½	0.285	1	max.50% uneven thick cot.lint.	119.5	400	12000	scattered	1/4	10°	"
	62	C	.213	Ti	½	0.253	2	cot.lint.	73	400	13000	1	0	20°	"
	63	C	.213	Ti	½	0.253	2	" "	125	400	11200	scattered	0	10°	"
	64	C	.213	Ti	½	0.30	3	" "	158	400	12600	1	0	10°	"
MK III	3.2	D	.214	Ti	½	0.28	3	" "	113.1	400	12700	1	1/4 secondary	15°	"
	3.3	D	.214	Ti	½	0.29	3	" "	79.5	400	11980	1	1/4	15°	"
	3.4	D	.214	Ti	½	0.28	3	" "	176.5	400	13200	1	1/4	15°	"
	3.5	D	.214	Ti	½	0.28	3	" "	129	400	13300	1	1/2	15°	"
	3.6	D	.214	Ti	½	.278	3	" " in foam	143	400	13500	1	0	15°	"
	3.7	D	.214	Ti	½	.298	3	cot.lint. in foam	142	400	13400	scattered (but proj. intact from X-ray)	0	15°	"

TABLE 3(a)

CONTAINED RUNS - GAS

Run No.	Loading Gas Pressure psi	Imprint on Copper Witness Plug	Implosion Distance from Origin mm	θ	Remarks
1	200	no		0°	
2	200	no		0°	
3	400	sharp	4	0°	
11	400	sharp	1	0°	chamber pointing up
12	400	sharp	1	0°	" "
13	400	sharp	0	0°	" " fast pumping of gas 3 mins. settling time
14	400	no		0°	chamber pointing up, H_2 in first, 3 min. settling
15	400	no		0°	same as 14, 5 min. settling
16	400	diffuse	1	0°	same as 14, 30 min. settling
17	400	no		0°	same as above, no settling
18	400	sharp	0	0°	chamber launching direction, fast pumping of gas, submerged electrode
19	400	sharp	0	0°	chamber launching direction, fast pumping of gas
20	400		1	0°	same as 19
21	400	whole plug surface non-uniformly deformed		0°	copper witness plug recessed 3/4" from origin
22	400			0°	same as 21
23	400			0°	copper witness plug recessed 1.5 in.
37	400	sharp	0.1	10°	
39	400	no		10°	conical plate has 3" dia. centre hole

Table 3 (a) continued.....

40	400	no		10^{o}	conical plate has 3" dia.centre hole
41	400	no		10^{o}	" " "
42	400	no		10^{o}	" " "
43	400	no		0^{o}	
44	400	sharp		0^{o}	
45	400	no		10^{o}	same conical plate as used in Runs 39-42
46	400	faint	0	10^{o}	same as 45
47	400	sharp	0.5	10^{o}	new design of conical plate, reduce centre hole diameter less abrupt change in surface slope
54	400	sharp	0	10^{o}	done to prove cavity geometry
3.1	400	sharp	0	15^{o}	MK III Launcher

BLE 3(b) CONTAINED RUNS - EXPLOSIVE

Run No.	Explosive		Gas Loading Pressure psi	Imprint on Cu Witness Plug	Implosion Distance from Origin mm	θ	Remarks
	Binding Agent	Weight gm					
24	Plastic Foam	88	400	very symmetrical	0	0°	fast pumping of gas
26	Cotton Linters	103	400	non symmetrical	5	0°	
38	Cotton Linters	122	400	symmetrical	0	10°	
48	Cotton Linters	85	400	not very symmetrical	0	10°	
53	Plastic Foam	79	400	non symmetrical	24	10°	change ignition wire direction
55	Cotton Linters	94	400	1-1/2" long elongated imprint	24	10°	
56	Cotton Linters	94	400	elliptical imprint	6	10°	

TABLE 4. SUMMARIZED RESULTS OF RUNS WITH IMPLOSION WITHIN 1-INCH DIAMETER OF ORIGIN

Run No.	Proj. Recess Distance Lr (in.)	Projectile			Projectile Integrity*	Explosive Weight(gm)	Projectile Velocity (fps)	θ
		Length (in.)	Material	Weight (gm)				
25	0.5	.11	Lexan	.06	D	109		0°
27	0.5	.11	Mg	.11	D	88		0°
28	0.5	.22	Mg	.23	D	98	14500	0°
29	0.5	.22	Mg	.23	D	82	13000	0°
30	0.5	.22	Ti+Lexan	.35	D	85	14000	0°
31	0.5	.22	Ti + Mg	.40	I	102	11000	0°
32	0.5	.22	Ti + Mg	.40	I	142	10000	0°
49	0.5	.11	Ti	.32	D	89	17000	10°
57	1.0	.11	Ti	.27	D	102	9300	10°
58	1.0	.11	Ti	27	D	122	7460	10°
60	1.0	.11	Ti	.285	D	105	10600	10°
61	1.0	.11	Ti	.285	D	120	12000	10°
62	2.0	.11	Ti	.25	I	73	13000	20°
63	2.0	.11	Ti	.25	D	125	11200	10°
35	3.0	.22	Ti + Mg	.35	D	89	13300	0°
64	3.0	.11	Ti	.30	I	158	12600	10°
3.2	3.0	.11	Ti	.28	I	113	12700	15°
3.3	3.0	.11	Ti	.29	I	80	11980	15°
3.4	3.0	.11	Ti	.28	I	176.5	13200	15°
3.5	3.0	.11	Ti	.28	I	129	13300	15°
3.6	3.0	.11	Ti	.278	I	143	13500	15°
3.7	3.0	.11	Ti	.288	I	142	13400	15°

*I = Intact Projectile

D = Disintegrated Projectile

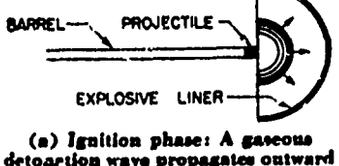

(a) Ignition phase: A gaseous detoartion wave propagates outward from the origin in a $2H_2 + O_2$ mixture

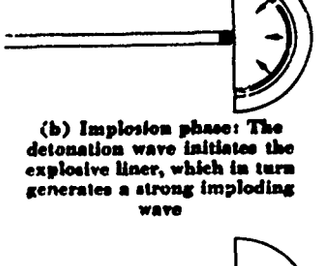

(b) Implosion phase: The detonation wave initiates the explosive liner, which in turn generates a strong imploding wave

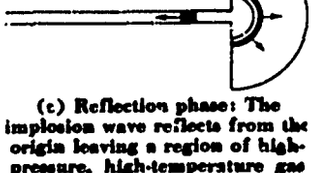

(c) Reflection phase: The implosion wave reflects from the origin leaving a region of high-pressure, high-temperature gas which bursts the diaphragm behind the projectile accelerating it to hypervelocity

Figure 1
Schematic diagram illustrating the principle of operation of the implosion-driven hypervelocity launcher

FIG.2 THE UTIAS IMPLOSION-DRIVEN HYPERVELOCITY LAUNCHER,MK III, IN FIRING POSITION

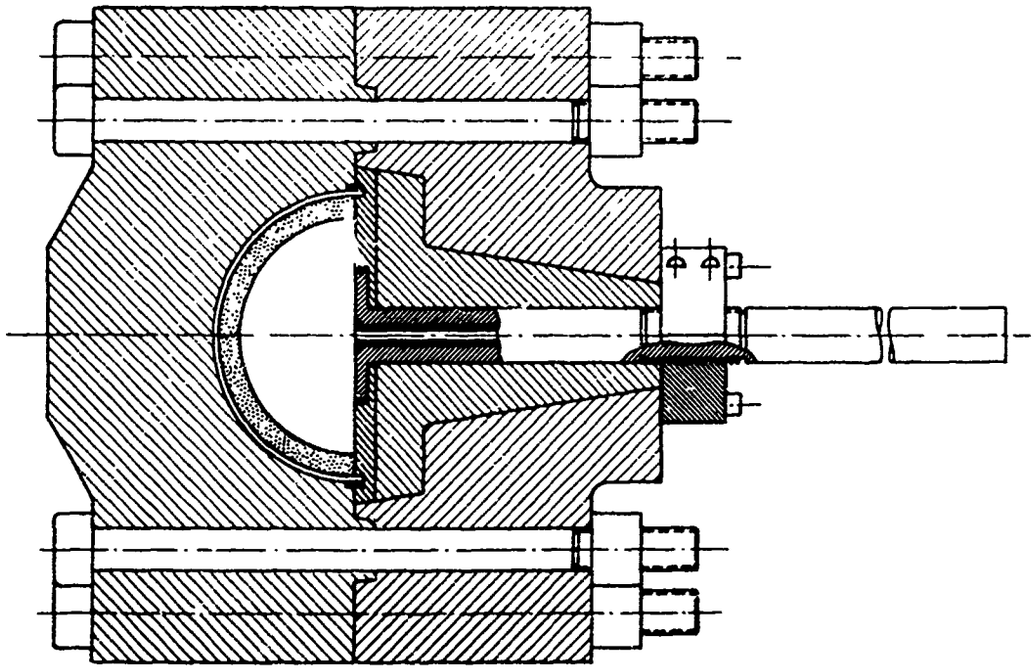

FIG.3 THE UTIAS IMPLOSION-DRIVEN HYPERVELOCITY LAUNCHER,MK II, 24 IN.DIA.OR 8 IN.DIA.CAVITY,1 IN.OR 0.22IN.DIA.BARREL.

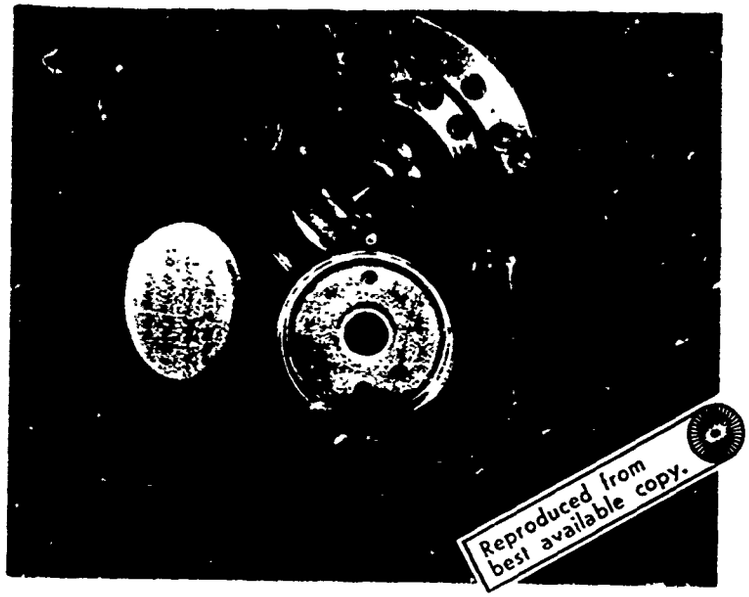

FIG.4 PHOTOGRAPH OF THE TOP HALF OF THE 8 IN.DIA. MK II LAUNCHER IN EXPLODED VIEW.

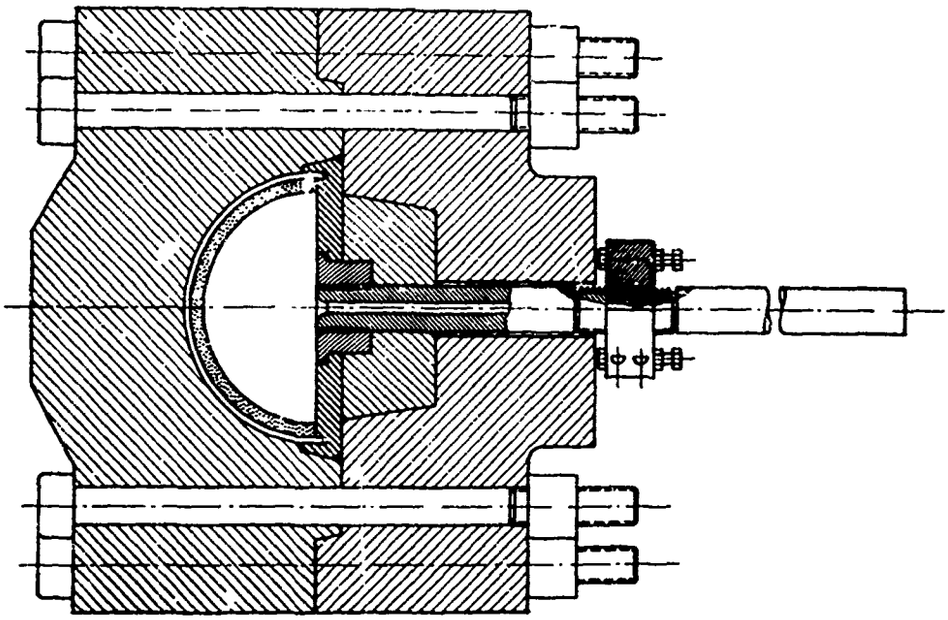

FIG.5 THE CTIAS IMPLOSION-DRIVEN HYPERVELOCITY LAUNCHER, MK III, 24 IN.DIA. OR 8 IN.DIA. CAVITY, 1 IN.DIA. OR 0.22 IN.DIA. BARREL.

FIG. 6. PHOTOGRAPH OF THE TOP HALF OF THE MK III LAUNCHER IN EXPLODED VIEW.

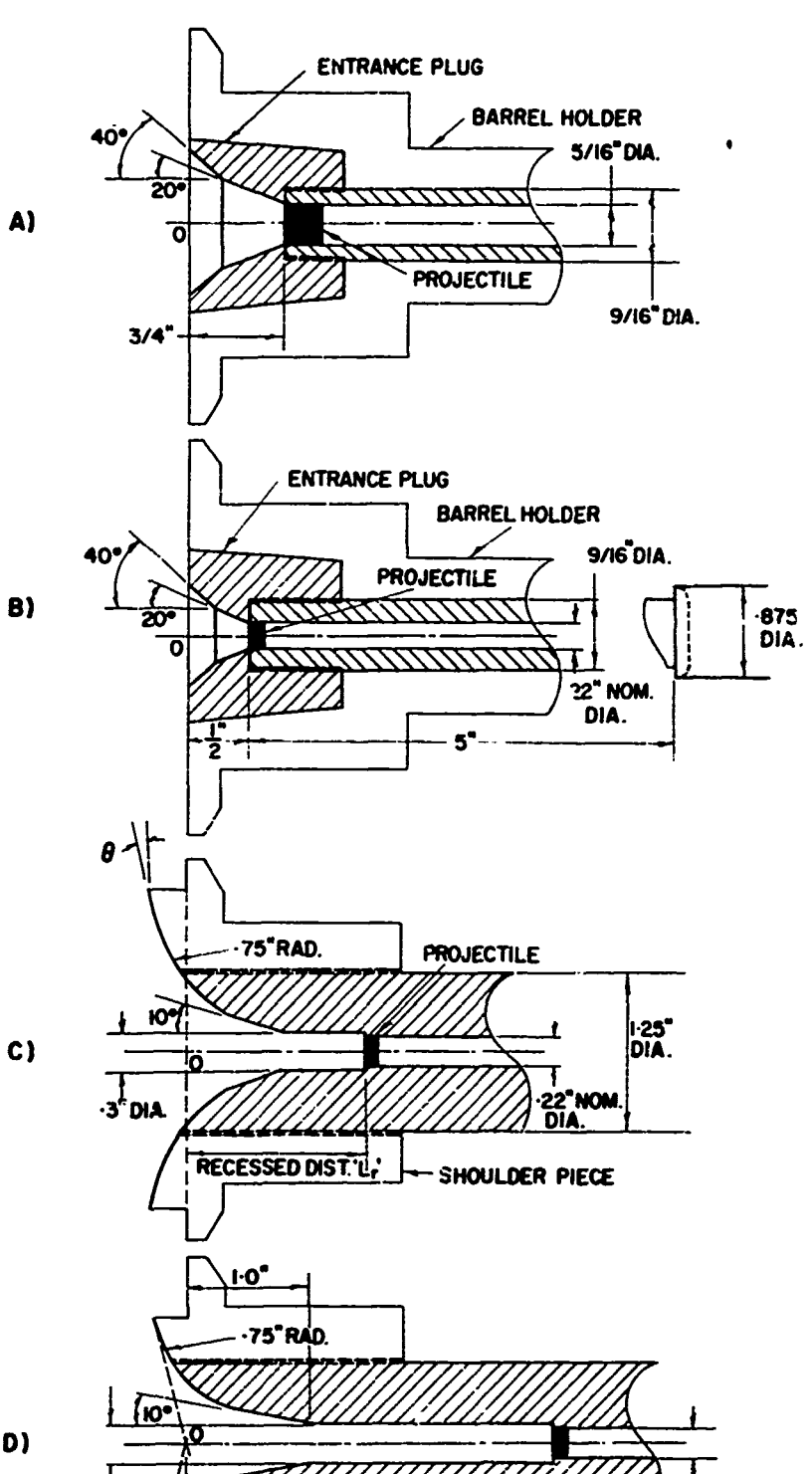

FIG. 7. BARREL ENTRANCE GEOMETRIES.

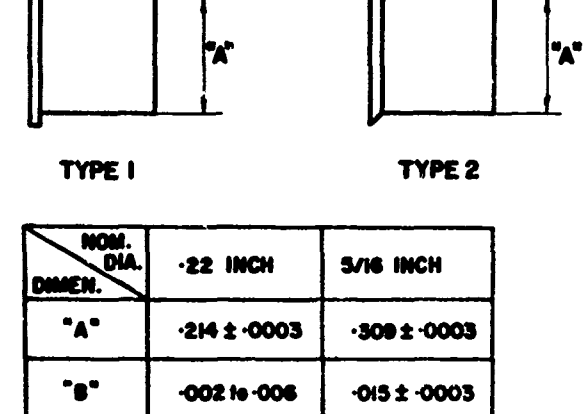

NOM. DIA. / DIMEN.	·22 INCH	5/16 INCH
"A"	·214 ± ·0003	·309 ± ·0003
"B"	·002 to ·006	·015 ± ·0003
"C"	·220 or ·110	·309

FIG. 8. PROJECTILE CONFIGURATIONS.

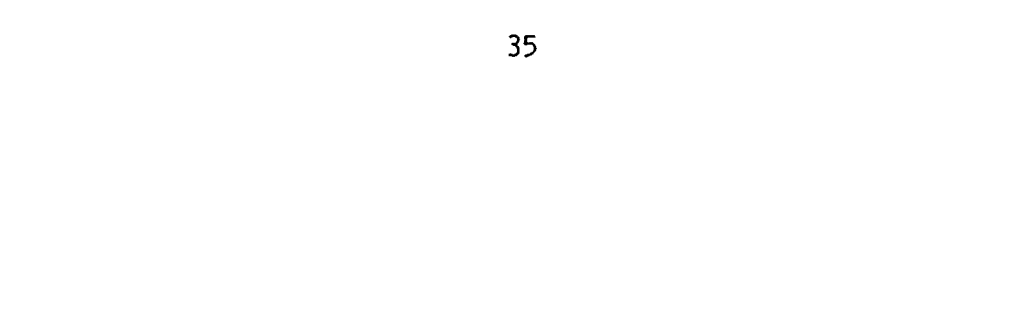

FIG 9. SCHEMATIC DRAWING SHOWING THE RELATIVE POSITIONS OF THE IMPLOSION CHAMBER, BLAST TANK RANGE, OBSERVATION STATIONS AND THE TARGET.

(A)

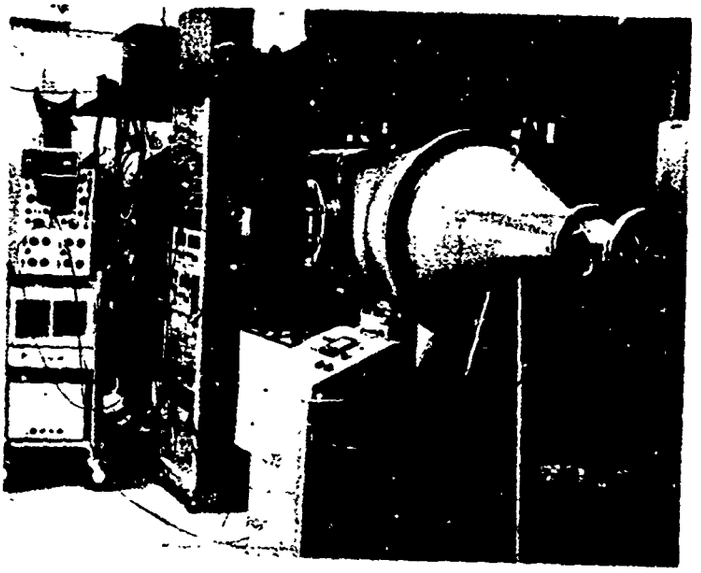

(B)

FIG.13 TWO VIEWS OF THE RANGE AND INSTRUMENTATION

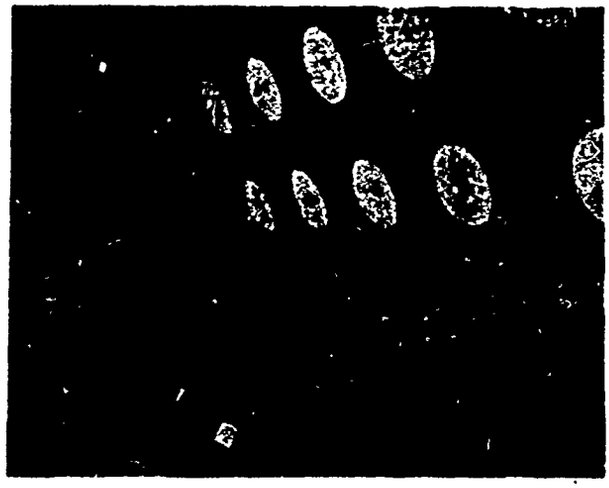

FIG. 11. CONTROL PANEL.

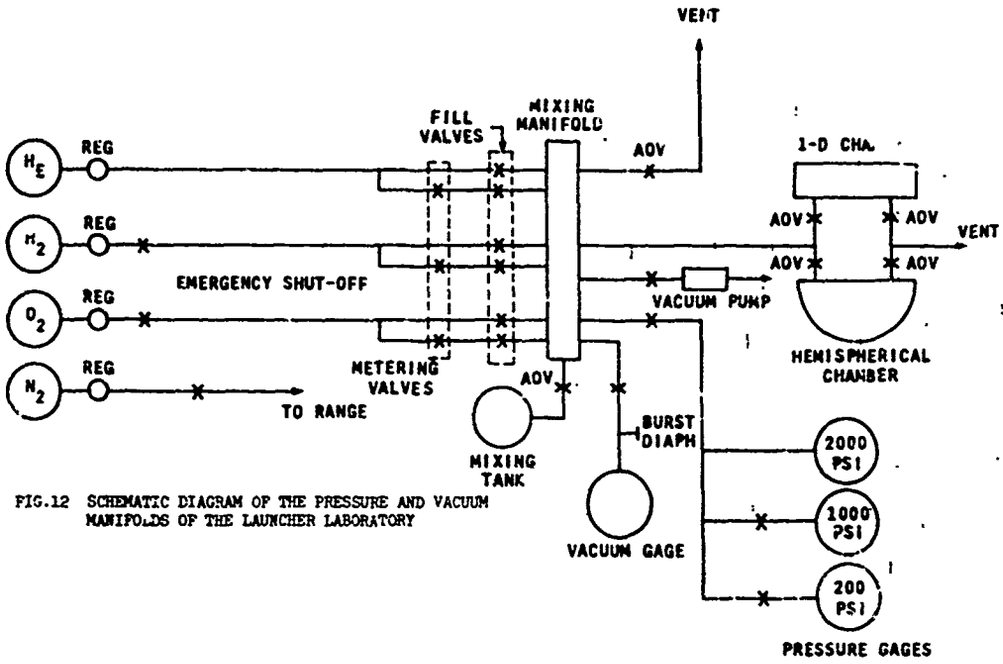

FIG.12 SCHEMATIC DIAGRAM OF THE PRESSURE AND VACUUM MANIFOLDS OF THE LAUNCHER LABORATORY

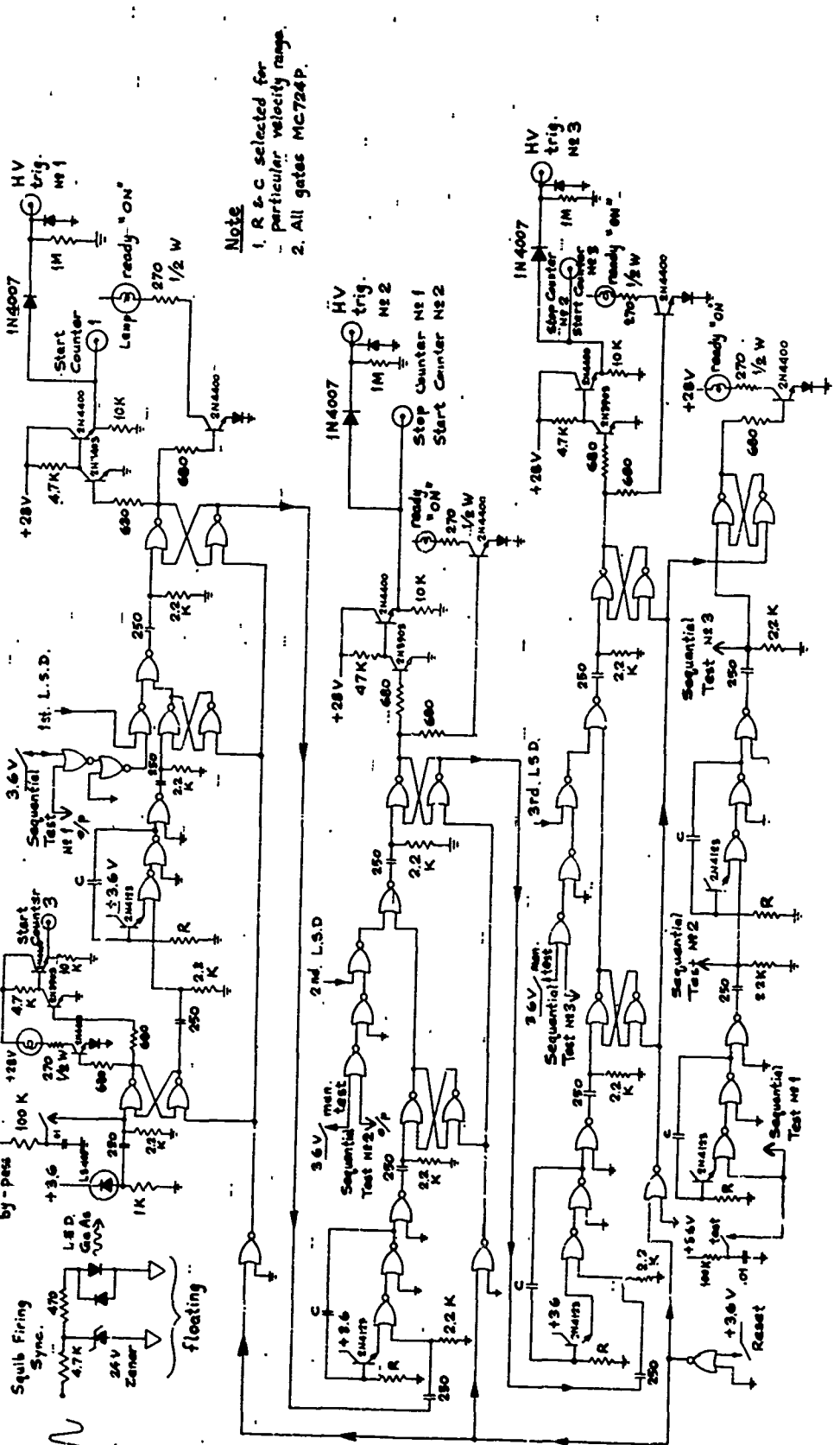

FIG. 13 SEQUENTIAL HOLD-OFF PA[illegible] CIRCUIT DIAGRAM

FIG. 14 SEQUENTIAL PROGRAMMER OUTPUT PULSES AND PROJECTILE IMPACT ACCELEROMETER OUTPUT
TIME SCALE : 200 μS/CM
VOLTAGE SCALE : 1 V/CM

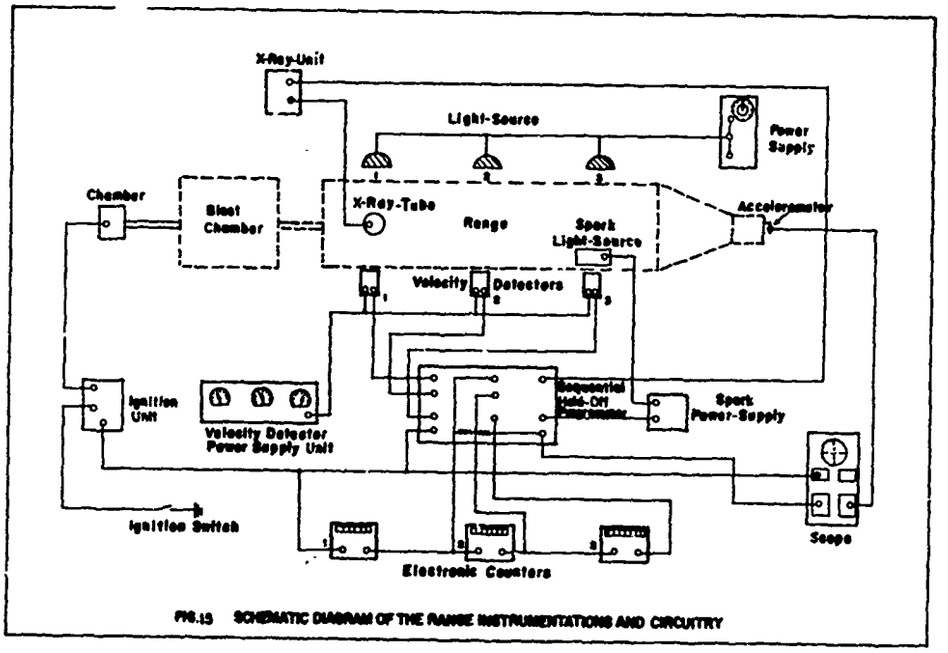

FIG.15 SCHEMATIC DIAGRAM OF THE RANGE INSTRUMENTATIONS AND CIRCUITRY

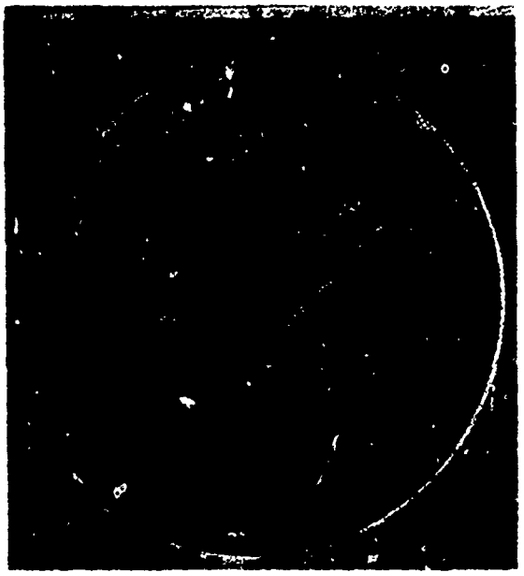

FIG. 16 FULL VIEW OF A MOCK-UP SHOWING THE STEPS TAKEN IN THE MANUFACTURE OF THE EXPLOSIVE LINER PACKAGE
1 COPPER LINER
2 THIN COAT OF CEMENT
3 OPEN CORE FOAM PLASTIC MATRIX
4 PETN SLURRY FORCED INTO PLASTIC MATRIX

FIG. 17 EXPLOSIVE LINER [illegible]

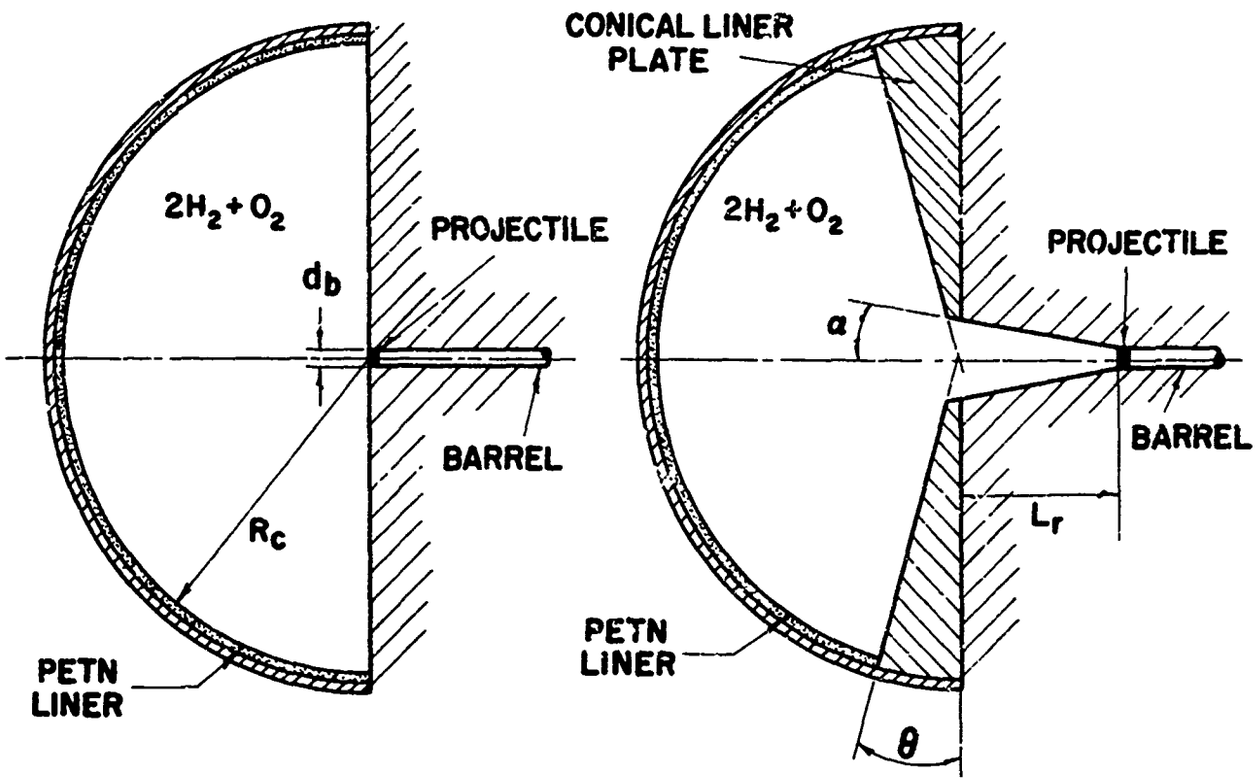

a) HEMISPHERICAL CAVITY

b) HEMISPHERICAL CAVITY WITH THE ADDITION OF A CONICAL LINER PLATE

Figure 18

IMPLOSION CHAMBER GEOMETRIES USED IN THE COMPUTER CODES

The actual geometries were not very different except that smooth flared entrances to the barrel were provided in both cases.

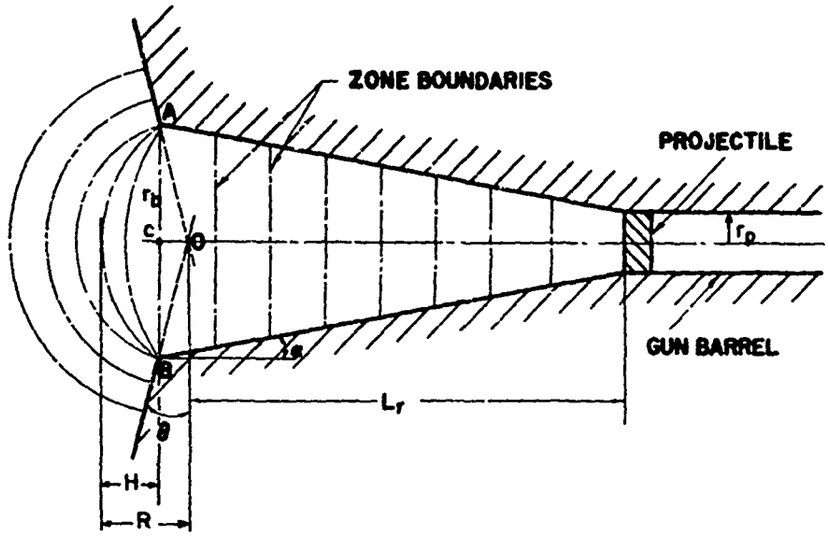

FIG. 19. BARREL ENTRANCE GEOMETRY AND ZONING SCHEME USED IN THE NUMERICAL PROGRAM.

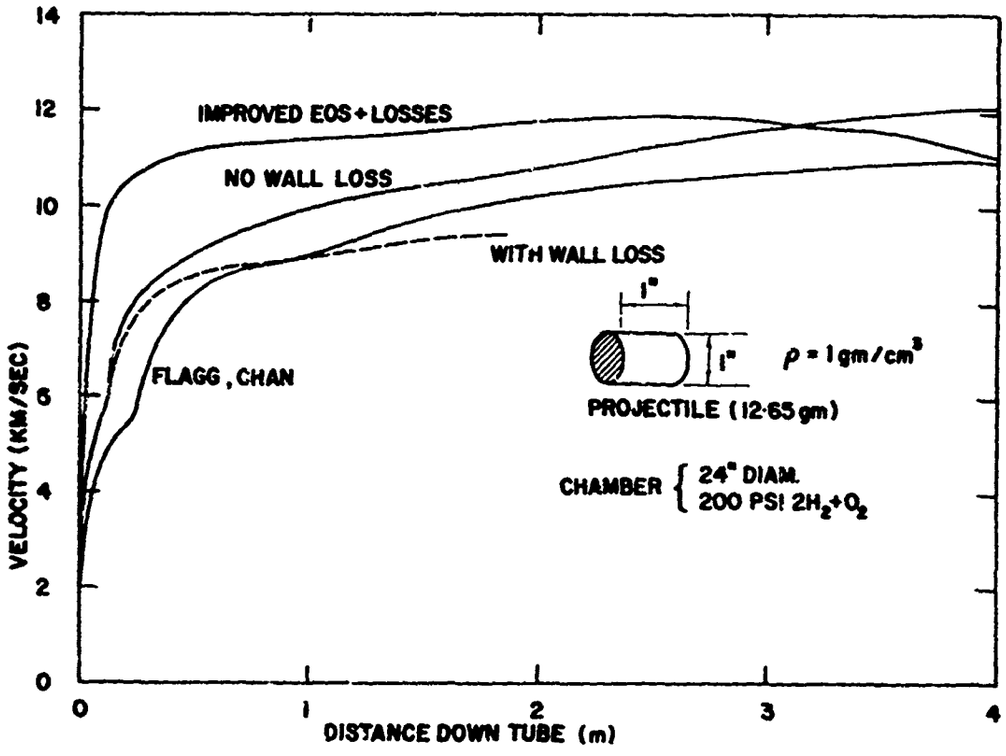

Figure 20

PROJECTILE VELOCITY VS LAUNCHER BARREL LENGTH FROM SEVERAL SOLUTIONS BY BRODE (REF. 39) AND THE PRESENT REPORT

Brode's no wall loss may be compared with Flagg-Chan showing very good agreement between the two independent analyses. Brode's improved equation of state (EOS) losses shows a suprising improvement in performance, despite losses, resulting from increased pressure and density from the eroded barrel constituents.

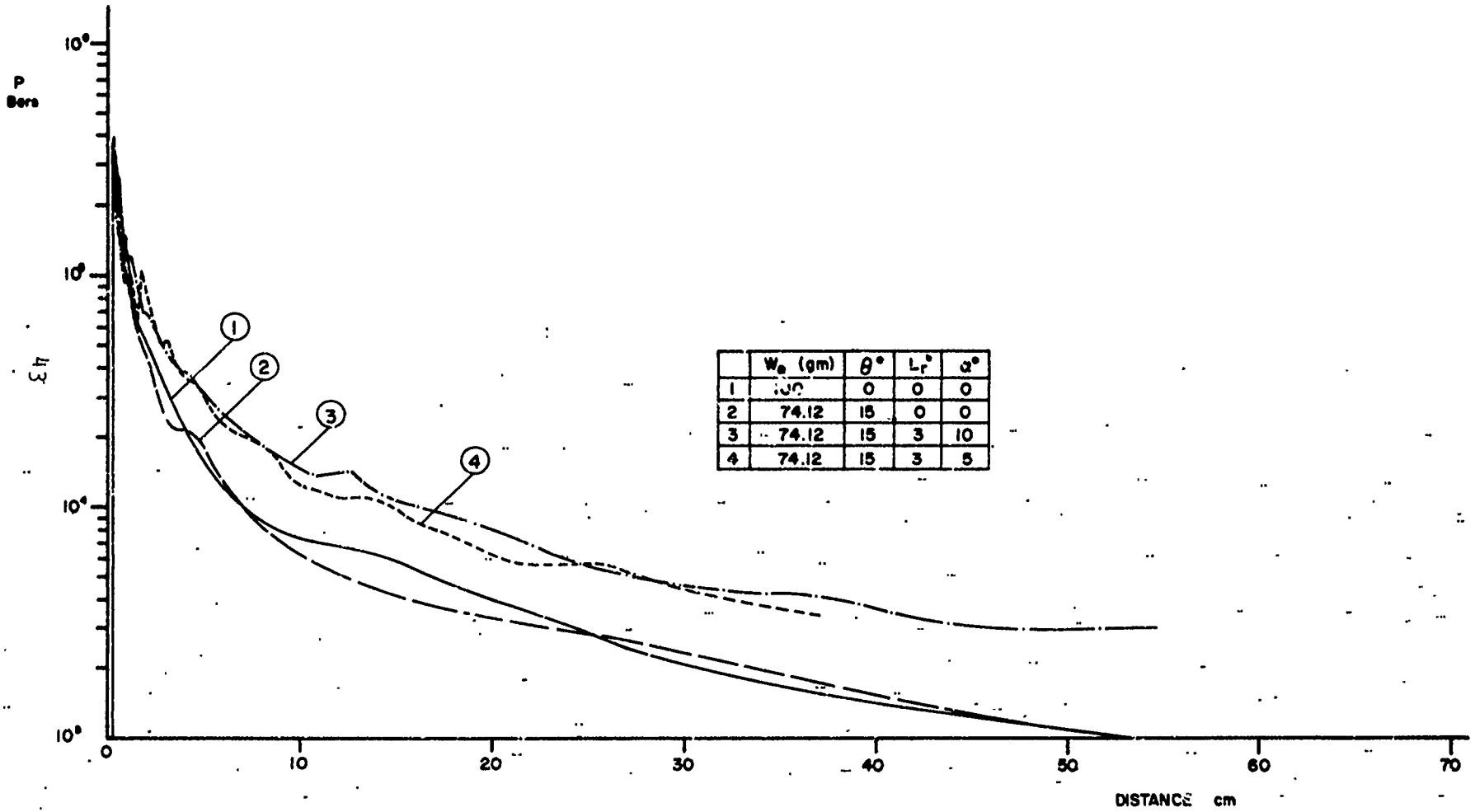

	W_e (gm)	$\theta°$	$L_r°$	$\alpha°$
1	[illegible]	0	0	0
2	74.12	15	0	0
3	74.12	15	3	10
4	74.12	15	3	5

FIG. 21 PROJECTILE BASE PRESSURE VERSUS PROJECTILE TRAVEL DISTANCE 7-7/8 INCHES DIAMETER CHAMBER, 400 PSI $2H_2+O_2$ AND A 0.292 GM PROJECTILE

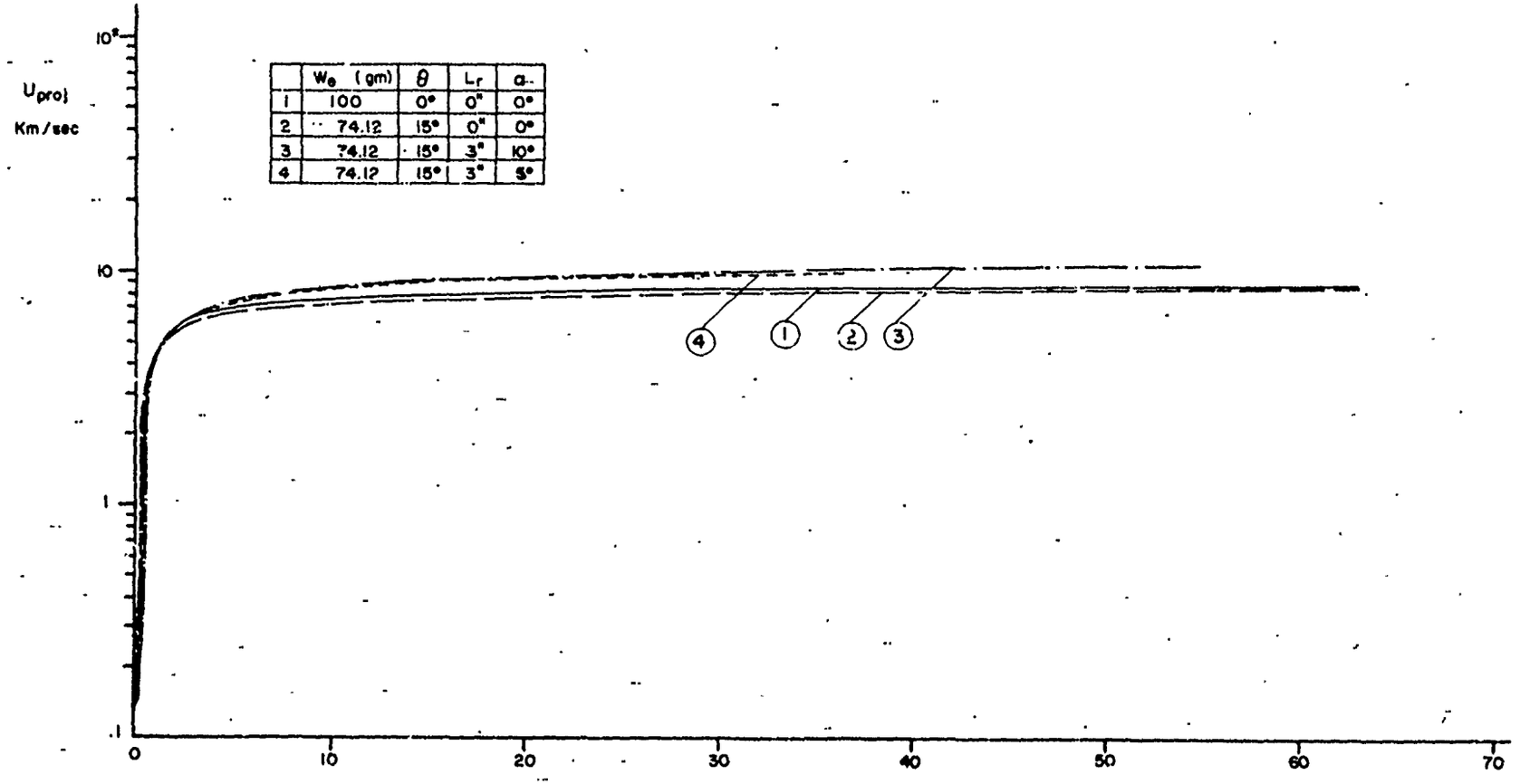

	W_e (gm)	θ	L_r	α
1	100	0°	0"	0°
2	74.12	15°	0"	0°
3	74.12	15°	3"	10°
4	74.12	15°	3"	5°

Figure 22

NUMERICAL SOLUTION OF PROJECTILE VELOCITY VS DISTANCE ALONG THE BARREL OF A TYPICAL EXPERIMENTAL RUN

Driver gas $2H_2 + O_2$, 400 psi initial, half-calibre (0.22 in dia) titanium projectile, 0.29 g, and a 7 7/8 in dia chamber. Various weights of explosives with and without a conical liner, recess, and flare angle are shown in the table. The amount of explosive and geometrical factors have not been optimized for maximum muzzle velocity.

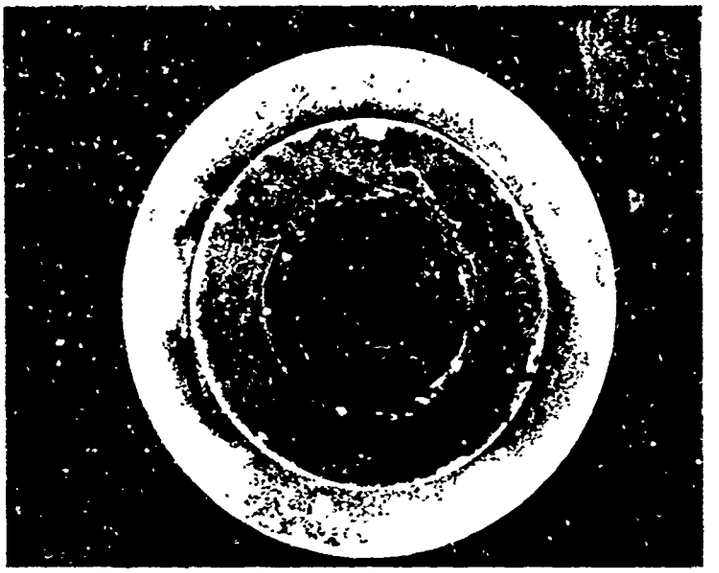

FIG. 23 IMPRINT OF OFF-CENTRE IMPLOSION 1/4 IN. FROM THE ORIGIN (RUN NO.3.4, 176.5 GM PETN WITH COTTON LINTERS, 400 PSI $2H_2+O_2$, WITH 15° CONICAL LINER PLATE, 1/2 CALIBRE, 0.22 INDIA. PROJECTILE IMPACTED 3 IN. FROM THE ORIGIN)

FIG. 24 IMPRINT OF OFF-CENTRE IMPLOSION AT THE RIM OF THE HEMISPHERICAL [illegible] (RUN NO.36, 255 GM PETN WITH COTTON LINTERS, [illegible] PSI $2H_2+O_2$)

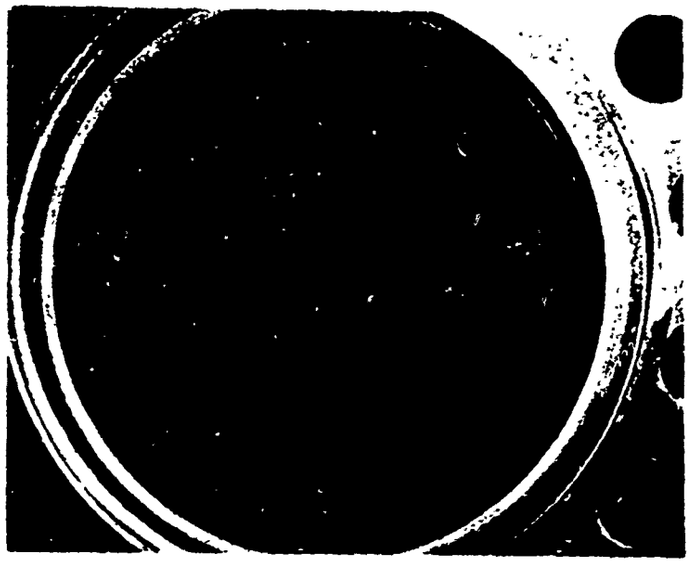

FIG. 25 IMPRINTS OF PRIMARY (p) AND SECONDARY (s) OFF-CENTRE IMPLOSIONS (RUN NO.59 , HEMISPHERICAL CAVITY CONFIGURATION, 129 GM PETN WITH COTTON LINTERS, 400 PSI $2H_2+O_2$, A 1/4 IN. GAP EXISTED BETWEEN THE EXPLOSIVE LINER EDGE AND THE INNER PLATE)

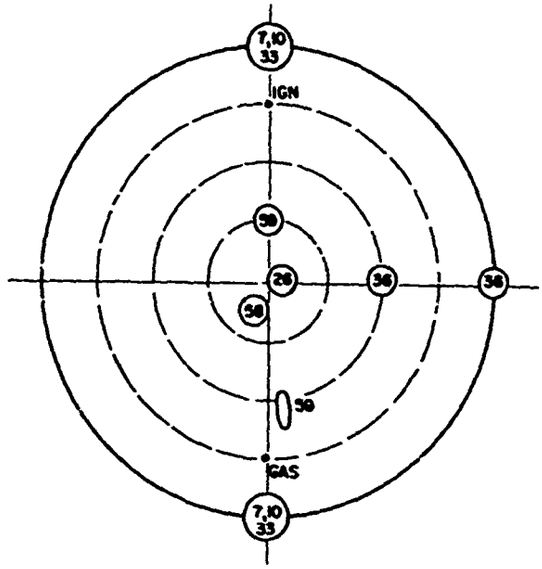

IGN-IGNITION ELECTRODE INLET
GAS-GAS INLET PORT

FIG.26 SCHEMATIC DIAGRAM SHOWING THE POSITIONS OF THE OFF-CENTRE IMPLOSIONS (IMPLOSION CHAMBER WITH HEMISPHERICAL CONFIGURATION)

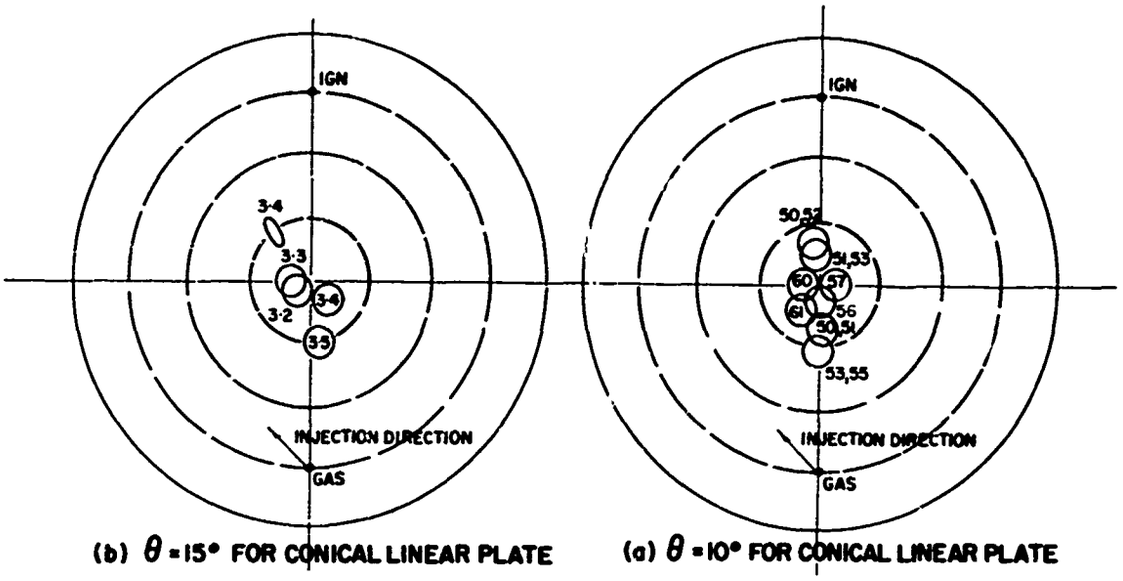

FIG. 27 SCHEMATIC DIAGRAM SHOWING THE POSITIONS OF THE OFF-CENTRE IMPLOSIONS (IMPLOSION CHAMBER WITH (a) 10° CONICAL LINER PLATE AND (b) 15° CONICAL LINER PLATE)

FIG. 28 IMPLOSION IMPRINTS ON COPPER WITNESS PLUGS FROM CONTAINED GAS AND EXPLOSIVE RUNS WITH 400 PSI $2H_2+O_2$

RUN NO.	EXPL.WEIGHT GM	CON.LIN.PL.ANGLE θ
13	0	0°
3.1	0	15°
24	88(FOAM)	0°
26	103(COT.LINT.)	0°
56	94(COT.LINT.)	10°

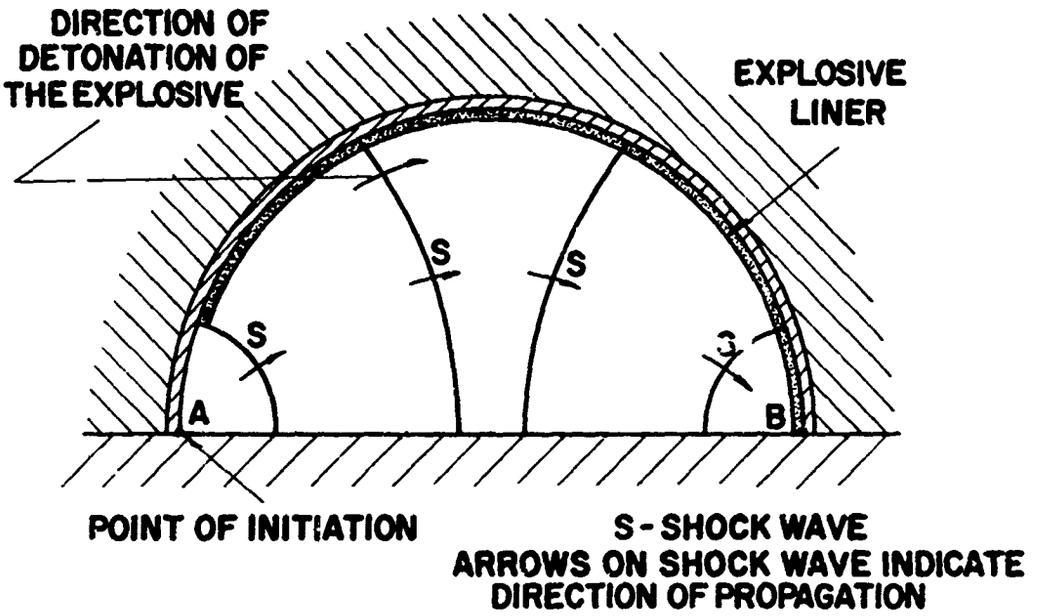

(a) HEMISPHERICAL CONFIGURATION

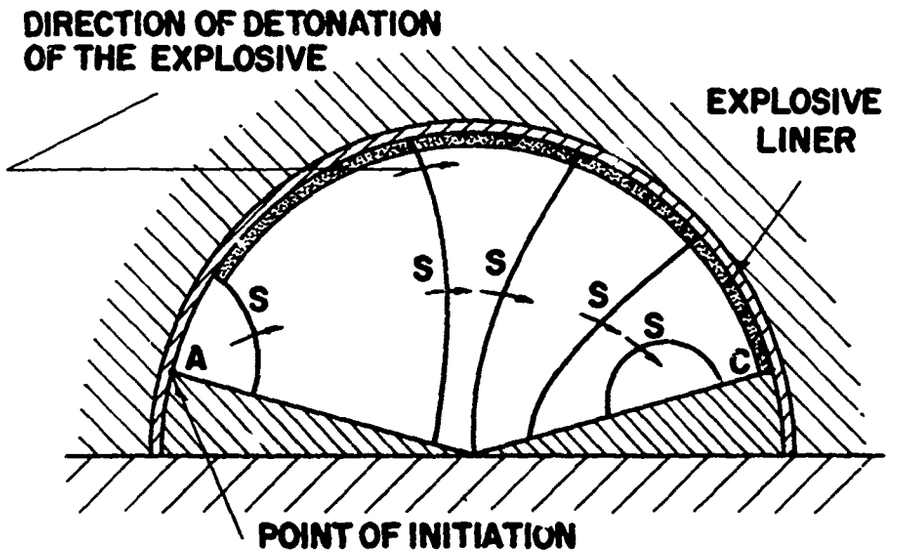

(b) CAVITY WITH THE ADDITION OF CONICAL LINER PLATE

FIG. 29 SCHEMATIC OF THE POSTULATED IMPLOSION WAVE PATTERN DUE TO SIDE INITIATION OF THE EXPLOSIVE LINER

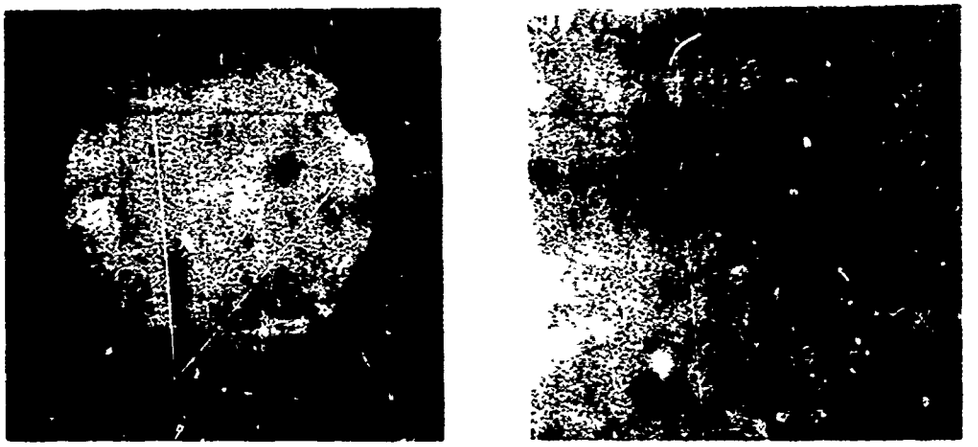

FIG. 30 SHADOWGRAPH (LEFT) AND X-RAY (RIGHT) PHOTOGRAPHS OF THE 0.22 IN.DIA. HALF CALIBRE TITANIUM PROJECTILE IN FLIGHT TRAVELLING FROM LEFT TO RIGHT (PROJECTILE VELOCITY = 13,200 FT./SEC.)

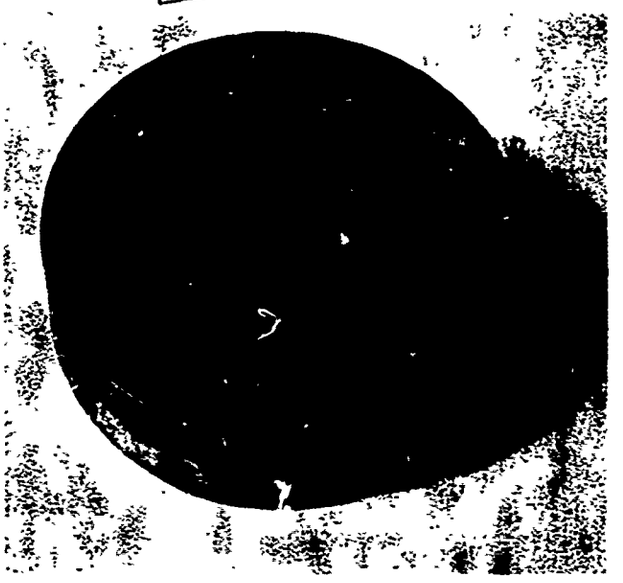

FIG. 31 CRATER FORMED BY A 0.20 GM 0.22 IN.DIA. HALF CALIBRE TITANIUM PROJECTILE AT VELOCITY OF 13,200 FPS ON A 6 IN.DIA. LEAD TARGET

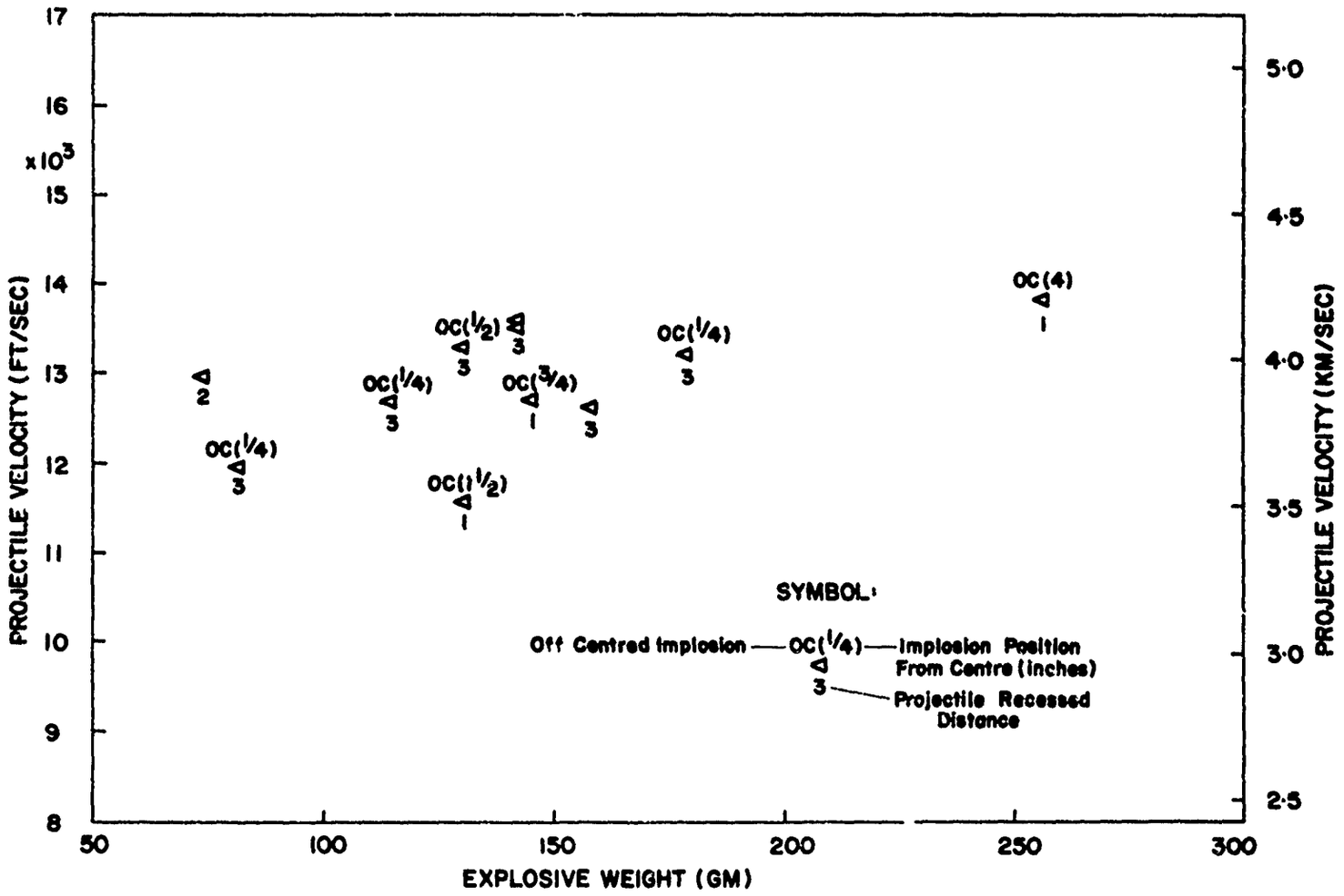

FIG. 32 IMPACT PROJECTILE VELOCITY VERSUS EXPLOSIVE WEIGHT (FROM MK II AND MK III LAUNCHERS, 1/2 CALIBRE, 0.22 IN.DIA. TITANIUM PROJECTILE WEIGHING APPROX. 0.28 GM, 40 PSI $2H_2+O_2$)

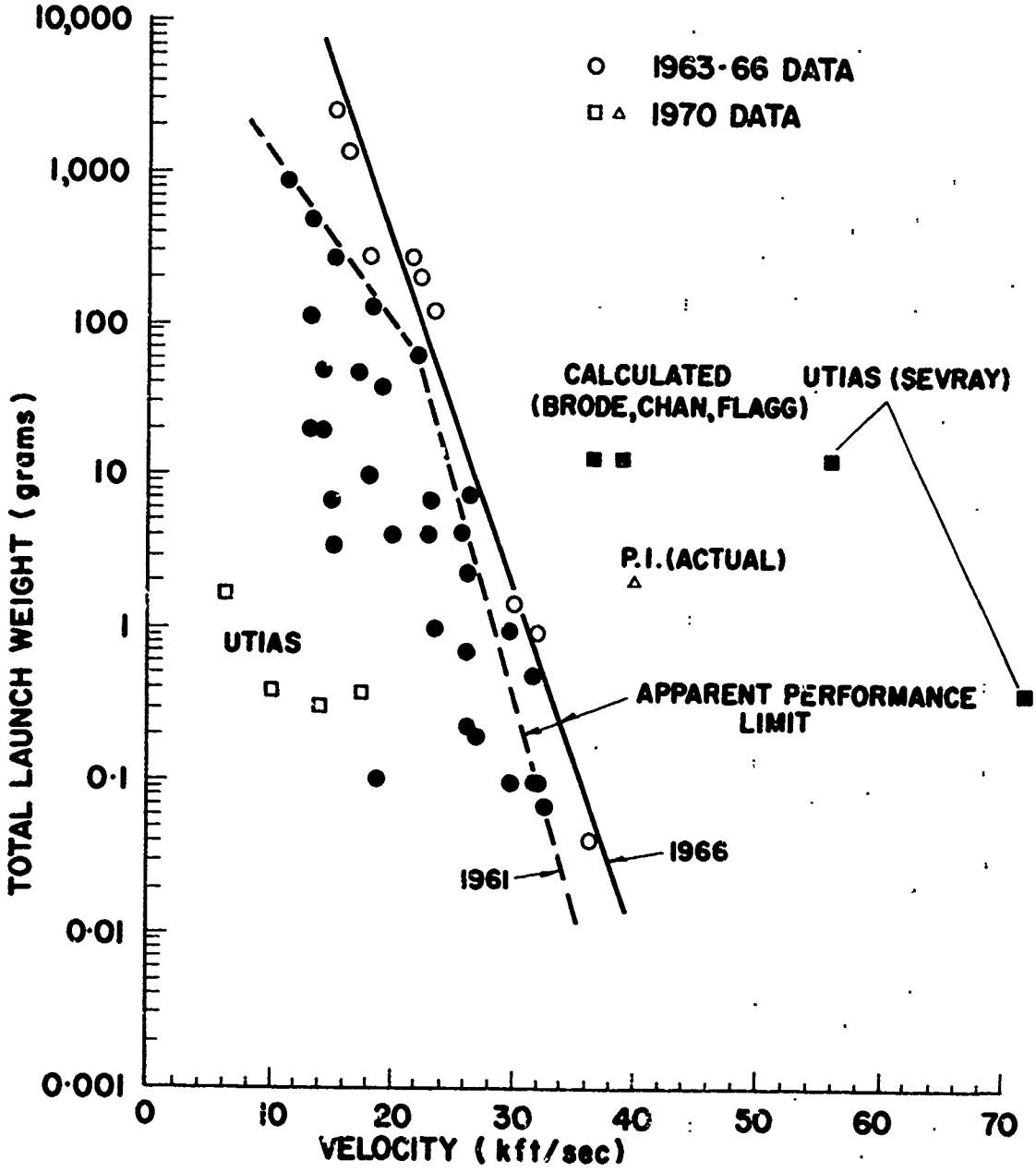

Figure 33

ACTUAL AND CALCULATED PROJECTILE MUZZLE VELOCITY VS PROJECTILE WEIGHT (AFTER REFS. 47, 48) WITH ADDED RESULTS FROM UTIAS (REF. 8 AND THE PRESENT REPORT) AND PHYSICS INTERNATIONAL (REF. 49) AND CALCULATED PERFORMANCE FROM UTIAS (REFS. 21, 23 AND THE PRESENT REPORT)

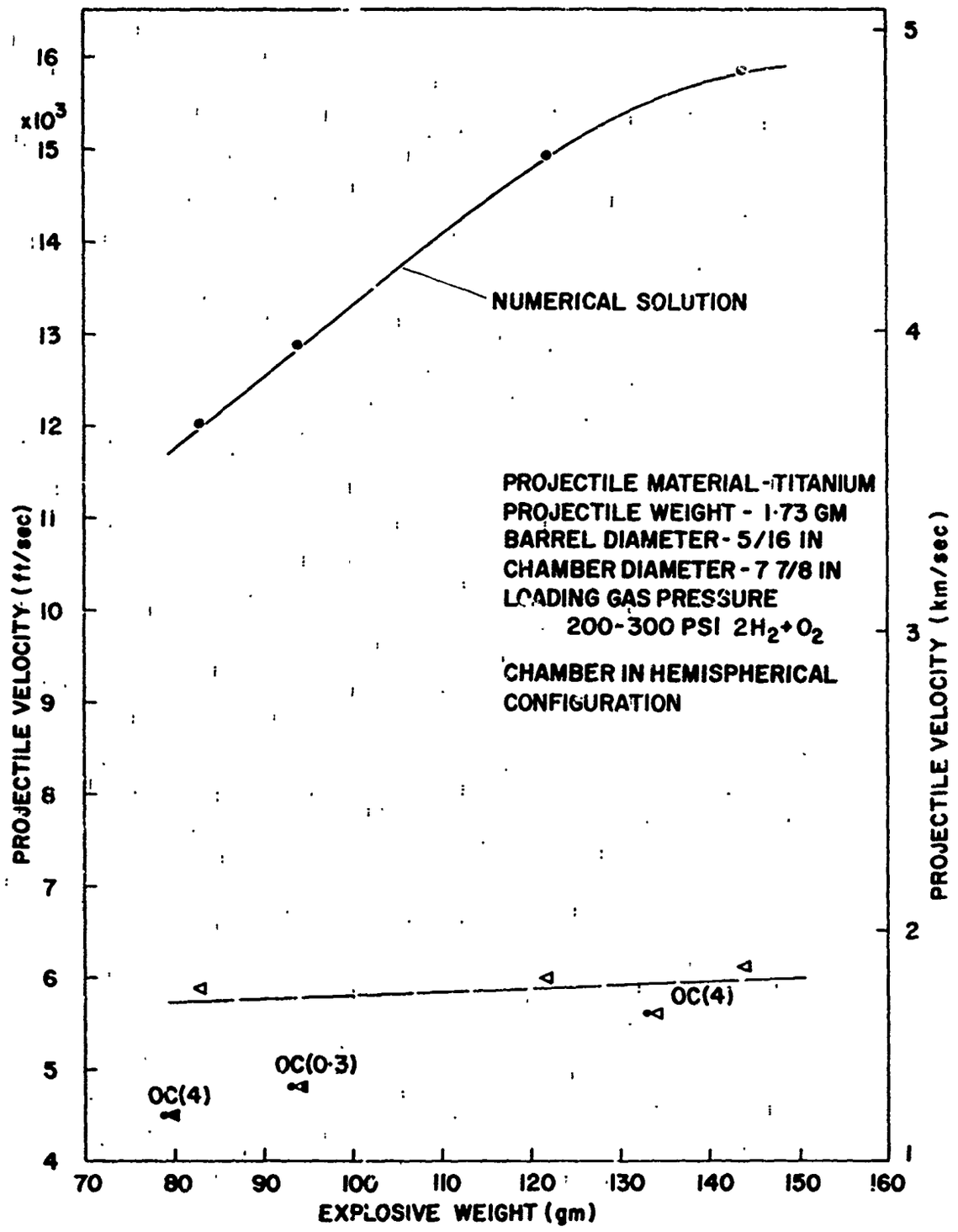

FIG. 34 THEORETICAL AND EXPERIMENTAL PROJECTILE VELOCITY VERSUS EXPLOSIVE WEIGHT FOR A SINGLE-CALIBRE TITANIUM PROJECTILE (OPEN SYMBOLS INDICATE INTACT PROJECTILES, FILLED SYMBOLS INDICATE DISINTEGRATED PROJECTILES, OC--OFF-CENTRE IMPLOSION, FIGURE INSIDE BRACKETS ABOVE THE SYMBOL INDICATES THE OFF-CENTRE IMPLOSION DISTANCE FROM THE ORIGIN)

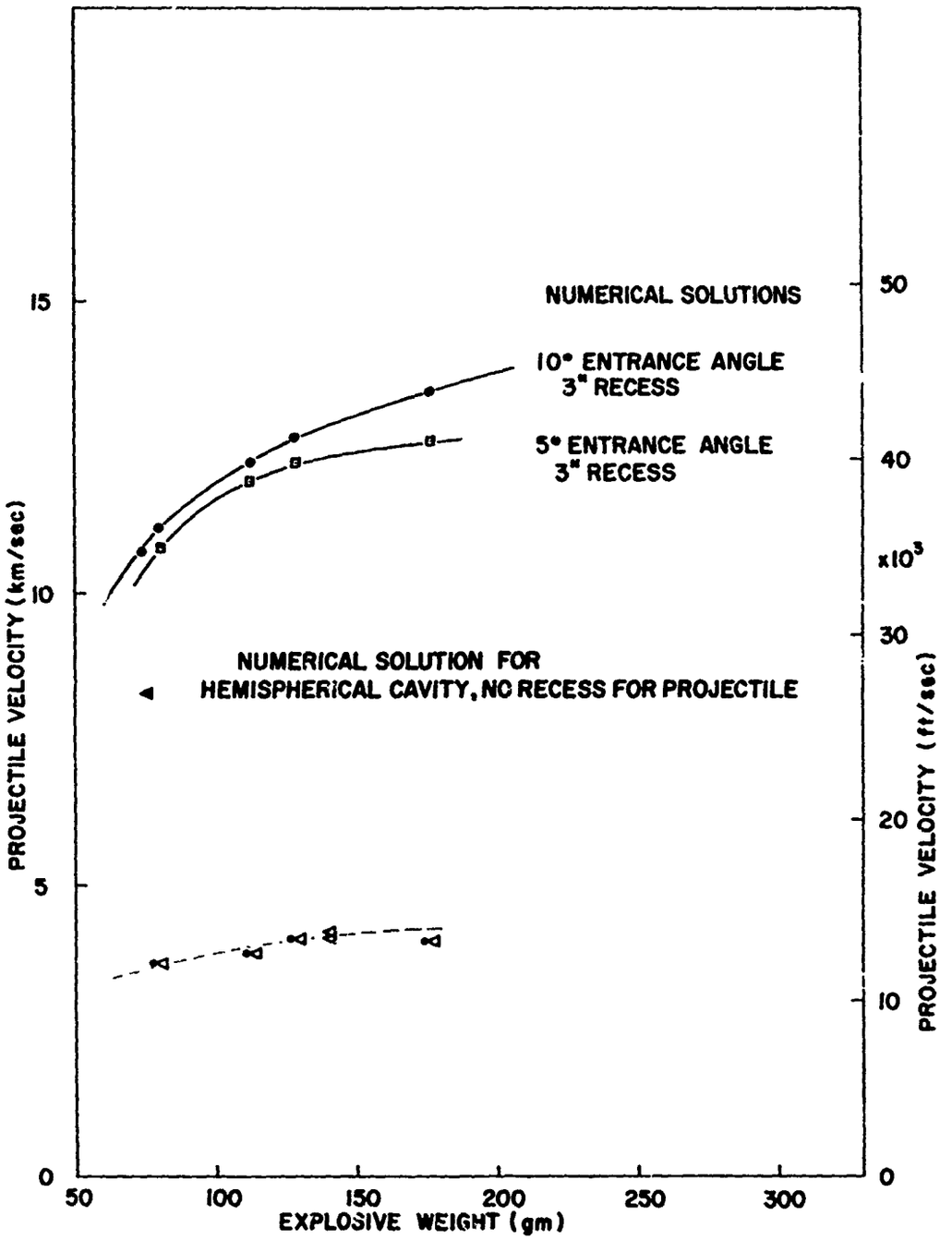

FIG. 35

...ON OF NUMERICAL AND EXPERIMENTAL PERFORMANCE OF THE MARK III LAUNCHER OF PROJECTILE VELOCITY VS PETN WEIGHT

...$2H_2+O_2$, 400 psi initial; half-calibre (0.22 in dia) titanium projectile, 0.29 g; upper ... points are numerical results, lower discrete points are for focused implosions (open triangle) and off-focus runs (attached circle). The amount of explosive is by no means an optimum nor that of the recess or entrance angle for the 15-degree protector plate-optimum calculated values yield about 50,000 ft/sec.

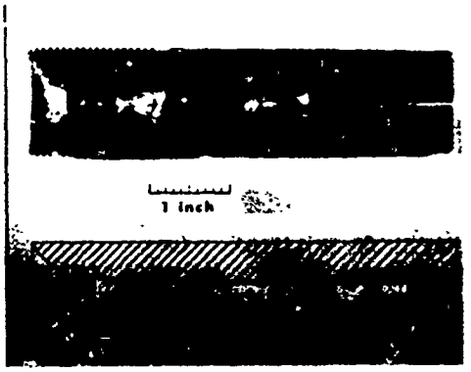

A SECTIONAL VIEW OF THE FIRST 5 1/4-INCHES OF THE LAUNCHER BARREL

Upper: Barrel after a run using 400 psi $2H_2 + O_2$ and 143 g PETN and a titanium projectile, half calibre (0.22 in dia), 0.28 g. Note that 45 g of barrel material was eroded during the run-about 160-fold the mass of the projectile.

Lower: Sketch of the original geometry of the barrel. The step in the bore is where the projectile flared base is seated.

FIG. 36

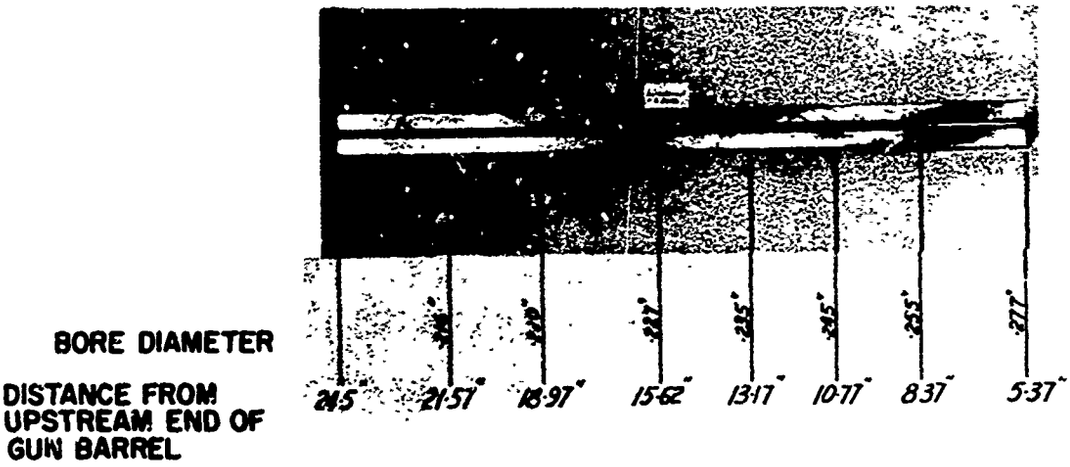

FIG. 37 SECTIONED VIEW OF AND THE MEASUREMENTS OF THE BORE DIAMETER ALONG THE GUN BARREL AFTER A RUN WITH 143 GM PETN, 400 PSI $2H_2+O_2$ AND A 0.28 GM HALF CALIBRE TITANIUM PROJECTILE

APPENDIX A: THE INVESTIGATION OF A TECHNIQUE OF INITIATING THE PETN LINER BY A LIGHT-SENSITIVE EXPLOSIVE (by G. Cappelli)

Simultaneous initiation of the entire explosive surface is one of the most important factors in the successful operation of the UTIAS Implosion-Driven Hypervelocity Launcher. The use of a light-sensitive explosive seems to be very attractive in this respect. In addition, by using a light-initiation technique, it is also possible to utilize a cold, light driver gas, rather than the heavier stoichiometric oxygen-hydrogen mixture, which is necessary for the present way of initiating the explosive liner (see Chapter 1). Because of these advantages, an investigation into the initiation of the light-sensitive explosive technique was carried out and is reported in the following.

In this work a primary light-sensitive explosive was used. This primary explosive is sprayed on or mixed with PETN. The experiment was conducted using the one-dimensional, cylindrical chamber (see Fig. A1). The distance between the explosive and the exploding wire is equal to the radius of the hemispherical implosion chamber (approx 4"). The exploding wire used was a 0.005 in. diameter silver rather than a copper wire. A voltage of 6 KV was applied and the wire was vaporized giving a strong flash of light in the blue region, which was conducive to initiation.

A.1 Silver Acetylide - Silver Nitrate as a Light-Sensitive Explosive

The light-sensitive explosive silver acetylide-silver nitrate ($Ag_2C_2.AgNO_3$) is a complex salt. It can be prepared by bubbling a stream of acetylene through a neutral solution of silver nitrate ($AgNO_3$). It can also be prepared in a non-neutral solution (ammonia solution, nitric acid soluation, etc.,) obtaining a product with slightly different properties. The most probable chemical reaction in the formation of $Ag_2C_2.AgNO_3$ is:

$$3\ AgNO_3 + C_2H_2 \rightarrow Ag_2C_2AgNO_3 + 2HNO_3$$

with the formation of nitric acid after the reaction.

Not much information is available from the literature on the dependence of the light-sensitivity of the salt on the way of preparation. It was found that the following factors have to be taken into account:

(1) The $Ag_2C_2.AgNO_3$ being a light-sensitive salt is decomposed by light. Experimental data show that high-frequency light (blue, violet or ultraviolet) is responsible for fast decomposition of the salt. On the other hand, low-frequency light (red) decomposes the salt very slowly. As a consequence, the salt has to be prepared in darkness or under red light to have a product which is not desensitized.

(2) The concentration of the salt in the solution is important. For instance, with a concentration greater than 25% we will obtain $Ag_2C_2.6AgNO_3$ instead of $Ag_2C_2.AgNO_3$; the $Ag_2C_2.6AgNO_3$ has slightly different properties. Also using a 5% neutral solution the final product appeared yellowish, while using a 10% neutral solution the final product was white.

(3) The way of washing the final product and the time waited before

washing can be also important. The way the $Ag_2C_2.AgNO_3$ was washed will be described later.

The safety problem is very important when handling this kind of explosive. The dry product ignites at a temperature slightly over 200°C (this temperature also depends on the method of preparation). To get an idea of the sensitivity of the explosive, the dry product was ignited by striking it with a small hammer. A small amount of dry salt was also put on a paper and, setting the paper on fire, the salt went off when the flame was more than two inches away from the salt.

On the other hand, when the $Ag_2C_2.AgNO_3$ is in the wet state, it is, in our opinion, quite safe. We tried to ignite the wet salt by hammering it and placing it on matches which were lit at their neutral end. In no case did we have ignition. This fact also suggests that to obtain good results with the light initiation the salt has to be very dry.

Being aware of the safety hazards, it was decided to try to ignite PETN by $Ag_2C_2.AgNO_3$ using different procedures, starting with what seemed to be the safest.

A.2 PETN Initiation by Light-Sensitive Explosive: First Attempt

The safest way of preparing light sensitive explosive ($Ag_2C_2.AgNO_3$) mixing it with PETN and drying it, is to carry out the whole process in a blast-proof chamber (in the present case in the one-dimensional chamber).

The first attempt was to mix $AgNO_3$ solution with PETN, press cut some liquid from this mixture in order to have the right consistency, put the wet mixture in the container (cup of the one-dimensional chamber) and put it in the chamber. After this, acetylene was injected in the chamber at a given pressure. It was hoped that the $AgNO_3$ ions had enough mobility to react with acetylene (at least in the vicinity of the contact surface between the gas and the PETN mixture) giving $Ag_2C_2.AgNO_3$ or $Ag_2C_2.6AgNO_3$.

The method has some good points:

(1) It is perfectly safe because we are handling wet PETN and a silver nitrate solution. The $Ag_2C_2.AgNO_3$ is only formed when the chamber is closed.

(2) Because $Ag_2C_2.AgNO_3$ is formed inside the chamber, that is in complete darkness, it is not desensitized by any light.

The initial experimental apparatus is shown schematically in Fig. A2. In this case the acetylene in the chamber is at a pressure equal to atmospheric pressure plus or minus the pressure corresponding to the height h of the water. An attempt was made to measure the volume of acetylene absorbed.

The procedure was as follows:

(1) Closing valve A, the system was evacuated to a pressure corresponding to the equilibrium between the speed of the pump and the speed of

evolution of water in the burette. The intent was to remove most of the air from the system trying to avoid any possibility of explosion with the air-acetylene mixture. The equilibrium pressure was about 15 mm Hg.

(2) Opening valve C, acetylene was injected into the system at about 1 atm pressure.

(3) Opening valve A, atmospheric pressure was applied to the acetylene in the burette. The starting situation was with a height h equal to zero (the reservoir was moved to obtain this value) and readings of water level in the burette, atmospheric pressure, and room temperature were noted.

(4) For each experiment a certain period of time was allowed to elapse and then the reservoir was raised in order to adjust the initial pressure. The reading of the water level in the burette was noted. The difference between this and the previous reading of the graduation gave the volume absorbed in that particular time. Knowing the pressure and temperature the mass of acetylene absorbed was determined approximately.

(5) Closing valve B, we again evacuated the system in order to dry the PETN - $Ag_2C_2.AgNO_3$ mixture. The indication that the mixture was dry came from closing the vacuum pump from the remaining system and the pressure read on the vacuum gauge remained constant.

(6) After drying, gas was injected into the chamber (driver gas) and attempts were made to ignite the PETN - $Ag_2C_2.AgNO_3$ mixture with light generated by an exploding wire.

It was not possible to ignite the mixture with light. Only in a few cases, after exploding the wire, did the surface of the mixture turn partially gray (this is an indication that some reaction started).

Attempts were made to put acetylene at higher pressure in the chamber (up to 5 atm) in order to have a greater absorption of acetylene. In no case was there ignition of the PETN - $Ag_2C_2.AgNO_3$ mixture.

In some cases formation of $Ag_2C_2.AgNO_3$ was observed. However, owing to the increase in volume when going from $AgNO_3$ to $Ag_2C_2.AgNO_3$, the surface of the explosive which was smooth at the beginning, became quite uneven.

It should be mentioned that the exploding wire was not the only light source which was tried. Different kinds of flash bulbs were tried in order to have more light going into the light-sensitive explosive. In no case was there ignition of the explosive with the preceeding method of preparation.

It was decided to try another method less safe than the previous one, but in our opinion safe enough to be handled and perhaps safe enough to be used in the hypervelocity launcher.

A.3 PETN Initiation by Light Sensitive Explosive: Second Attempt

In the first attempt an effort was made to prepare $Ag_2C_2.AgNO_3$ from a silver nitrate solution mixed with PETN when the mixture was enclosed in the chamber. In that case it was not possible to determine the percentage of $Ag_2C_2.AgNO_3$ formed or if it had formed at all.

In the second attempt, $Ag_2C_2.AgNO_3$ was prepared with a separate procedure and after it was formed, it was mixed with PETN or PETN was coated with it. In this regard, the easiest way of loading the explosive would be to mix $Ag_2C_2.AgNO_3$ with PETN. On the other hand, loading and compressing the PETN - $Ag_2C_2.AgNO_3$ mixture is not very safe, even if they are wet. It was therefore preferred to have first the PETN layer put down and compressed and then a coat of $Ag_2C_2.AgNO_3$ applied on top of it.

For the preparation of $Ag_2C_2.AgNO_3$ we proceeded as follows:

(1) First we tried to avoid any light from getting inside the container in which the $Ag_2C_2.AgNO_3$ was prepared. So the container, a glass jar, was coated with two layers of sprayed varnish. The first layer (sprayed on the outside) was black; the second layer, sprayed over the first one, was white. In this way any light coming from outside was reflected by the white surface and light going inside was absorbed by the black surface.

(2) After some attempts it was decided to use an $AgNO_3$-water solution with a concentration of 10% of $AgNO_3$. The solution was put in the jar and the jar was closed; the cover of the jar had two small pipes through it in order to bubble acetylene through the solution.

(3) The acetylene was bubbled through for about ten minutes, then allowed to stand ten minutes more before opening the jar. The jar was opened in darkness to wash the precipitate

(4) Under red light the precipitate was poured on a filter and washed three times with water, stirring every time. In this way most of the nitric acid, formed during the chemical reaction, was washed away.

(5) The $Ag_2C_2.AgNO_3$ was stored in a jar similar to the one used for the preparation.

The second phase was to load the PETN and Ag_2C_2 $AgNO_3$ in the cups used in the one-dimensional chamber. One of these cups is shown in Fig. A4. A disk of open core plastic foam is glued to the bottom of the cup to hold the explosive and PETN is squeezed into this. To press the explosive a steel cylinder was used. The problem was that, after compression, the explosive was sticking to the cylinder and some patches of explosive were torn off. To solve this problem, a thin plastic foil was put between the explosive and the cylinder. After compression the cylinder came off very easily and the plastic was peeled off with no damage to the explosive surface

Over the moist PETN we put a layer of $Ag_2C_2.AgNO_3$. Operating in red light the two different procedures described below were followed:

(a) Some wet $Ag_2C_2.AgNO_3$ was put approximately evenly over the PETN and then it was pressed using the same procedure as before (plastic foil). The consistency of the wet $Ag_2C_2.AgNO_3$ was like toothpaste. The thickness of the layer obtained was generally over 0 5 mm.

(b) It was also tried to spray $Ag_2C_2.AgNO_3$ over the PETN. In this case, the complex salt was in a much more dilute suspension in water in order not to obstruct the nozzle of the sprayer. Nevertheless, the nozzle was obstructed many times because of the fact that the $Ag_2C_2.AgNO_3$ crystals sometimes stick together forming particles of the same magnitude as the nozzle hole. Also, in some cases, the water coming out with $Ag_2C_2.AgNO_3$ started washing away the PETN.

In summary, even if this second method was sometimes successful, it was generally preferred to use the first method because it was more convenient with the one-dimensional chamber.

Having put the explosive in the cup, the cup was placed in the one-dimensional chamber and the chamber was closed working under red light. The chamber was evacuated to dry the explosive and, as before, it was pumped until the gauge showed a steady reading (the reading was generally a fraction of mm Hg).

With this method the explosive was ignited by the light coming from the exploding wire.

A.4 Possible Dependence of the Ignition on the Pressure of the Driver Gas

In the first few experiments (following procedure (a) described above) the explosive was ignited right after vacuum drying. In these cases the pressure of the driver gas was less than one mm Hg.

In subsequent experiments, the driver gas (generally He) was used at higher pressure and in some cases, with pressures in the range of 15 to 30 psi, there was no ignition. Because of this we started to determine the percentage runs with ignition as a function of gas pressure (He) in the chamber. The number of runs for every fixed pressure was 4. Up to the end of the present experiments Table A1 was obtained.

The use of this technique in the hemispherical launcher is more complicated. We must always keep in mind that $Ag_2C_2.AgNO_3$ is a dangerous material and in many aspects an unpredictable explosive.

We feel that more tests have to be done before using this explosive with large quantities of PETN. A series of tests could be made to determine at what degree of dryness the $Ag_2C_2.AgNO_3$ can be ignited, for instance, by hammering it.

We should keep in mind that loading a hemispherical liner with 60-fold the amount of explosives is more complicated than loading a cylindrical cup. In the case of the hemispherical liner the best results will probably be achieved by spraying the $Ag_2C_2.AgNO_3$ on the PETN. Hence a better technique of spraying should be developed.

REFERENCES

A.1 J. D. McCowan — "Decomposition of Silver Acetylide". Faraday Society Transactions (1963) Vol.59, pp.1860-1864.

A.2 W. E. Baker, F. O. Hoese, S. Silverman — "Development of Capabilities of a Light-Initiated, Sprayed Explosive". Tech. Report. IR, Project No. 02-9008-01. Southwest Research Institute, San Antonio, Texas, (1969).

A.3 R Stadler — "Analytic and Explosive Technical Investigations on Silver Acetylide". Tech. Report No.2. Project No. 02-1770(1R). Southwest Research Institute, San Antonio, Texas, (1966).

Pressure p.s.i.	1	3	6
% of runs with Ign.	100	100	100

Table A.1

Percentage of Runs with Ignition Versus Pressure of the Driver Gas

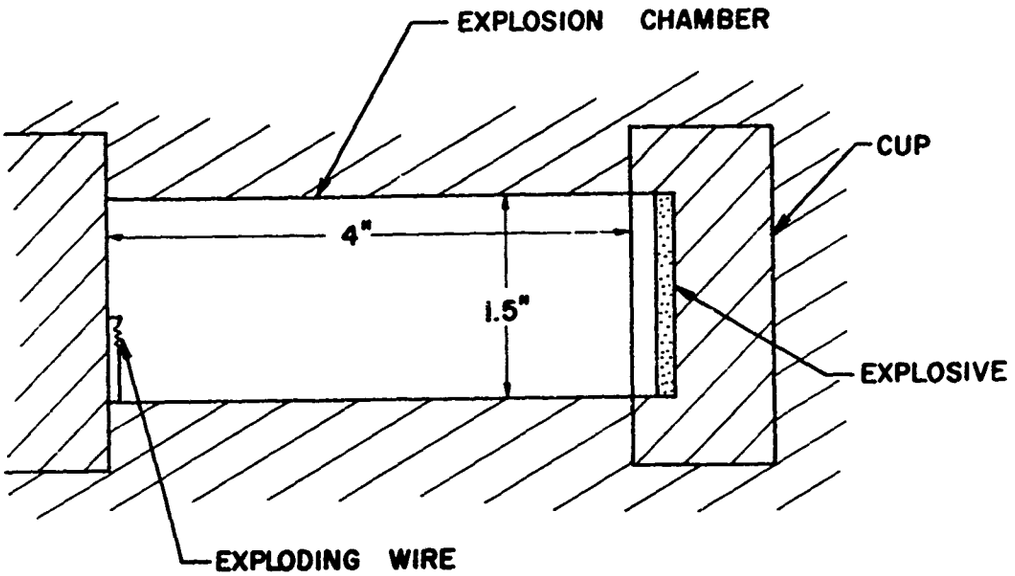

FIG. A1 SCHEMATIC DIAGRAM OF THE ONE-DIMENSIONAL CHAMBER

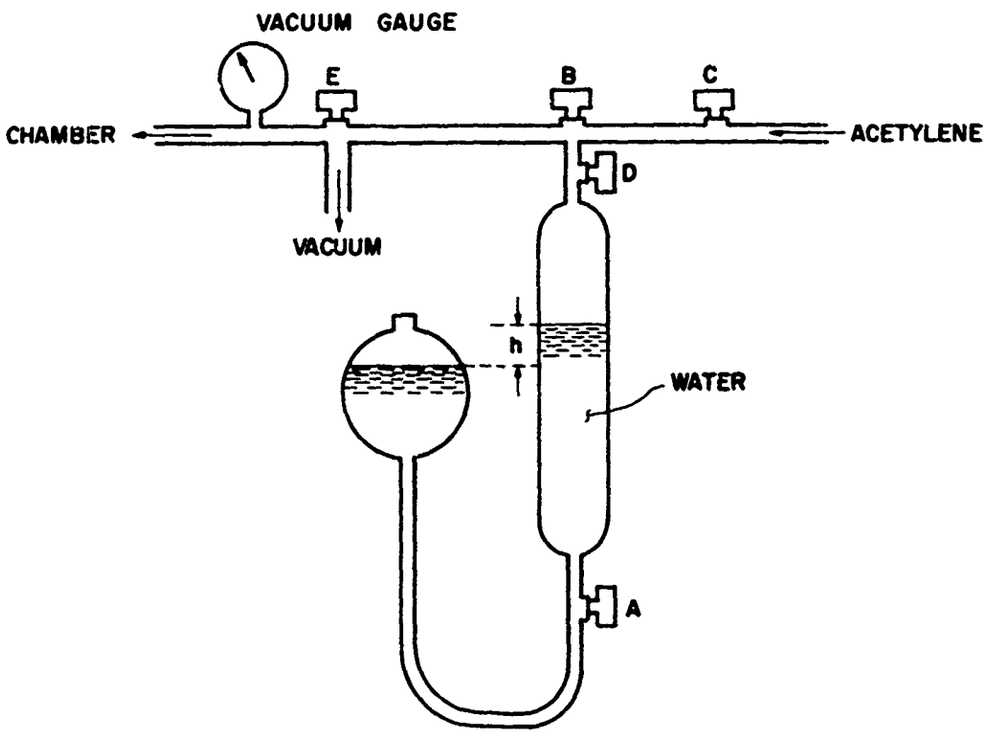

FIG. A2 SCHEMATIC DIAGRAM OF THE APPARATUS FOR MEASURING THE AMOUNT OF ACETYLENE ABSORBED

FIG. A3 STEEL CUP AND PLASTIC FOAM PAD

APPENDIX B: AN INVESTIGATION OF A LASER INTERFEROMETER TECHNIQUE FOR PROJECTILE VELOCITY MEASUREMENT IN THE BARREL OF THE UTIAS IMPLOSION-DRIVEN HYPERVELOCITY LAUNCHER (by G. Cappelli)

B.1 Introduction

From Newton's Second Law the pressure behind a projectile is proportional to the acceleration neglecting friction and counter pressure. Therefore a detailed measurement of the acceleration history can give direct information for the pressure history. On the other hand a knowledge of the pressure history can give useful information on the wave system developed inside the hemispherical implosion chamber Up to now the only information available on the pressure and velocity histories of the launcher were from numerical solutions of a one-dimensional computer code. While there was some doubt on the validity of this code, it is therefore desirable to obtain some experimental verification. Elsenaar (Ref. B.1) used a microwave technique to measure the projectile velocity quite successfully in the gas runs. However, signals from explosive runs were found to be affected by leakage of gas in front of the projectile and no conclusive results were obtained for the explosive runs. In the following a laser interferometer technique based on the work of L. M. Barker (Ref. B.2) will be described. This was an attempt to overcome the difficulty encountered by the microwave technique.

B.2 Theory

Figure B.1 shows a schematic setup of the apparatus and the optical path of the laser light beam. The light beam reflected from the projectile is split in two by beam splitter B1. One beam goes to the photomultiplier and the other follows a delay path which differs from the previous one by a delay leg with length of, to a good approximation,

$$\ell = N \lambda \tag{B.2.1}$$

where N is an integer constant and λ is the wavelength of the laser light. When the projectile moves, λ undergoes a Doppler shift according to the formula:

$$\Delta\lambda(t) = \frac{2\lambda_o u(t)}{c} \tag{B.2.2}$$

where λ_o is the initial laser light wavelength, u(t) is the velocity of the projectile while c is the velocity of light in air. $\Delta\lambda$ will be observed in the photomultiplier as interference fringes. Since any practical projectile velocity is much smaller than the speed of light, therefore $\Delta\lambda(t) \ll \lambda_o$.

Differentiate Eq. (B.2.1) and get

$$dN = - \frac{\ell}{\lambda^2} d\lambda \tag{B.2.3}$$

Combine Eqns. (B.2.2) and (B.2.3) and get

$$u(t) = \int_o^t \frac{c}{2\ell} \frac{\lambda^2}{\lambda_o} dN \tag{B.2.4}$$

Since $\lambda \approx \lambda_o$

$$u(t) = \int_0^t \frac{c\lambda_o}{2\ell}\, dN = K\ \Delta N \qquad (B.2.5)$$

This relation gives the speed of the projectile, starting from rest, as a function of the total number of interference figures, ΔN, observed in the photomultiplier. The constant of proportionality $K = c\lambda_o/2\ell$ can be accurately determined. The time rate of change of the velocity then gives the acceleration of the projectile.

B.3 Experimental Apparatus

B.3.1 General Setup

A schematic drawing of the setup of the experimental apparatus is shown in Fig. B.1. The laser is a 1 mW University Laboratories He-Ne gas laser. The beam divergence is 0.8 milliradians. The mirrors are first surface mirrors flat to within a quarter wavelength. The beam splitters have 50% reflection and are also flat to within a quarter wavelength. All mirrors and beam splitters are mounted on adjustable holders. The photomultiplier was an EMI type 9558, with S-20 spectral response, with approximately 6% quantum efficiency at 6328°A. A 6328°A interference filter was used to protect the photomultiplier from extraneous light. The photomultiplier housing and the dynode chain circuit are shown in Figs. B.2 and B.3 respectively.

The delay leg of the present setup has a length of $\ell = 68$ cm. Hence the constant K in Eq. (B.2.5) has a value of

$$K = \frac{c\lambda_o}{2\ell} = 140 \text{ m/sec}$$

Therefore every interference fringe observed at the photomultiplier-oscilloscope system will correspond to a velocity change of 140 m/sec. Assuming that only half of a cycle can be read on the oscilloscope record of the photomultiplier output then the present system should have a lower limit on the resolution of a velocity measurement of 70 m/sec. While the photomultiplier-oscilloscope system had a frequency response of up to 1 MHz, the maximum frequency of the observed interference fringes in the present experiment was expected to be of the order of 10 KHz only.

The experiment was carried out using different types of firearms for ease and economy of operation instead of the hypervelocity launcher, namely a 0.22 caliber rifle and a 12-gauge shotgun loaded with special bullets. (The latter was used in most of the experiments). The choice of the bullet is very important and will be discussed later.

The oscilloscope was triggered in two different ways, one using the internal trigger system regulated to trigger at a chosen amplitude, the other using an external signal (this method was often used with the shotgun). The circuit for the external trigger is shown in Fig. B.4. The contact to ground was closed in the way shown in Fig. B.5. When the firing pin of the shotgun hits the primer of the shotgun shell, the circuit is closed to ground giving the trigger signal.

B.3.2 Use of Projectiles in a 0.22 Calibre Rifle

As mentioned before, the choice of the right bullet configuration is extremely important in this experiment. In fact we can say that we have

not been able to find an ideal bullet configuration which would reflect the incident laser beam back parallel to itself in the way shown in Fig. B.1. In the present case, when the projectile starts moving, it is subjected to vibrations causing the reflected beam to be completely out of alignment with the incident beam.

Also, the laser light (and the light reflected by the bullet) carries a noise signal that gives, with a photomultiplier output of 1 V, a noise output of about 50 mV. This ratio of 1/.05 is not constant but decreases when the total output decreases and depends also on the type of projectile used. The frequency of the noise signal is about 10 KHz, as shown in Fig. B.6. If the amplitude of the signal due to beating is of the same order of magnitude as this signal, it is impossible to read any cycle due to the Doppler effect. In other words, the light reflected by the head of the bullet has to be strong enough to give an eventual beat signal stronger than the noise signal. In any case the total signal registered by the photomultiplier has to be well above the noise signal.

A first attempt to reduce variations of the light reflected by a moving bullet was made using a 0.22 calibre rifle as follows: the 0.22 bullet was shot into a 5/16 in. dia. aluminum bullet placed in a 5/16 in. dia. barrel. Different reflecting surfaces at the head of the bullets were used. The oscilloscope traces were not reproducible in the experiments; the traces generally indicate very strong variations of light in the photomultiplier. It was then decided to accelerate bullets using a different system.

B.3.3 Use of a 12-Gauge Shotgun

A second attempt to obtain reasonably small variations of light reflected from a moving projectile was made using a 12-gauge shotgun loaded with special plastic bullets. The optimum diameter of the plastic bullet for a good fit in the shotgun barrel and high velocity was found to be .731 in. Different types of bullets were tried; three of them are shown in Fig. B.7. The one on the left shows a concave pyramidal shaped reflecting surface. Every face of the pyramid is at 45° with respect to the axis of the bullet. With this configuration, the in-going beam having a certain angle with respect to the axis of the projectile will emerge parallel to itself as can be seen in Fig. B.8, using simple geometrical considerations. In practice it is very difficult to obtain the desired 45° angles with respect to the axis of the bullet and all attempts with this kind of projectile were unsuccessful. Also, we have to consider the fact that in the launcher, 0.22 in. dia. projectiles are generally used and the difficulty of obtaining the desired pyramidal configuration would be much greater because of the small dimensions.

A second kind of bullet tried is the central one shown in Fig. B.7. In this case the head of the bullet is hemispherical and made out of polished aluminum. The laser beam will be reflected back in spherical waves by the head of the bullet. Only a small fraction of light will go back in the same direction as the in-going beam; however, owing to the spherical surface, there will always be a fraction of light going back parallel to the in-going beam, no matter what oscillations the projectile can be subjected to. The difficulty with this configuration was that, at least with the laser used, the fraction of light reflected parallel to the in-going beam was not strong enough to give a signal bigger than the noise signal of the laser. Also, it was very difficult to obtain a good spherical reflecting surface.

The third bullet shown on the righthand side of Fig. B.7 was used in most of the shotgun runs. More details of this bullet are shown in Fig. B.9. The total weight of this bullet is approximately 4.2 gm. and the shell was loaded with approximately 3.1 gm of smokeless gunpowder type 700-X. The reflecting surface was obtained from a piece of stainless steel sheet, .015" thick, with a good polish. The reflecting disk is convex with a radius of curvature of about 4 in. These disks obtained their curvature from the punching process when they are stamped out of the sheet with a 7/16 in. punch. The light reflected by the convex surface is enough to give a total signal from the photomultiplier at least 10 times bigger than the noise signal. The reason for using this bullet becomes clear from Fig. B.10. Because of the convex surface the laser beam is reflected back in a cone of light. If the aperture of the cone is sufficiently large there will always be a portion of light going back to the mirror M2 in the same direction as the in-going beam. This is true if the vibrations of the projectile do not exceed certain limits. This convex-headed bullet represents an intermediate situation between the hemispherical headed bullet and a flat-headed bullet. A loaded shell is shown in Fig. B.11. The edge of the plastic shell is important obtaining high projectile speed. The edge has been obtained using a 12-gauge case trimmer. The speed obtained with this bullet was generally over 1,000 m/sec.

Because of the smaller variations of reflected light with respect to previous types of bullets, it was decided to use this bullet for further investigations. Also, it was found that, using this bullet, an almost repeatable signal from the photomultiplier was obtained.

B.3.4 Other Experimental Details

The 12-gauge shotgun was mounted on a heavy adjustable stand as shown in Fig. B.12. Before every run it was checked so that the in-going laser beam was coincident with the axis of the shotgun barrel. This operation is important because if the laser beam is not parallel to the barrel axis, it can meet the moving reflecting surface in different regions of the reflecting surface itself, giving variations of light. Also, to initially have the axis of the reflected cone of light coincident with the in-going beam, the laser beam must be coincident with the barrel axis.

Before every run the shotgun shell was moved and rotated in the barrel to choose the position that gave the maximum reflected light back into the photomultiplier (this was done in order to have similar initial conditions every time). Many times the position chosen was too critical, that is, a small rotation or movement of the shell was sufficient to give strong variations of light received by the photomultiplier (and hence large signal changes to the oscilloscope). In such a case the shell was always replaced.

B.4 Analysis of Experimental Results

With the convex-headed bullet described above, we started to study the light reflected back by the bullet accelerated in the shotgun barrel. We intended to answer the following questions:

1. How much variation of the amplitude of the reflected beam was due to projectile vibrations?

2. How can these variations interfere with a possible beat signal due to the Doppler effect?

In Fig. B.13, three oscilloscope traces registering photomultiplier outputs corresponding to three different shotgun runs are shown. Of these three runs the one on top can be considered a good run; the other two are average runs, as will be discussed later. To interpret these oscilloscope traces and also to answer the previous questions, we have to consider the following calculations.

B.4.1 Calculation of the Exit Time of the 12-Gauge Bullet from the Shotgun Barrel

In all oscilloscope traces shown in Fig. B.13, a strong variation of light is observed after a time of approximately 1.1 - 1.5 msec. This variation of light could have been due to the bullet leaving the barrel. Hence it is important to calculate the travelling time of the bullet in the barrel and to compare this time with the time observed in the oscilloscope traces. Moreover, more data will be found from this calculation as it will be seen later. Also the projectile can only accelerate while still in the barrel and so we can expect beat fringes only within this travelling time.

For simplicity we assumed a linearly decreasing acceleration profile for the bullet as shown in Fig. B.14. This profile is only a first approximation and consequently the time calculated will give an approximate value. With the linear profile assumed for the acceleration we can write:

$$a_o x + Sa = a_o S \qquad (B.4.1)$$

where a_o is the initial acceleration and S the length of the barrel.

From (B.4.1) we have

$$a = \frac{a_o}{S} (S-x) \qquad (B.4.2)$$

Also we can write for the projectile acceleration:

$$a = \frac{du}{dt} = u \frac{du}{dx} \qquad (B.4.3)$$

Using (B.4.3) and (B.4.2) we have:

$$\frac{ao}{S} (S-x) = u \frac{du}{dx} \qquad (B.4.4)$$

From this:

$$ao \int_o^S (S-x)dx = S \int_o^{u_1} udu \qquad (B.4.5)$$

u_1 is the muzzle velocity and it was measured with a standard method (interrupted light beam technique) (see Section 2.4 of this report).

From (B.4.5):

$$a_o = \frac{u_1^2}{S} \qquad (B.4.6)$$

This is the initial acceleration expressed in terms of u_1 and S.

Using again equation (B.4.4) we have:

$$a_o \int (S-x)\, dx = S \int u\, du \qquad (B.4.7)$$

This gives the solution:

$$a_o \left(Sx - \frac{x^2}{2} \right) = \tfrac{1}{2} Su^2 + C$$

where C is a constant of integration.

For $x = 0$, $u = 0$ and hence $C = 0$.

We have:

$$2\, a_o Sx - a_o x^2 = Su^2 \qquad (B.4.8)$$

From (B.4.8) we can write:

$$u = \frac{dx}{dt} = \left[\frac{a_o}{S} (2Sx - x^2) \right]^{1/2} \qquad (B.4.9)$$

Integrating (B.4.9), we obtain the time it takes the bullet to travel a distance x in the barrel:

$$\int dt = \frac{S}{a_o} \int \frac{dx}{\sqrt{-x^2 + 2Sx}} \qquad (B.4.10)$$

The integral on the right side of Eq. (B.4.10) has the general form:

$$I = \int \frac{(Ax + B)}{\sqrt{-x^2 + px + q}}$$

with the general solution:

$$I = -A \sqrt{-x^2 + px + q} + (B + \frac{Ap}{2}) x \arcsin \left(\frac{x - p/2}{\sqrt{q + p^2/4}} \right) + \text{Cons.} \qquad (B.4.11)$$

In the present case:

$$A = 0;\ B = 1;\ p = 2S;\ q = 0$$

So we have:

$$\int \frac{dx}{\sqrt{-x^2 + 2Sx}} = \arcsin \left(\frac{x-S}{S} \right) + \text{Const} \qquad (B.4.12)$$

From (B.4.12)

$$t = \sqrt{\frac{S}{a_o}} \left(\arcsin \left(\frac{x}{S} - 1 \right) + \text{Const} \right)$$

At $t = 0$, $x = 0$ and:

$$\text{Const} = \frac{\pi}{2} \qquad (B.4\ 13)$$

so from (B.4.13) and (B.4.6):

$$t = \left(\frac{\pi}{2} + \arcsin \left(\frac{x}{S} - 1 \right) \right) \frac{S}{\mu_1} \qquad (B.4.14)$$

Equation (B.4.14) gives the time taken the bullet to travel the distance x inside the barrel of length S when the muzzle velocity is u_1. For x = S we have the total travelling time of the bullet in the shotgun barrel:

$$t_a = \frac{\pi}{2} \frac{S}{u_1} \qquad \text{(B.4.15)}$$

For a gun barrel length of 70 cm and bullet muzzle velocity, u_1, of 1000 m/sec we have $t_a \tilde{=} 1.1$ msec. So it is correct to assume that the strong variation of light after 1.1 - 1.5 msec. is due to the emergence of the bullet from the barrel.

B.4.2 Further Analysis of the Oscilloscope Traces

Continuing with the analysis of the oscilloscope traces, we see that, in the average case, there are strong variations of light within the first 0.4 msec., that is, within 1/3 of the total time taken by the projectile to come out of the muzzle. How can these variations affect the velocity measurement? In other words, how many fringes can we expect within 0.4 milliseconds? To answer this question we have to find a relation between time and velocity of the projectile.

From equations (B.4.8) and (B.4.6) we can write:

$$x^2 - 2Sx + S^2 (u/u_1)^2 = 0 \qquad \text{(B.4.8a)}$$

From this

$$x = S \pm S \sqrt{1-(u/u_1)^2} = S\left(1 \pm \sqrt{1-(u/u_1)^2}\right) \qquad \text{(B.4.16)}$$

Since we are considering $x \leq S$ we have to drop the + sign in Eq. (B.4.16) which becomes

$$x = S\left(1 - \sqrt{1-(u/u_1)^2}\right)$$

Substituting this value in Eq. (B.4.14), we have

$$t = \left(\frac{\pi}{2} + \arcsin\left(-\sqrt{1-(u/u_1)^2}\right)\right) \frac{S}{u_1}$$

or

$$t = \frac{S}{u_1}\left[\frac{\pi}{2} - \arcsin\left(\sqrt{1-(u/u_1)^2}\right)\right] \qquad \text{(B.4.17)}$$

Instead of solving this equation to obtain u = u(t) we can choose a value of u and find the time t corresponding to it. For $u = 0.5\, u_1$ we have

$$t \tilde{=} 1/3\, t_a$$

This calculation shows that in 1/3 of the time t_a, the bullet has reached 50% of the final speed and consequently in 1/3 of the time t_a we can expect 50% of the fringes due to the Doppler effect. This means that because of the strong variations of light within this time, generally we will not be able to read 50% of the fringes. This conclusion answers question (2) posed before Section B.4.1.

B. 4.3 Another Possibility for Inaccurate Readings

As already noted, the pictures of Fig. B.13 show strong variations of light in the photomultiplier occurring within about 1/3 of the total bullet travelling time. It is important to know the intensity of the variations of light, due to projectile vibrations, with respect to the total signal received by the photomultiplier. Also, the beat signal will have an amplitude proportional to the total signal that generates it. This total signal has minima and maxima as shown in Fig. B.13 and correspondingly the amplitude of the fringes will have a minimum or a maximum.

Experimentally it has been observed that the variations of light occurring within the first 0.4 msec can go from less than 30% of the total signal to more than 90% of the total signal. Every case is different. However we still have to determine the amplitude of the beat signal with respect to the amplitude of the total signal from the photomultiplier. To do so we have to give some further consideration to the beat signals and the interference signals. In general, we can say that an interference signal can be obtained by combining two waves of the same frequency but one out of phase with respect to the other. If the difference in phase is changing in time we will be able to detect, at a fixed point in space, minima and maxima of the resultant signal. A maximum will occur when the maxima of the two waves combine together. A minimum will occur when the minima of the two waves combine together. A beat signal can be obtained by combining two waves of different frequency. A maximum of the signal occurs when the maxima of the two waves combine together and a minimum occurs when the minima combine.

In the case under study the light reflected by the projectile is split into two beams that follow two paths of different length. The length of these paths is changing in time by a small amount because of the vibrations of the optical system. The output of the photomultiplier due to these vibrations is like the one shown in Fig. B. 15; the signal is modulated at a frequency of about 180 cycles/sec. These interence fringes are due to changes of the optical path length producing a phase change between the two beams when they recombine in the photomultiplier. The fringes disappear when one of the mirrors is rotated causing a non-coincidence of the direct and the delayed beams. So these fringes are also an indication of the coincidence of the two beams which is necessary to have beat fringes. Also by tapping on the optical system we observed a change in the frequency of these fringes but practically no change in the amplitude. If the variations of the optical path length were less than half a wavelength (in this case the amplitude of the fringes would not be the biggest possible) we should have obtained variation in the amplitude of the fringes by tapping on the optical system. In fact, it is reasonable to think that by tapping on the optical bench, the amplitude of the oscillations of the mirrors should increase. As a consequence, if initially the variations of the optical path length were less than half a wavelength, after tapping the variations should be bigger (perhaps half a wavelength) giving a bigger interference signal.

In conclusion, the amplitude of the interference fringes obtained is a maximum for every case and configuration. From what was said above, we can expect that the amplitude due to the Doppler beat will be the same as the amplitude of these fringes. In all cases observed, the interference fringes have an amplitude of about 1/5 of the total signal coming from the photomultiplier. This means that, if for example the total signal is varying from 1.0 V to 0.2 V, the amplitude of the fringes will vary from 0.2 V to 0.04 V. This shows another

difficulty in reading the eventual Doppler beat fringes.

Also, it can be noted from Fig. B.1 that because of the beam splitters, a reflected beam of light entering the interferometer with intensity A, will give an intensity 3/8A, in the photomultiplier. The frequency of the beat signal is expected to be about 8 KHz, and so the optical system can be considered almost stationary in the time the beat signal is expected.

B.4.4 Attempt to Eliminate the Effects of Variations of Light Received by Photomultiplier

As pointed out in the previous section, the variations of light in the photomultiplier caused by vibrations of the projectile presented a serious problem. It can be said that, at least in the case of the shotgun bullet, these variations are so strong that a velocity measurement is impossible with the optical system previously used.

In an effort to eliminate the effects of variation of light, the experimental apparatus was modified as shown in Fig. B.16. A beam splitter B4 was added to the optical system. The laser beam reflected back by the projectile passing through the beam splitter B1 is split again by the beam splitter B4. One half of this beam follows the same path as before, going into the photomultiplier P1 and recombining with the delayed beam. The other half of the beam is going into the photomultiplier P2. The outputs from the two photomultipliers are fed into the differential amplifier plug-in unit of the oscilloscope, so that the oscilloscope displays the difference between the two signals.

The system was tested by turning the delayed beam away. Before every run, the system was adjusted in such a way that the maximum signals from the photomultipliers gave no signal in the oscilloscope when subtracted by the differential amplifier.

We obtained many kinds of different oscilloscope traces; one of these traces is shown in Fig. B.17. In this particular run there was some improvement and in the first 1 msec. there are no strong variations of the signal. In other cases the variations were more pronounced. Generally we had different oscilloscope traces for every run.

Notice that the delayed beam still carries variations in light due to vibrations of the projectile. To correct these vibrations we could insert another beam splitter between B2 and B3 in Fig. B.16 and use another photomultiplier, P3, to detect the portion of delayed beam coming from the new beam splitter. The signal from P3 should be added to the signal from P2.

Other systems of correction of the variations of light could be applied using two or more photomultipliers. In any case we feel that as far as this investigation is concerned, the method using two photomultipliers did not give a good correction of the variations of light due to projectile vibration.

B.4.5 Possible Effects Due to Modulation of Laser Light

According to an article by Ashby and Jephcott (Ref.B.2), the light emitted from a laser into a moving mirror and reflected back into the laser can affect the laser light itself. The intensity of the laser light will be

modulated at a frequency dependent on the velocity of the reflecting surface. Minima occur as the reflecting surface moves through successive half wavelengths. About 50% depth of modulation of the laser output can be produced even with a small fraction of light (less than 1%) reflected back into the optical cavity of the laser. The depth of modulation depends on the frequency of the modulation itself and decreases with increasing frequency. The depth of modulation decreases below 50% as the frequency increases above 100 KHz; at 1 MHz the depth of modulation is about 5%.

The present problem is to investigate what effect this modulation can have on the laser hypervelocity measurements. Let us consider the first half fringe due to the Doppler beat. From the calculations developed in Section B.4.2 we can write for $x = x(u)$:

$$x = S\left(1 - \sqrt{1-(u/u_1)^2}\right) \qquad \text{(B.4.18)}$$

Let ϵ be the fraction of muzzle velocity corresponding to the first half cycle, we have:

$$x_\epsilon = S\left(1 - \sqrt{1-\epsilon^2}\right) \qquad \text{(B.4.19)}$$

This is the distance travelled by the projectile to reach the speed ϵu_1. The number of modulations due to the projectile passing through successive half wavelengths will be:

$$n = \frac{x_\epsilon}{\lambda/2} = \frac{2x_\epsilon}{\lambda} \qquad \text{(B.4.20)}$$

The time t_ϵ that takes the projectile to travel the distance x_ϵ is from Eqs. (B.4.14) and (B.4.19)

$$t_\epsilon = \frac{\pi}{2}\,\frac{S}{u_1}\left(1 - \frac{\arcsin\sqrt{1-\epsilon^2}}{\pi/2}\right) \qquad \text{(B.4.21)}$$

To obtain an order of magnitude estimate we will consider a constant modulation of light within the time t_ϵ. In this case the frequency of modulation will be:

$$f_m = \frac{n}{t_\epsilon} = \frac{4}{\lambda}\,\frac{\left(1 - \sqrt{1-\epsilon^2}\right)u_1}{\pi\left(1 - \frac{\arcsin\left(\sqrt{1-\epsilon^2}\right)}{\pi/2}\right)} \qquad \text{(B.4.22)}$$

If the final speed is 1100 m/sec. and half a cycle of the Doppler beat signal correspond to 70 m/sec., one has:

$$\epsilon \simeq 0.06, \quad u_1 = 1{,}00 \text{ m/sec}$$

and also:

$$\lambda = 0.6328\mu = 6.328 \times 10^{-7} \text{ m}$$

Putting these numbers in Eq. B.4.22 we have:

$$f_m \simeq 3 \times 10^8 \text{ HZ}$$

This frequency is at least two orders of magnitude bigger than one MHz and consequency the depth of modulation is negligible. We can conclude that, except

for the very beginning of the accelerating process, the effect of modulation of the laser light is insignificant.

B.5 Conclusions

The possibility of velocity measurements using a laser interferometer technique has been investigated. Of the problems that have been encountered, the oscillations of the projectile have been the most serious. For this reason most of the effort has been spent trying to reduce the effects of these oscillations. This problem has been only partially solved going from the 5/16 in. dia. bullet to the 12-gauge plastic bullet. Some oscillations were still present and the calculations show that they can affect up to 50% of the expected beat fringes.

The use of two photomultipliers to eliminate the variations of light due to oscillations of the projectile has not been successful up to now. This is possibly due to an imperfectly convex reflecting surface at the head of the bullet. Also the position of the photomultipliers is critical in order to have total cancellation of the signals due to oscillations of the moving bullet.

An investigation has been carried out with a 12-gauge shotgun and the results apply to the 12-gauge bullet. The use of other launching devices could give rise to different problems. It is reasonable to think that oscillations of the projectile will always be present, even if in different proportion.

Also, the alignment of the launcher barrel with the laser beam could present problems. On the other hand, it is possible that the oscillations of the projectiles from the hypervelocity launcher are smaller than the oscillations of the 12-gauge bullets. No experiments have been done using the hypervelocity launcher.

In conclusion we can say that, in the case of the 12-gauge bullet, it has not been possible to find a bullet or any other device that could produce the ideal situation of a bullet moving with its reflecting surface perpendicular to the in-going laser beam and consequently quantitative data on projectile accelleration, velocity, and base pressure were not obtained.

REFERENCES

B.1 Barker, L. M. "Fine Structure of Compressive and Release Wave Shapes in Aluminum Measured by the Velocity Interferometer Technique". Sandia Laboratory Preprint SC-DC 66-2447.

B.2 Ashby, D.E.T.F. Jephcott, D.F. "Measurement of Plasma Density Using a Gas Laser as an Infrared Interferometer". Applied Physics Letters. Vol.3, No.1, p.13 (July, 1963).

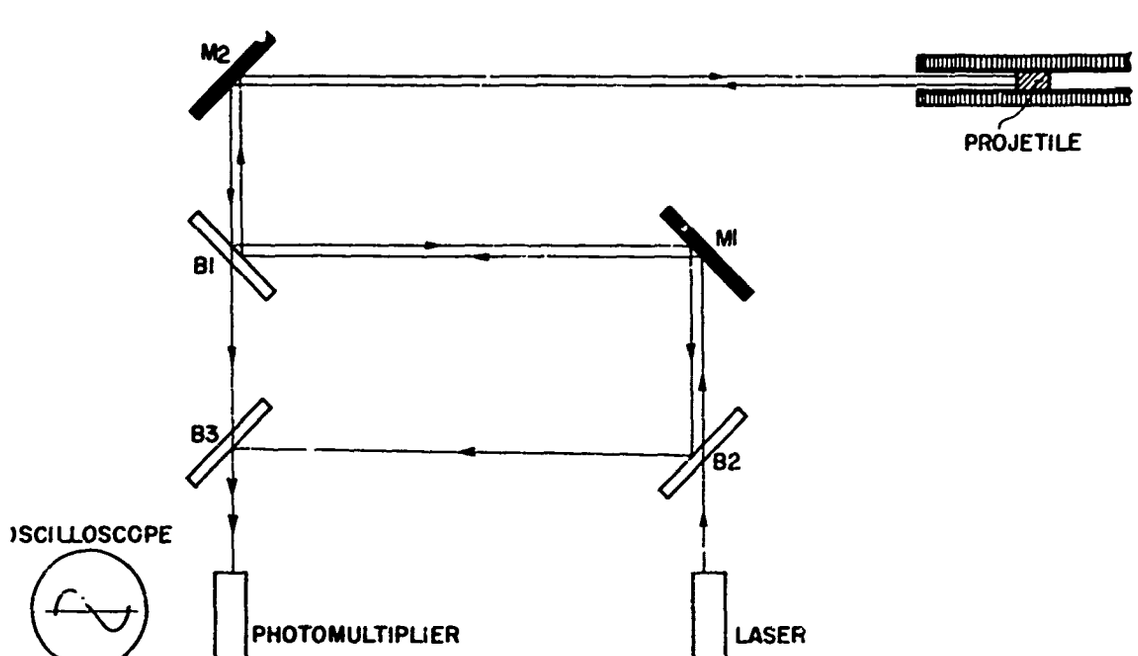

FIG. B.1 SCHEMATIC OF THE EXPERIMENTAL APPARATUS

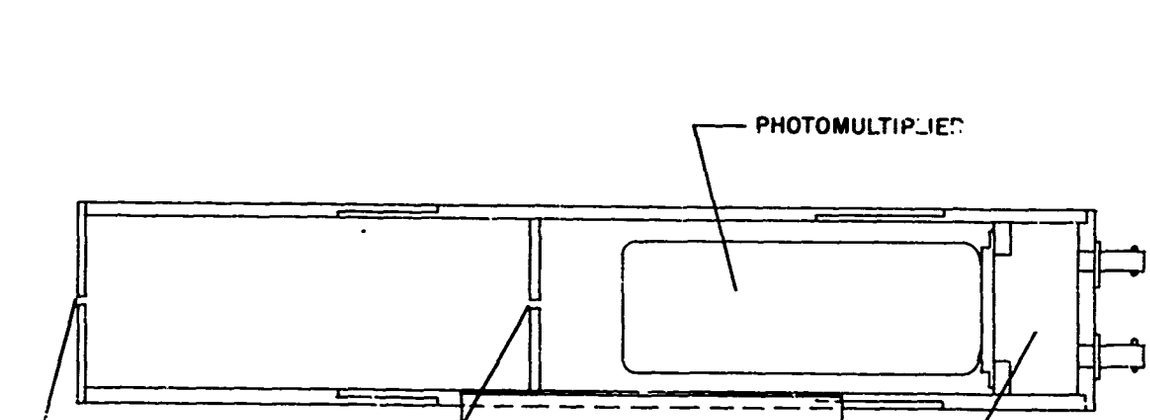

SCALE :- 1:2

FIG. B.2 SCHEMATIC OF THE PHOTOMULTIPLIER HOUSING

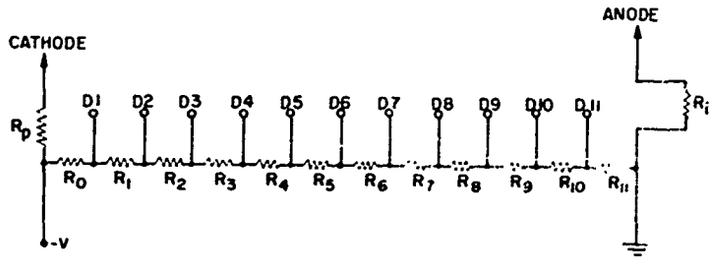

(D1, D2, D3 ·· D11) DINODES

$R_0 = 25K\,\Omega$

$R_1 = R_2 = R_3 \quad = R_{11} = 25K\,\Omega$

$R_p = 25K\,\Omega$

R_i = oscilloscope internal resistance $\sim 1M\,\Omega$

FIG. B.3 PHOTOMULTIPLIER CIRCUIT

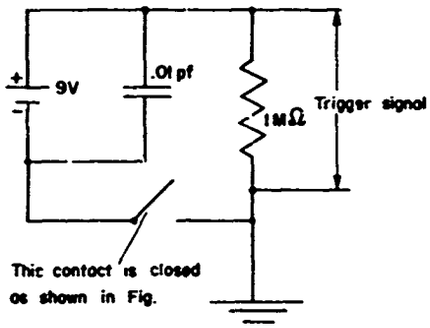

FIG. B.4 TRIGGER CIRCUIT

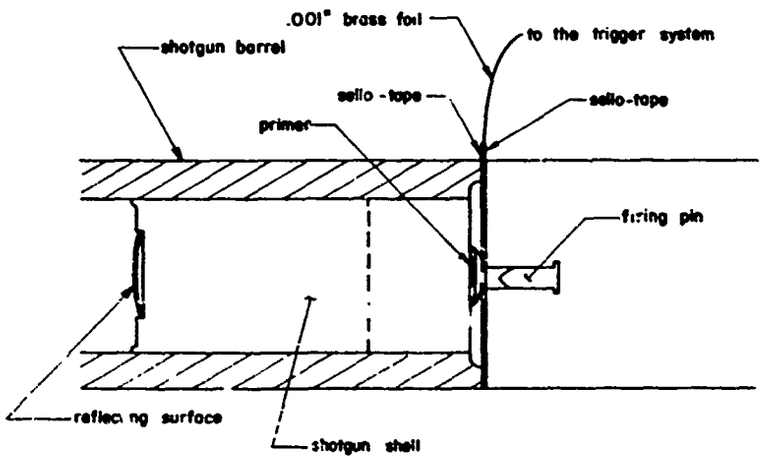

FIG. B.5 SCHEMATIC OF THE 12 GAUGE SHOTGUN TRIGGER SYSTEM

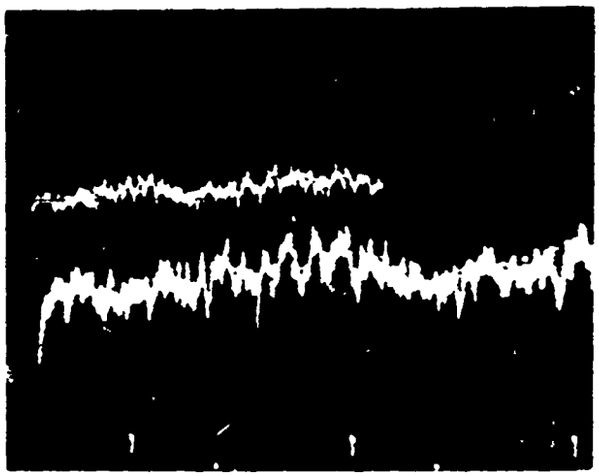

FIG. B.6 NOISE SIGNAL FROM THE LASER
UPPER BEAM: 0.2V/cm; 2msec/cm
LOWER BEAM: .05v/cm; 1msec/cm

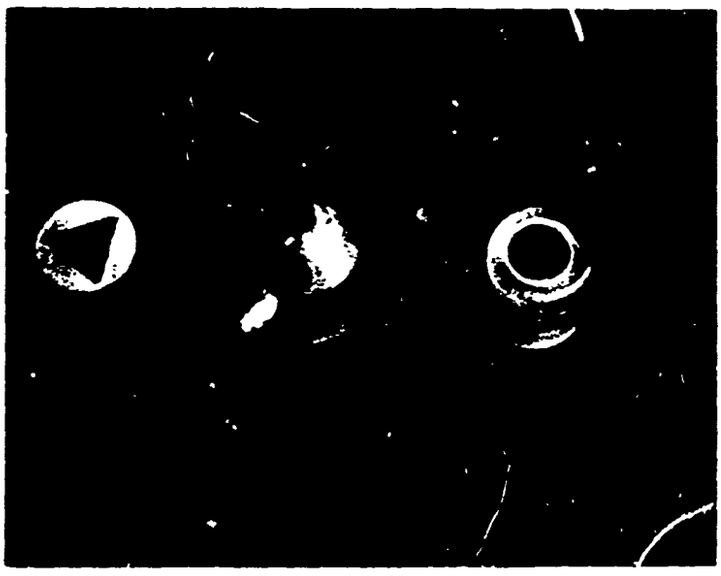

FIG. B.7 TYPES OF BULLETS USED

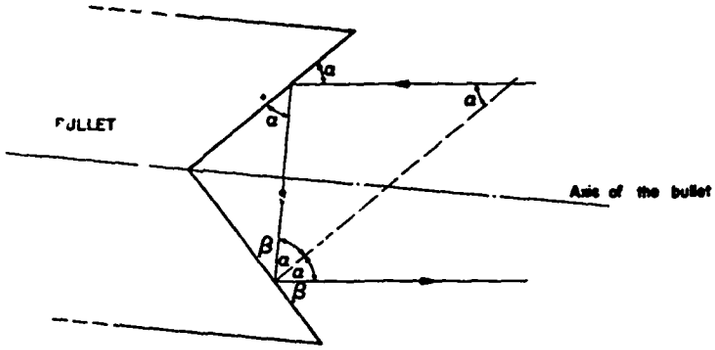

FIG. B.8 SCHEMATIC OF THE INCIDENT AND REFLECTED LIGHT BEAM BY A CONCAVE PYRAMIDAL SHAPED BULLET HEAD

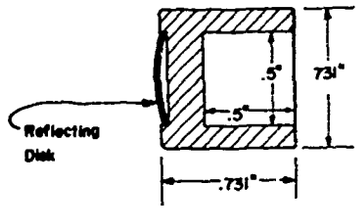

FIG. B.9 CROSS-SECTION OF THE 12 GAUGE BULLET

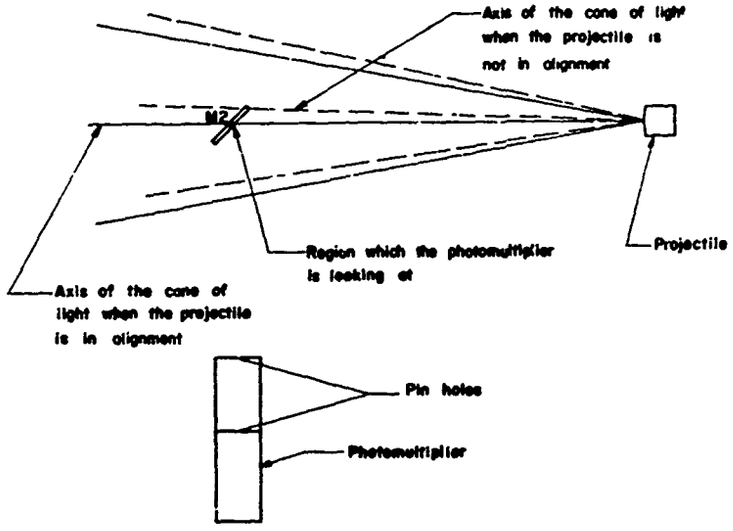

FIG. B.10 SCHEMATIC SHOWING THE POSSIBLE MISALIGNMENT OF THE CONE OF LIGHT REFLECTED BY THE BULLET

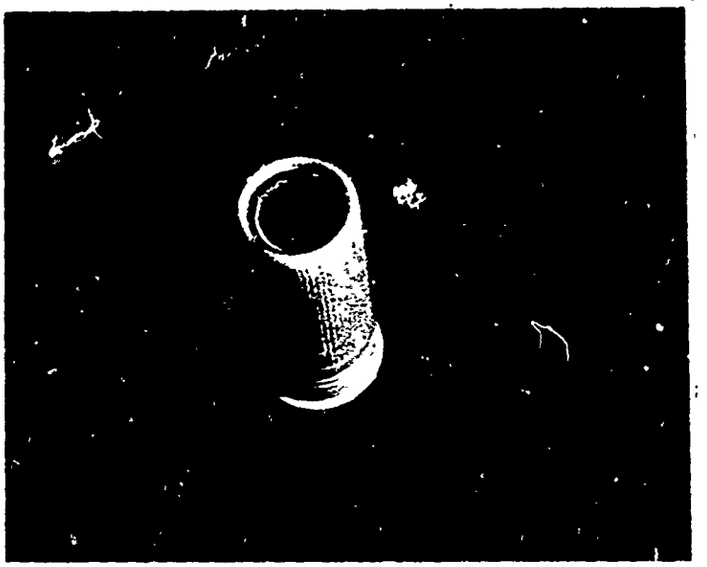

FIG. B.11 PHOTOGRAPH OF A 12 GAUGE BULLET

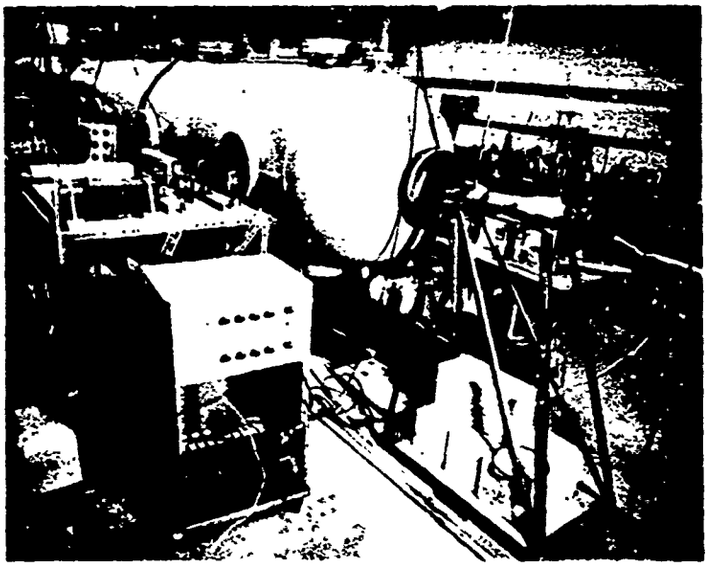

FIG. B.12 GENERAL VIEW OF THE EXPERIMENTAL APPARATUS

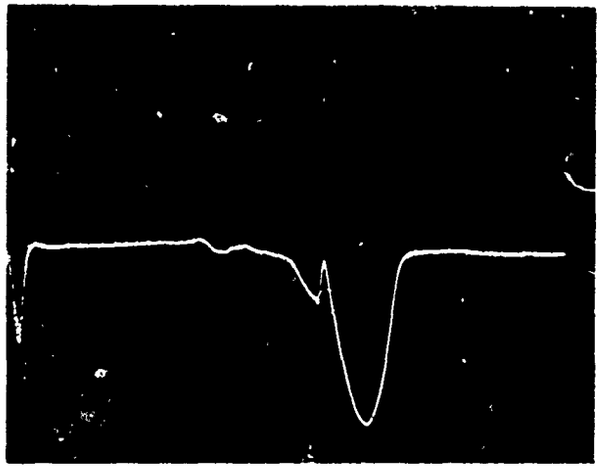

5.0v/cm;0,2msec/cm;
Internal trigger at 2V.

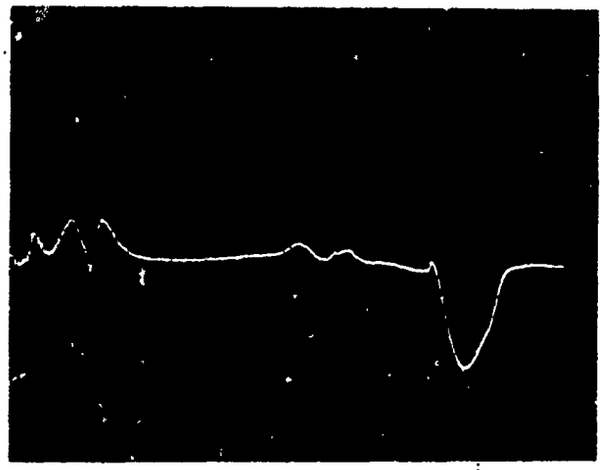

5.0v/cm;0.2msec/cm;
External trigger.

5.0v/cm;0.5msec/cm;
External trigger.

FIG. B.13 OSCILLOSCOPE TRACES SHOWING VARIATIONS OF LIGHT REFLECTED BY THE BULLET INTO THE PHOTOMULTIPLIER

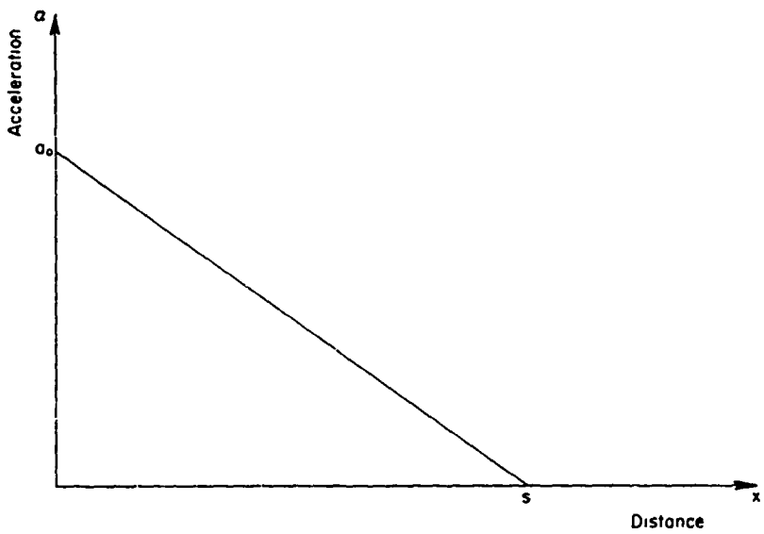

FIG. B.14 ASSUMED ACCELERATION PROFILE AS A FUNCTION OF PROJECTILE TRAVEL DISTANCE IN THE SHOTGUN BARREL

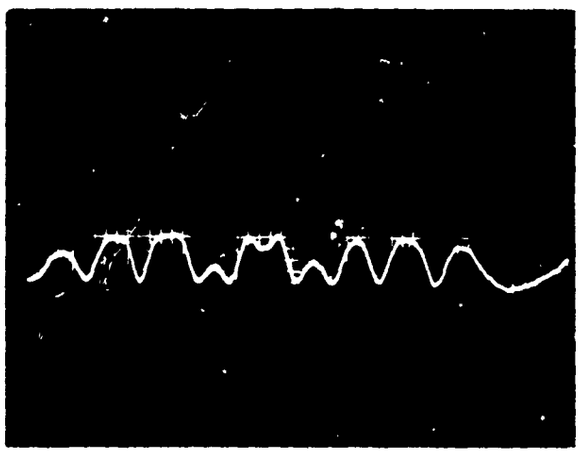

FIG. B.15 INTERFERENCE SIGNAL DUE TO VIBRATIONS OF THE OPTICAL SYSTEM

SCALE: 0.5V/cm
SCALE: 0.5V/cm; 5msec/cm.

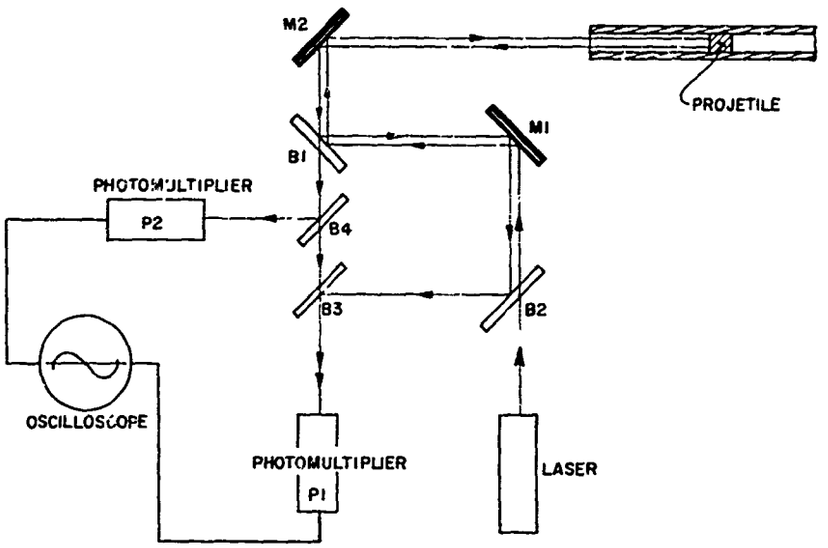

FIG. B.16 SCHEMATIC OF THE MODIFIED EXPERIMENTAL APPARATUS

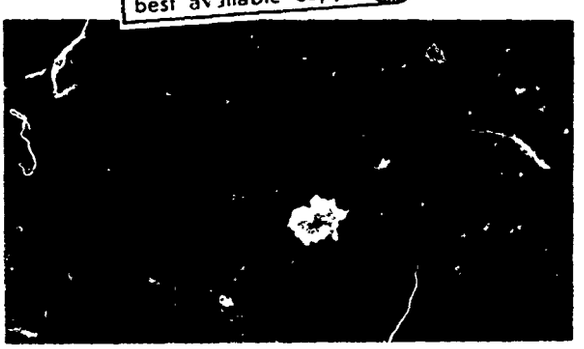

FIG. B.17 OSCILLOSCOPE TRACE OBTAINED USING A DIFFERENTIAL AMPLIFIER

SCALE: 0.5V/cm ;)
SCALE: 0.5V/cm ; 0.5μsec/cm.

APPENDIX C: SUMMARY OF WORK ON THE MK I LAUNCHER AND PROJECTILE INTEGRITY

C.1 Introduction

Some development and operational aspects are described in the following that were done on the MK 1 launcher and also a number of problems that are concerned with the question of projectile integrity. Various projectile materials were tested as well as the effect of locating the projectile in the barrel. This led to attempts to observe the projectile in the barrel with X-ray equipment in order to obtain insight into projectile failure.

Since the conditions at the origin of the implosion chamber were not always repeatable, it would have been difficult to make a consistent study of projectile behaviour using the launcher. It was therefore decided to test projectiles by impacting a stationary one in the barrel by a moving projectile producing high pressures and possible spall. Calculations were made on one-dimensional (plane) impact with spall. The literature on spall was searched and some of this data is being tested for applicability in carrying out calculations using a two-dimensional computer code.

C.2 Evaluation of Impacts on Lead Targets

Measurements were made of the crater sizes produced by plastic projectiles on the early series of runs made by Watson (Ref. C.1) and Flagg (Ref. C.2). These runs were primarily with 0.22 inch barrels and targets were made from lead. The projectiles were mainly polyethylene, with some made of Teflon. The crater depth, diameter, and volume were measured. The velocities were in the low range of hypervelocity impact (up to 8000 ft/sec.) and the craters did not have the expected symmetry and the ratio of diameter/depth did not approach 2, as one would have at high impact velocities.

The data were correlated by the method of Ref. C.3 and are shown in Fig. C.2.1. The factors Z and X are functions of the material properties of the target and projectile. The line shows the curve representing the best fit for a multitude of materials with the points representing the UTIAS polyethylene-on-lead impacts.

On later runs the crater formation was used primarily to monitor the projectile integrity just before impact by observing whether one or several craters were formed and occasionally the crater was used to estimate the velocity of the projectile, usually when the light screen velocity detectors failed to function.

C.3 Summary of Runs Made with the 0.22 and 5/16 Inch Barrels

A number of runs was made with the MK I launcher using both gas and explosive drivers to test various materials and the effect of recessing the projectile.

C.3.1 Test of Some Projectile Materials

A series of gas runs was made to check whether some materials would be suitable for projectiles. This was done with barrels made of stainless steel high pressure tubing, approximately 10 ft. long, at initial gas pressures of 400 psia.

The results for various projectile tests with gas only in the launcher are summarized in Table C.3.1.

TABLE C. 3.1

Run No.	Material	Barrel Diameter (in.)	Projectile Mass (gm)	Velocity (ft/sec.)	Condition after Launch
230	Polyethylene	.312	0.40	5610	intact
231	Carbon	.312	0.65	-	failed
232	Carbon	.312	0.65	4600	failed
233	Titanium	.312	1.73	3810	intact
234	Titanium	.312	1.73	3880	intact
235	Fibre Glass →	.187	0.15	5100	intact
238	Fibre Glass ↑	.187	0.15	5000	failed
239	Fibre Glass ↑	.187	0.14	5650	failed
236	Boron Nitride	.312	0.83	5100	failed
237	Boron Fibres	.187	0.17	4880	intact

The boron fibres were arranged axially and had an epoxy matrix. The largest diameter that could be tested with the specimen obtained was 3/16 inch. The arrows for the fibreglass projectile indicate the alignment of the fibres. The axially aligned fibres were launched intact. An earlier run by Flagg (Ref. C. 2) with an axially aligned fibreglass projectile and an gas driver had shown that the matrix had failed. This made it seem unlikely that resin bonded fibres would withstand launching with an explosive driver with its higher pressures and possibly more uneven load distribution on the base of the projectile, even if strong fibres were used.

C.3.2 Runs with Laminated Magnesium-Lexan Projectiles

A number of runs was made with laminated projectiles and recessing of the projectile away from the origin. The advantage of a laminated projectile is that the tensile stresses caused in the material are lower than in a homogeneous one, as explained in section C.8.5. The materials used were magnesium and Lexan, a half calibre long cylinder of each being bonded together with Eastman 910 contact cement. Figure C. 3.1 shows the entrance configuration used and Table C.3.2 lists the results from these runs. The figure shows the four configurations used: there were two barrel sizes (0.22 and 0.312 inch) and for both runs were made with the projectile located near the entrance of the barrel and with the projectile recessed down the barrel.

TABLE C.3.2

Run No.	Material	Barrel Dia. (in.)	m_{proj} (gm)	m_{expl} (gm)	P_i (psia)	Recess (in.)	Velocity Measured ft/sec)	Calc.	Proj. Condition
242	Mg/Lex.	0.22	0.21	99	200	3/8x2.75	14300	30000	intact
243	Mg/Lex.	0.22	0.21	116	200	-	10800	28800	failed
263	Mg/Lex.	0.312	0.6	130	400	.35x2.75	6900	24800	failed
250	Mg/Lex.	0.312	0.6	130	400	-	12000	23000	intact
274	Ti	0.312	1.73	116	200	3/8x2.75	5740	13800	intact
258	Ti	0.312	1.73	90	200	-	5000	15200	intact

The velocities attained with the 0.22 in. magnesium-Lexan projectiles were the best that have been obtained with the Hypervelocity Launcher. These runs showed that locating the projectile downstream in the barrel made a significant difference in the case of the 0.22 barrel, but did not have much effect on the 0.312 inch barrel. In the 0.312 inch barrel the wall thickness of the tube was 0.125 inch, allowing expansion of the barrel and possible distortion of the projectile, causing its failure.

Calculations that were made to assess the effect of a recess are also listed in Table C.3.2, and show that the trend on the 0.22 inch barrel is the same as obtained experimentally, while in the other cases the correspondence is less good, due to projectile failure.

Table C.3.3 is an overall summary of pertinent projectile runs that were made with the MK I model launcher with various barrels and projectile materials. The explosive driver was PETN, where used, and the gas was a stoichiometric mixture of hydrogen and oxygen.

C.3.3 Conclusions

(a) The data shows considerable scatter, even between runs which have reasonably identical initial conditions. This is mainly ascribed to projectile failure and unsymmetrical implosions, which give rise to unpredictable pressures at the origin.

(b) Variations in the barrel length/projectile diameter ratio do not seem to be important, in line with calculations which showed only small increases in velocity with increased barrel length and experimental data of Watson (Ref. C.1) where the projectile velocity was found to be proportional to $L^{0.2}$.

(c) The variations in projectile mass affected the velocity and from gas runs it appeared that the velocity changes proportional to $m_{proj}^{-.23}$, when the same initial driving pressure is used. In an ideal launcher with infinite chambrage the muzzle velocity depends on the conditions in the driver, barrel length, projectile mass and barrel area. At high velocities or with a cool driver gas, when $u_{proj} \rightarrow \hat{u}_4$ (escape speed of the driver gas) $u_{proj} \sim m^{-.125}$, and at low velocities when $u_{proj} \rightarrow 0.05\ \hat{u}_4$, then $u_{proj} \sim m^{-.43}$. The implosion driven launcher

is not strictly speaking comparable to the ideal chambered driver because of the impulsive loading due to the implosion, but the results show that the velocity variations were in the expected range.

(d) When the efficiency of the launcher is calculated as the ratio of the kinetic energy of the projectile to the total energy in the chamber (gas and explosive internal energy), this varies between 0.05 and 0.5%. Here again the scatter in the data is noticeable due to projectile failures and unsymmetrical implosions.

TABLE C.3.3

Run No.	PROJECTILE Material	Size	Mass gm	Location	P_i (psi)	m_{Expl} gm	L_{Barrel}	Velocity ft/sec	Impact	Source
214	Mg	5/16	.61	0	200	76.3		9000	OK	F
219				0	200	96.8		11600	OK	F
215		3/16		0	200	74.5		-	FAIL	F
216				0	200	70.9		-	"	F
276		.27		0	200	113.6	~ 12'	4960	FAIL	G
204	Polyethy-lene	5/16			200	-		6220	OK	F
205					200	81.3		13500	PARTIAL	F
209					200	209		-	FAIL	
210					200	213.8		7000	FAIL	F
230					400	-	10'-1"	5610	OK	G
213					200	91.5		10500	FAIL	F
206		3/16			200	-	~10'	-	OK	F
207					200	-	"	~ 4000	OK	F
208					200	-	"	4700	OK	F
		.22			200	-	6'	5900	OK	W
					400	-	6'	7200	OK	W
218	Fibre-glass			0	200	90.74		11100	FAIL	F
235	→	3/16		0	400	-	8'-6"	5100	OK	G
238	→	3/16	.151	0	400	-	7'-1"	~5000	FAIL	G
239	→	3/16	.145	0	400	-	9'-4"	~5650	FAIL	G
246	→	5/16	.757	0	400	-	9'-1"	4260	OK	G
237	Boron Fibres	3/16	.167	0	400	-	8'-9"	4880	OK	G
236	Boron Nitride	5/16	.82		400	-	7'-7-3/4"	5100	FAIL	G
231	Carbon	5/16	.65		400	-	9'-8"	-	FAIL	G
232					400	-	9'-6"	4600	FAIL	G
233	Titanium	5/16	1.73	0	400	-	9'-8"	3810	OK	G
234				0	400	-	8'-0"	3880	OK	G
258				0	200	90	9'-0"	~5000	OK	G
259				Recess	200	102	8'-0"	~5000	OK	G
274				Recess	200	116	7'-0"	5750	OK	G
240	Lexan	.22		Recess	400	98.3	3'-7"	14300	FAIL	G
241	Mg/Lex.	.22	.21	Recess	400	102	2'-11"	14800	OK	G
242				Recess	200	99	2'-4-5/8"	14300	OK	G
243				0	200	116.5	4'-7-1/2"	10800	OK	G
245				0	200	116	4'-5-3/4"	12500	FAIL	G
247				Recess	200	209.3	4'-8"	~13500	OK	G
248	Mg/Lex	5/16	.6	0	400	-	9'-0"	4500	OK	G
249				0	400	111.3	9'-0"	12500	PARTIAL	G
250				0	400	130	9'-0"	10-12000	OK	G
251				0	400	115	9'-0"	12100	FAIL	G
261				Recess	400	-	8'-0"	4700	OK	G
263				Recess	200	130	7'-0"	6900	FAIL	G
275				Recess	200	117	9'-0"	5360	FAIL	G

C.4 Stress Wave Propagation Into the Periphery of the Hemispherical Chamber

Calculations were made at UTIAS concerning the stress propagation into the periphery of the implosion chamber due to detonation of the explosive liner, when designs were made for the 30 inch diameter launcher (Ref. C.4). Two approaches were used:

(a) A finite difference scheme (Ref. 5) based on work by Davids and co-workers (Ref.6) and reported in Reference 5.
(b) A finite difference scheme with Lagrangian coordinates using the method presented by Wilkins (Ref. C.7), the results of which are given below.

To calculate the cavity expansion of the implosion chamber, a pressure pulse was applied to the wall of the cavity where the explosive liner would be located. This pulse was based on the calculations of launcher performance (Ref. C.8) and had the form

$$p = p_o \quad (= 57 \text{ kbar}) \qquad 0 < t \leq t_o \quad (= 1 \ \mu\text{sec})$$

$$p = p_o(t/t_o)^{-2/3} \qquad t > t_o$$

The material was assumed to have the following properties:

Young's Modulus	$E = 2040$ kbar
Shear modulus	$\mu = 816$ "
Yield Strength	$Y^o = 3.45$ "
Poisson's ratio	$\nu = 0.25$

Pressure - density relation: $p = 1360(\rho/\rho_o - 1)$ kbar (Ref. C.9).

The radial stress distribution is shown for various times in Fig. C.4.1. An elastic wave and a plastic wave front are moving into the material. Due to the pressure drop on the cavity wall an unloading wave moves into the material, overtaking the compression wave and decreasing its strength. The strength of the elastic wave front does not decrease until the plastic wave has decayed. The radial divergence of the stress waves causes a decrease in their strength, but in this case the decay of pressure on the cavity wall causes a fairly rapid decrease in peak stress transmitted into the material and the peak stress is expected to decay to the elastic limit at about 20 cm. from the surface. Depending on the thickness of the chamber it could be plastically deformed right through. The expected radial expansion of the cavity under these conditions is shown in Fig. C. 4.2. Also shown on this graph is the displacement for a material with a yield strength of 12 kbar in a plane geometry. The greater yield strength of this material results in less displacement, as would be expected. At 20 μsec the cavity has expanded roughly 0.1 cm for $Y^o = 12.2$ kbar and 0.13 cm for $Y^o = 3.45$ kbar. The calculations were not continued long enough to determine how much the cavity would contract again, but it is to be expected that some permanent deformation remains after the run.

In order to protect the chamber walls from the explosive a hemispherical liner is used which also acts as the explosive carrier. Calculations were made for a 10 cm thick liner which might be used with the 30 inch diameter launcher chamber. Copper and lead were considered and the results showed, as expected from considerations of acoustic impedance mismatch between copper and steel and lead and steel, (See also Table 1 in the main text), that copper and lead

cause an increase in the stress transmitted into the steel chamber, although copper causes a lower stress than lead.

C.5 X-Ray Observations of the Projectiles

In order to obtain more information about the projectile behaviour during launching, use was made of flash X-ray units to observe the projectile in the barrel after it has left the region of the top plate. A schematic diagram is shown in Fig. C.5.1. The closest one could observe the projectile from the origin of the hemisphere was the thickness of the top plate on the MK I launcher, which is about 7 inches. The lead separating screen prevented exposure of a cassette by an adjacent X-ray tube. The flash X-ray unit was a 300 kV Field Emission model which could penetrate a high pressure tube of 5/16 inch. I.D. and 9/16 inch. O.D. The timing of the X-ray system was achieved by computing the time-distance curve for the projectile and making corrections to the projectile path.

Typical computed x-t paths are shown in Figs. C.5.2 and C. 5.3. It was found that for the type of run being made (about 100 gm PETN and gas with 400 psi initial pressure) a reduction of 60% in the displacement from the calculated value allowed X-ray shots to be taken of the projectile at distances from 30 to 65 cm from the origin of the hemisphere. Figure C.5.2 shows the results for projectiles made of a half calibre magnesium and half calibre Lexan cemented together. These projectiles are not visible very well in the X-ray shots, since the magnesium and Lexan do not absorb enough energy in comparison to the barrel and also it is possible that the Lexan part of the projectile was damaged. In one case the X-ray shot showed a projectile which was at an angle in the barrel and this corresponded to an off-centre implosion which must have tilted the projectile.

Figure C.5.3 shows the results for titanium projectiles. Since the titanium absorbs more energy than the magnesium, identifying the projectile was easier and up to 90 cm the measured and corrected paths are fairly close. Runs were made with the projectile initially located at the origin of the chamber and with the projectile recessed 8 cm down the barrel. In both cases the 60% reduction from the calculated displacement agreed closely with the measured positions. These runs indicate that the pressures used in the calculations are too high and probably the approach of Elsenaar (Ref. 11), using an integrated pressure over the barrel area should give results closer to the measured values.

Further runs were made with a stationary projectile (magnesium-Lexan) located near the end of the barrel, which was impacted by a titanium projectile accelerated by the launcher. The purpose of these runs was to test the feasibility of making this kind of impact run to simulate conditions near the origin where the pressure is not known, and not repeatable. If the impact velocity is known, the pressures and deformations can be calculated.

The runs were made with gas drivers since impact at about 1.5 cm/μsec would cause pressures up to 100 kbar to occur. The impacing velocity was measured with contact pins spaced 6 inches apart. The problem here proved to be the timing of the X-ray units, since the contact pins sometimes triggered before the titanium projectile arrived, probably due to gas leaking around the projectile, causing a shock wave to trigger the gauges before the projectile passed them. The barrel was evacuated to the range pressure of about 1 mm Hg.

Since it would be of interest to recover the projectile after a run for visual examination, "end caps" were tried at the end of the barrel to catch the projectile. These consisted of a heavy piece of metal with a blind hole of the barrel bore diameter in it and with a sliding fit on the end of the barrel, as shown schematically in Fig. C.5.4. This recovery scheme was tentatively tried, since it would assure that the general shape of the projectiles was retained. Impacts into other softer materials were thought to be more likely to cause nonuniform deformation and possible break-up of the projectile. The impact in the bottom of a hole could be cushioned by having a low pressure gas between the end cap and the stationary projectile, which would be compressed and cause a slightly more gradual retardation, but this was not attempted in this series of runs.

A total of four runs was made with end caps. Points of interest are:

(a) The 5/16 inch I.D. barrel with its 1/8 inch thick walls expanded about 0.030 inch at the location where the impact occurred. This can be expected, since the pressures generated on impact exceed the yield strength of the material.

(b) A solid magnesium projectile was recovered intact from the end cap, although it did expand when it impacted on the bottom of the hold in the end cap. This expansion could be decreased by an air cushion as mentioned above.

(c) Magnesium-Lexan projectiles seemed to decelerate the titanium projectile more than the solid magnesium projectiles. The titanium was wedged into the barrel in two such runs. The Lexan was not recovered, and the magnesium was damaged, possibly due to gas leakage around the titanium projectile.

(d) The impact velocities were around 2500 ft/sec, which is lower than one would have expected for the initial pressure used, since usually velocities around 3800 ft/sec could be achieved with the same pressure in the driver. The reason for this is not clear, unless gas leakage and gas build up between the two projectiles decelerated the titanium projectile significantly before impact.

(e) To use this method one would have to prevent the gas leaking around the impacting projectile and be able to recover the stationary projectile without great deformation, which might mask the results one may be looking for. This made it seem more desirable to use a rifle to accelerate the projectile, which would have a lower peak pressure and the projectile would have to be made with a seal.

The best X-ray shots of the projectile can be obtained in free flight after leaving the barrel. A schematic view is given in Fig. C. 5.5 of the arrangements used. The steel barrel is connected to the dump tank by a Perspex tube and the stationary projectile was located just before the end of the barrel. The impact velocity was again obtained by contact pins and the X-ray shots were triggered by breaking a wire running normal to the axis of the barrel by the projectile. This kind of shot yields information on the exterior dimensions of the projectile but does not readily point up failure due to spallation, unless the material actually separates into sections. If only internal spalling occurs there will be little change in material thickness penetrated by the X-rays and hence there will be no change in the image

recorded on the photographic plate.

C.6 Calculations On One-Dimensional Spall

In order to predict projectile behaviour one would have to know the material properties and the forces acting on the projectile. If the forces are symmetric about the axis one can use a cylindrical coordinate system, which requires two space and one time variable and a large number of points have to be treated when the problem is cast in finite difference form. The problem would be simplified if one could consider a one-dimensional situation with only one space variable.

Some one-dimensional calculations were made for the following cases:

(a) Impact of a moving projectile on a stationary one.
(b) Application of a pressure pulse on the base of a projectile.

The numerical scheme used is the same as for the launcher performance calculations, except that equations of state were used which described the metals considered. The spall criterion is that given by Whiteman (Ref. C.10) which relates the maximum tensile strength to the rate of change of stress at a point.

The cases run under (a) are summarized below:

Materials	Impact Velocity (mm/μsec)	Spall
Cu → Al	0.4	No
	1.0	Yes
Al → Al	0.4	No
	0.72	No
	0.9	No
	1.0	Yes

These calculations, while not giving the precise limits at which spall could be expected to occur, did show that for the size of projectile considered (1 cm diameter) the impact velocity should be of the order of 1 mm/μsec.

A series of runs was made under (b) which examined the effect of peak base pressure and pressure decay rates. The basic pressure profile was based on work from Ref. C.11 which yields the average pressure on the projectile base and the implosion time. The base pressure was approximated by

$$p = p_c(t/t_\theta) \qquad t \leq t_\theta \quad (t_\theta \text{ - implosion time})$$

$$= p_\theta(t/t_\theta)^m \qquad t > t_\theta$$

The pulse shape is shown in Fig. C.6.1 and the results are plotted in Fig. C.6.2 for a decay rate of $m = -1$. Only the maximum pressure $p_\theta = 100$ kbar caused failure. The effect of changing the rise time by a factor of three is to lower the tensile stress by about 16%, which indicates a small dependence on t_θ. It was also estimated that the peak tensile stress is proportional to the square root of the decay rate m, which would make this a more important

factor when considering the effect of loading on a projectile. These figures apply only over a small range, since when t_o is made large compared to the transit time of a sound pulse through the projectile, the decay rate will be less important on the tensile stress caused.

C.7 Two-Dimensional Calculations of Projectile Impact

Since the projectile, when it is launched, is able to deform both radially and axially, a two-dimensional approach would lead to a better representation than the one-dimensional model. Work on this has been done by Watson and Godfrey (Ref. C.12) and Mitchell (Ref. C.13) and is presently being carried on at UTIAS (Ref. C.14). The results show that the barrel wall expansion causes unloading waves to decrease the strength of the pulse propagating through the projectile. Not enough data is available at the moment to judge whether any detrimental effects occur which might cause reinforcement of the tensile waves. The radial expansion at the periphery of the projectile and the uneven stress distribution across a diameter results in larger axial velocities at the axis and hence a bulging of the projectile at the centre line.

Figure C.7.1 shows the axial pressure distribution at two radii at times 0.5 and 1.0 μsec after the collision of a titanium projectile with an aluminum projectile in a barrel of 0.8 cm diameter. The barrel wall is chosen thick so that reflected waves from the outer wall will not affect the projectile in the early stages of the collision. Figure C.7.1(a) shows the hydrostatic pressure along the centre line of the projectile and near the circumference at the barrel wall at 0.5 μsec after impact. The difference in pressure along the two lines is due to radial expansion near the barrel wall which results in a rarefaction wave propagating into the centre of the projectile while a compression wave propagates outward through the barrel wall. In Fig. C.7.1(b) at 1 μsec a rarefaction wave is reflecting from the left free surface and the shock moving into the aluminum is close to the front end of the projectile. The elastic wave is hardly seen because of the low value of the yield strength, (5.2 kbar for Ti and 2.8 kbar for Al) compared to the hydrostatic pressure developed in the impact. Computations are presently being made to understand the projectile behaviour in the barrel and to obtain limits up to which the projectile should be able to withstand the accelerations, using spall data from the literature. Figure C.7.2 shows the deformation of the projectiles and the barrel wall at 2.0 μsec. The barrel expands at the collision plane of the projectiles and compresses the front end of the aluminum projectile due to differences in the sound speed of the two materials.

C.8 Considerations in Projectile Integrity

C.8.1 Introduction

The pressures generated in the Hypervelocity Launcher create severe conditions under which the projectile is accelerated. Attention had to be given to this aspect when the amount of energy, and hence the peak pressures generated, was increased. There were generally no problems in launching projectiles with gas only as the driver, but when an explosive driver is used the pressures generated are of the order of 100 kbar (according to calculations by Sevray (Ref. C.16) and projectiles were more likely to fail and various measures were taken to improve the performance of the projectiles.

C.8.2 Launcher Geometry and Conditions at the Entrance

The geometry of the launcher has been described in a number of reports (Ref. C.1 and C.2) and here the interest is centred around the origin of the chamber and the barrel entrance. The implosion converges on the origin either driven by the explosive or the reflection of the detonation wave from the cavity wall in a gas only case. The pressure peaks at the centre and drops off radially. Pressure histories at the centre have been calculated by Sevray and others and a typical profile is shown in Fig. C.8.1. Radial pressure profiles have been given by Flagg (Ref. C.2) and this is shown schematically in Fig. C.8.2.

Since the projectile has a finite area over which the accelerating pressure is acting (typically 8 mm diameter) the pressure on the area is not uniform if the projectile is placed at the origin of the hemisphere. The pressure in the implosion rises above 100 kbar and drops off with radius as $r^{-1.5}$, so that a doubling in the radius represents a drop in pressure by a factor of 2.8. Hence a non-uniform pressure acts on the base of the projectile which is not desirable.

C.8.3 Forces Acting on the Projectile

The purpose of the launcher is to accelerate the projectile to high velocities (of the order of 50,000 ft/sec). Ideally this would be done with the application of a pressure profile on the base of the projectile which rises with time and accelerates the projectile over the whole length of the barrel. The pressure on the base should be uniform so that shear deformation in the projectile is avoided. In the implosion-driven launcher the transition from the hemispherical chamber to the barrel causes a rather complex system of waves which propagates through the projectile and the chamber and barrel walls. This is outlined in the following section.

When the implosion occurs stress waves are caused in the metal of the top plate or conical liner plate. These waves converge towards the origin and cause compression of the barrel and of the projectile as shown in Fig. C.8.3. As the gas shock front enters the barrel, the barrel walls will again expand and the projectile will be accelerated. Since the pressures are high, the metal will be in the plastic state and stress waves propagate through the projectile and the barrel walls. A shock is reflected upstream into the gas from the projectile - gas interface. The barrel expansion will decrease the driving pressure. The stress wave propagates through the projectile and reflects from the front surface as a rarefaction wave. This wave will propagate upstream and interact with the unloading wave due to expansion of the gas after the implosion travelling downstream in the projectile. This interaction can cause tension as explained in the next section. When the rarefaction wave reaches the rear free surface of the projectile another reversal of stress occurs and a shock wave will propagate downstream, while a rarefaction wave will propagate upstream. This sequence is illustrated in Fig. C.8.4.

The projectile is thus accelerated by stress waves propagating through the material and seen on a small time scale the particles are subjected to jumps in velocity whenever they are processed by a wave. On a larger time scale the projectile will seem to be accelerated rapidly by the pressure pulse from the implosion and further acceleration can take place when another wave caused by subsequent implosions overtakes the projectile in the barrel.

In the beginning of the motion the projectile is forced against the

wall by the radial expansion that takes place and there will be friction. The effect of this seems, however, to be low in terms of velocity. The maximum shear stress would be the shear strength of the material. The radial stress drops off as the pressure decreases behind the projectile and friction should decrease.

C.8.4 Possible Failure Mechanisms of the Projectile

The projectile may fail mainly due to the following mechanisms:

(a) Spallation
(b) Nonuniform Base Pressure

(a) Spallation - For a description of this phenomena see for example Ref. C.15. The conditions which lead to spallation are usually a pressure pulse which is followed by an unloading wave. Reflection of the pressure pulse form the free surface causes a reflected rarefaction wave to travel upstream and interaction of this with the unloading wave causes tension and this can lead to failure. These conditions are possible in the launcher because the pressure drops off rapidly after the implosion has occurred.

(b) The other possible mode of failure is due to nonuniform base pressures. This can mean either that the pressure is not uniform on the base but radially symmetric, or still worse, that the peak pressure occurs off-axis. If the pressure is not uniform the wave travelling down the projectile is not plane, since the wave speed depends on the compression and deformation is not uniform across the diameter of the projectile. It was found that placing the projectile downstream in the barrel increased the changes of survival. This would be due to changes in the pressure history and a more uniform pressure pulse which moves down the barrel bore. That off centre implosions affect the projectile was seen in an X-ray shot which showed a projectile with its base at an angle, and the state of the barrel entrance indicated that an off-centre implosion had occurred.

C.8.5 Means of Preventing Failure

In order to obtain a projectile that survives the launch and comes out intact from the barrel the following can be verified.

1. Material Choice: The ideal should be a super-strong material which does not break. This is unfortunately not available yet. The compromise one has to make is to choose a material with a high yield strength and a low density. Since the aim with a hypervelocity launcher is to obtain velocities in the meteoroid range (over 11 km/sec) the density has to be kept low, but low density materials generally exhibit lower yield strength. There are composite materials available which have high strength fibres imbedded in a matrix. Although these can achieve high strength in tension, their performance is doubtful in the launcher application because of the shear forces which act on the projectile due to uneven loading on the base. The material which was used most for the projectiles in the launcher was a titanium alloy which had a yield strength of about 120,000 psi with a density of 4.5 gm/cm^3.

2. Pulse Shape: The base pressure history is the most important parameter in the launcher since it determines the velocity attained by the projectile and the

acceleration which it is subjected to. Ideally the pressure profile should be continuously rising, or if there is a sharp front and pressure jump, the pressure after this should decay only gradually and should be such that after the pressure wave has reflected from the front of the projectile as a rarefaction wave and has reached the rear end, the pressure on the base has decayed by less than the yield strength of the material in tension. Figure C.8.5 shows the pressure distribution at a time when the wave has reflected back to the rear of surface of the projectile. The dotted lines indicate the shape of the incident and reflected waves. The base pressure has dropped from its initial value of p_o to p_1 and the material near the rear surface is under a tension of $p_T = p_1 - p_o$. If no tensile failure is to occur, Δp ($= p_1 - p_o$) should be less than the yield strength in tension Y^o.

If there is no control over the rate at which the base pressure decays due to the gasdynamics of the launcher, the rate of pressure drop $\Delta p/\Delta t$ should be such that in the time $\Delta t = 2L/c_o$ that it takes for the pressure wave to reflect back to the rear surface, the pressure on the base has not dropped by more than the yield strength.

i.e., if $\Delta p = Y^o$

then $\Delta p/\Delta t = \dfrac{Y^o c_o}{2L}$

This means that for fast decaying pressures the projectile should have a high yield strength, high sound speed and be as thin as possible. This would point to thin metallic projectiles. The launching of disks, however, where the ratio of length to diameter is small is only possible when the pressure is uniform on the base. In the UTIAS implosion driven launcher the base pressure is not uniform and the launching of disks is not feasible, however, projectiles with a half-calibre length have been launched successfully.

As was mentioned earlier, location in the barrel has an effect on the launching, since this changes the loading on the projectile, making it more uniform the further away from the barrel entrance the projectile is placed.

3. Laminated Projectiles For a given base pressure the pressure history in the projectile can be changed by using layers of various materials which have different acoustic impedances (product of density and sound speed). This can be achieved by having a stiff material upstream and a soft one downstream. This results in a reflected rarefaction wave from the interface of the two materials, which is lower than if there had been only one material with a free surface. This is shown schematically in Fig. C. 8.6 where $(\rho c)_I > (\rho c)_{II}$.

A combination magnesium-Lexan projectile was tested and gave satisfactory results, although the results were also affected by projectile location and it cannot be said whether the projectile survived due to location or material combination.

C.8.6 Conclusions

The projectile integrity problem is one of the limitations in the use of the hypervelocity launcher and it seems that one has to investigate what is happening to the projectile in the early launching period. This is presently being done by numerical simulation of the launching process and should give insight on the forces that are acting on the projectile and the limits to which

one could expect the present engineering materials could be subjected when used as projectile materials.

References

C.1 Watson, J. D. — Implosion-Driven Hypervelocity Launcher Performance Using Gaseous Detonation Waves. UTIAS T. N. No.113 May, 1967.

C.2 Flagg, R. F. — The Application of Implosion Wave Dynamics to the Hypervelocity Launcher. UTIAS Report No.125, June, 1967

C.3 Bouma, D. D. Burkitt, W. C. — Multivariable Analysis of the Mechanics of Penetration of High Speed Particles. NASA CR-664, December, 1966.

C.4 Dawson, V. C. D. Waser, R. A. Oakes, D. O. — The MK II Implosion-Driven Hypervelocity Launcher Design Analysis. UTIAS T.N. No.147, March, 1970.

C.5 Garg, S. K. — Numerical Solution for Spherical Elastic-Plastic Wave Propagation. ZAMPvol 19, pp.778-787, 1968.

C.6 Davids, N. Metha, P. K. Johnson, P. K. — Spherical Elastic-Plastic Waves in Materials. Behaviour of Materials Under Dynamic Loading. ASME, New York, p.125-137, 1966.

C.7 Wilkins, M. L. — Calculation of Elastic-Plastic Flow. Methods in Computational Physics. Vol.3. Academic Press, New York, 1964.

C.8 Flagg, R. F. Mitchell, G. P. — An Optimization Study of the UTIAS Implosion-Driven Hypervelocity Launcher MK II. UTIAS T.N. No. 130, December, 1968.

C.9 Taylor, J. W. Rice, M. W. — Elastic-Plastic Properties of Iron. J. Applied Physics. Vol.34, No.2 February, 1963.

C.10 Whiteman, P. — Preliminary Report on the Effect of Stress Rate on Dynamic Fracture of Steel, Brass and Aluminum. UNDEX 445, AWRE (U.K.) October, 1969.

C.11 Elsenaar, A. — A Numerical Model for a Combustion Driven Spherical Implosion Wave. UTIAS T.N.No. 144, October, 1969.

C.12 Watson, J. D. Godfrey, C. S. — An Investigation of Projectile Integrity Using Computer Techniques. Physics International. PITR 67-10, February,1967.

C.13 Mitchell, G. P. — A Computer Simulation of Projectile Collision in a Barrel. B.A.Sc.Thesis, University of Toronto, September, 1969.

C.14 Graf, W. O. — A Study of Projectile Integrity Under Extreme Conditions. Ph.D. Thesis (in progress), University of Toronto.

C.15 Rinehart, J. S. Pearson, J. — Behaviour of Metals Under Impulsive Loads. ASME. Cleveland, Ohio. 1954.

C.16 Sevray, P. A. L. — Performance Analysis of UTIAS Implosion-Driven Launcher, UTIAS T.N. No.121, January, 1968.

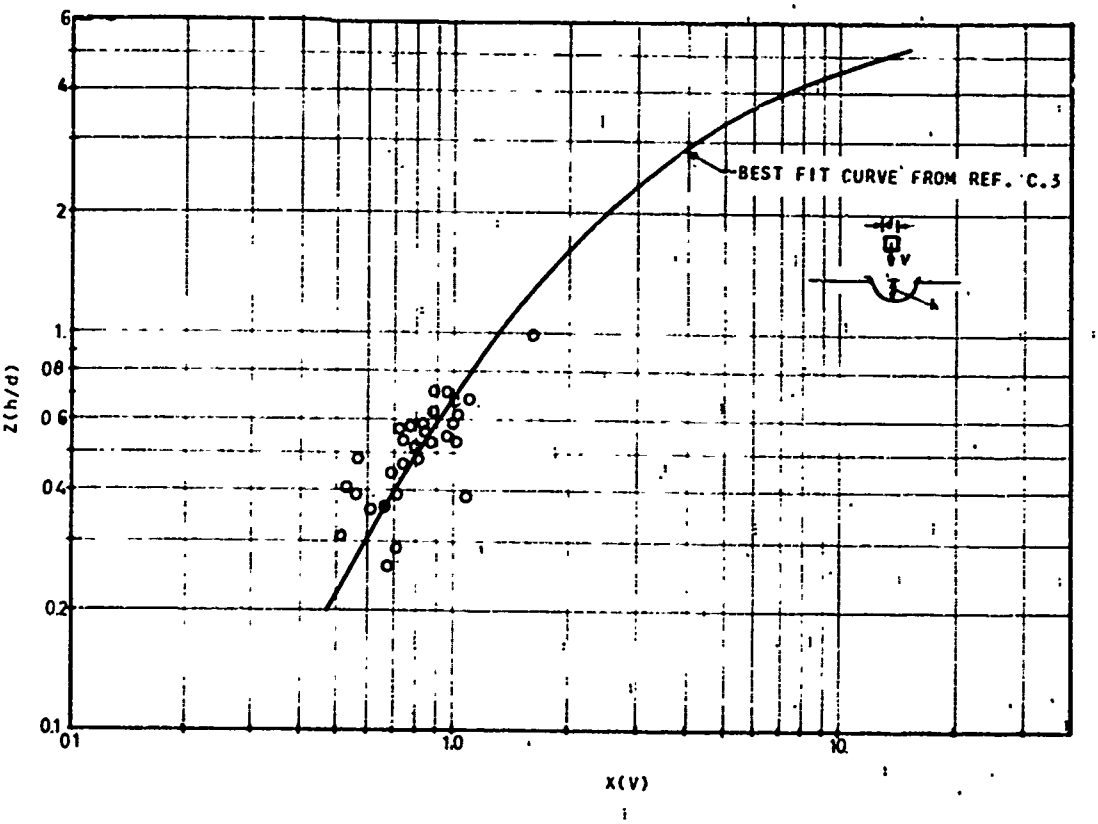

FIG. C.2.1 CORRELATION OF CRATER DEPTH AND PROJECTILE VELOCITY FOR LEAD TARGETS

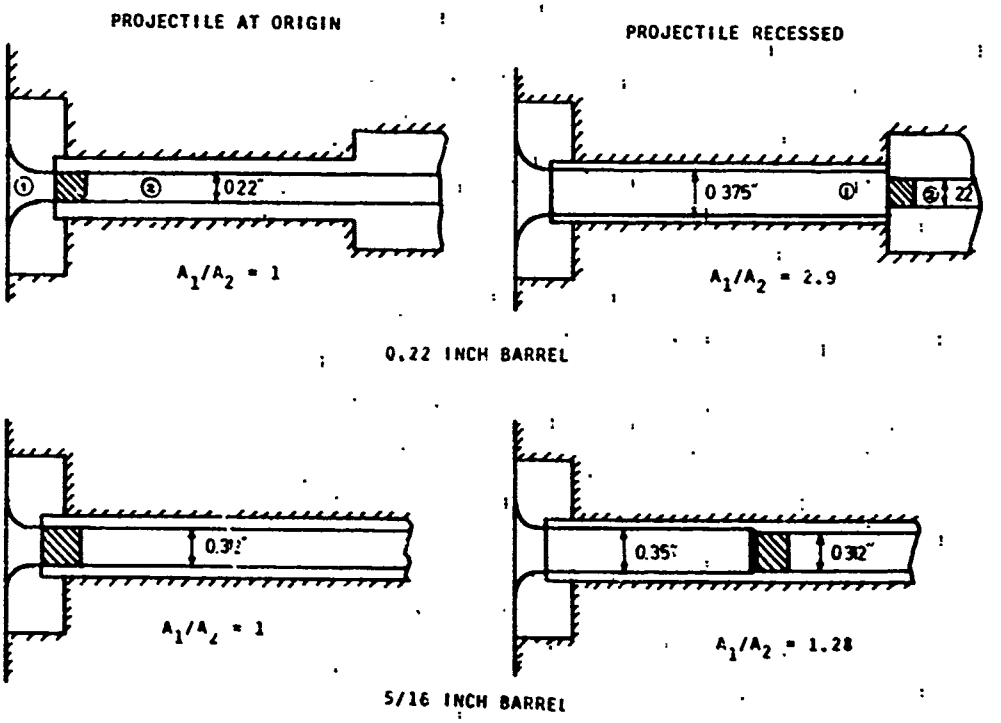

FIG. C.3.1 ENTRANCE CONFIGURATIONS FOR RECESSED AND UNRECESSED PROJECTILE LOCATIONS

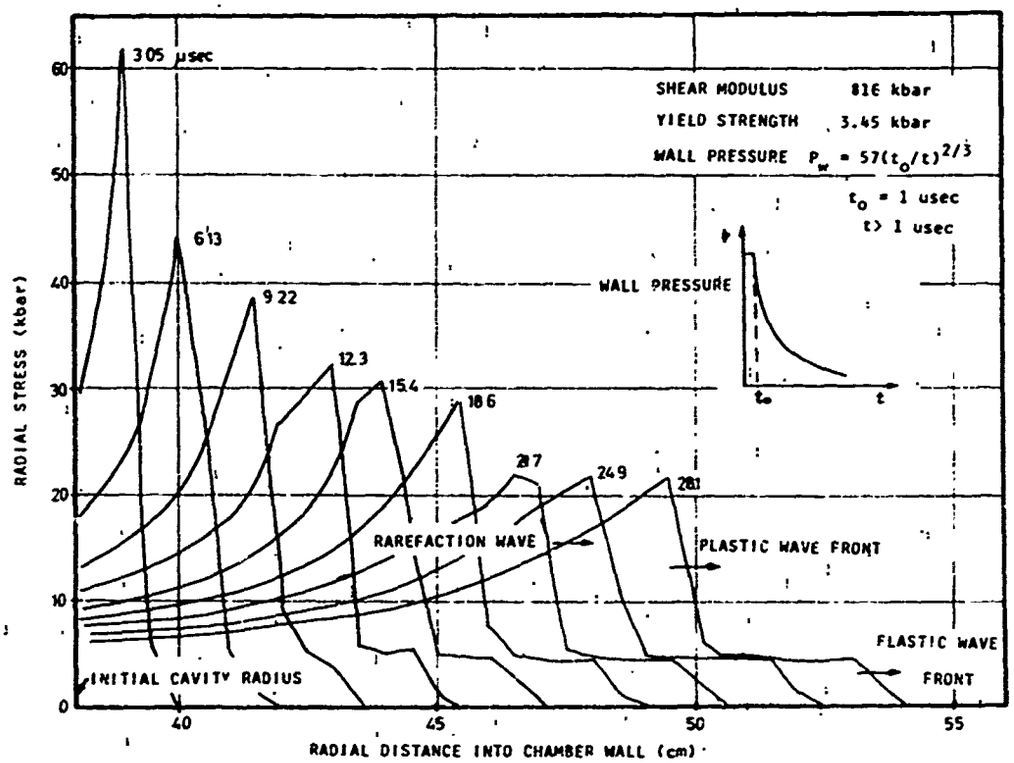

FIG.C.4.1 RADIAL STRESS PROFILES IN A 30 INCH DIAMETER CHAMBER

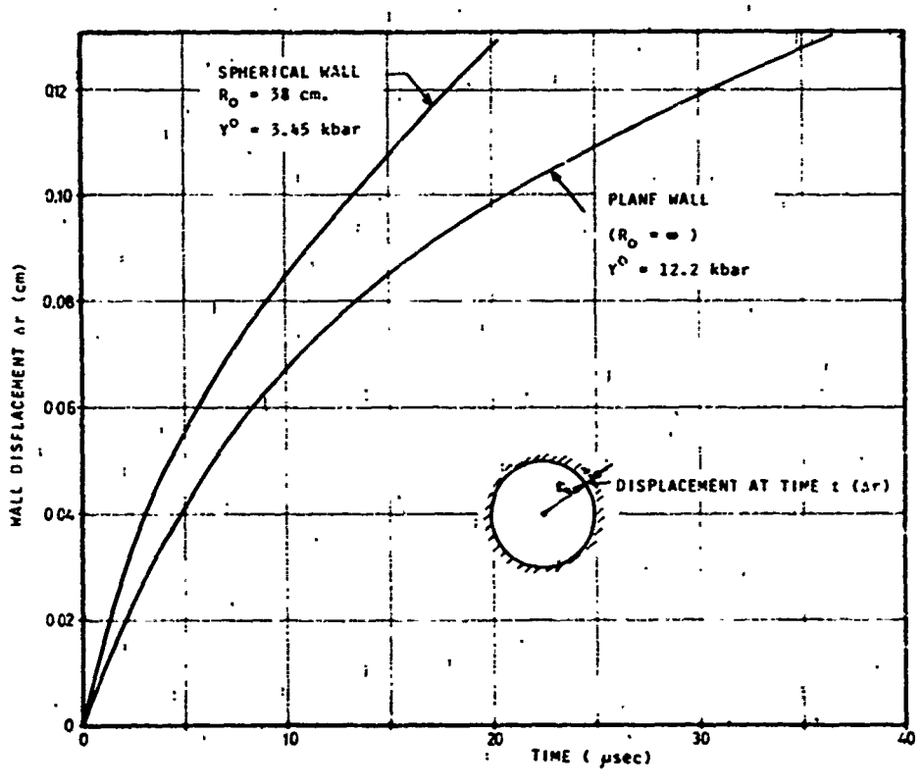

FIG. C.4.2 DISPLACEMENT OF CAVITY WALL WITH APPLIED PRESSURE PULSE

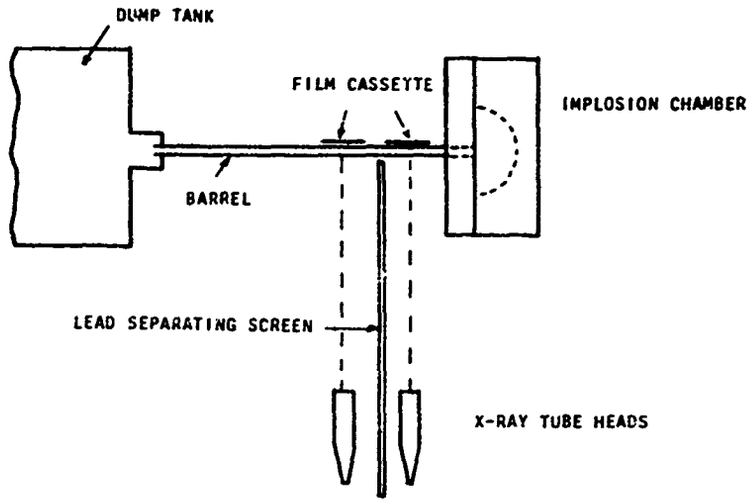

FIG. C.5.1 SCHEMATIC DIAGRAM OF ARRANGEMENT TO OBTAIN

X-RAY SHOTS OF THE PROJECTILE WHEN LEAVING THE IMPLOSION CHAMBER

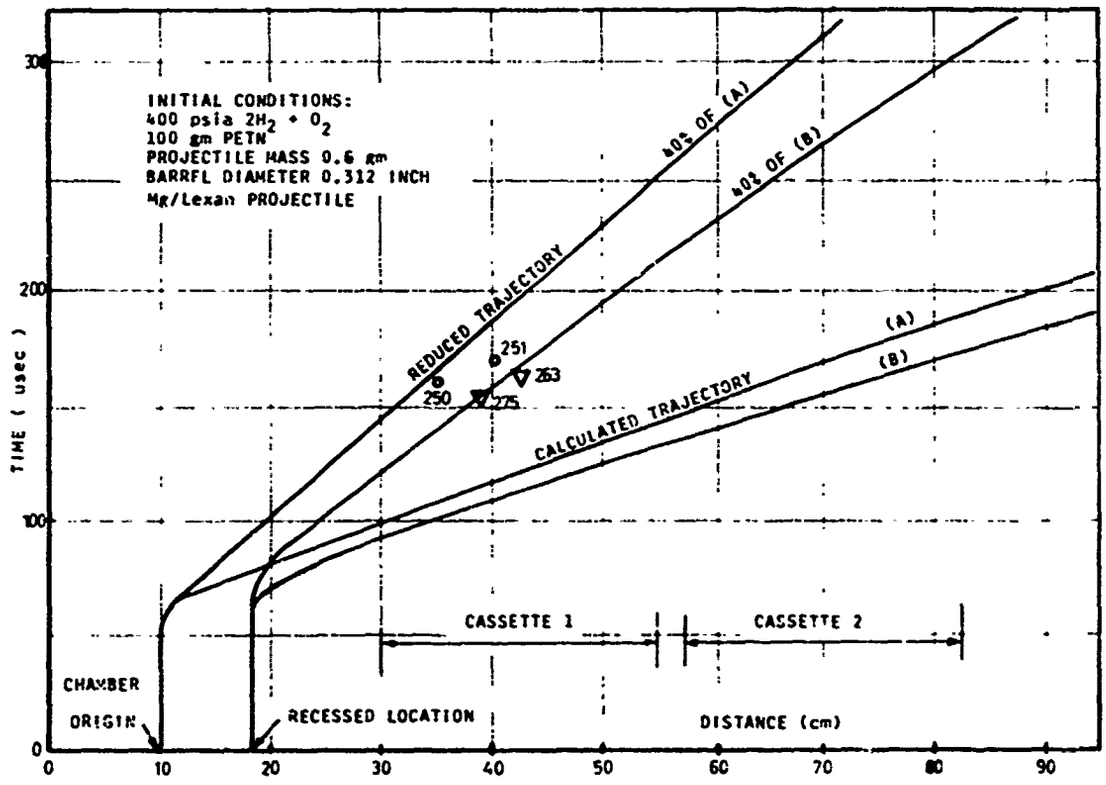

FIG. C.5.2 CALCULATED x-t PLOTS OF PROJECTILE MOTION AND OBSERVED LOCATIONS FROM X-RAY SHOTS.

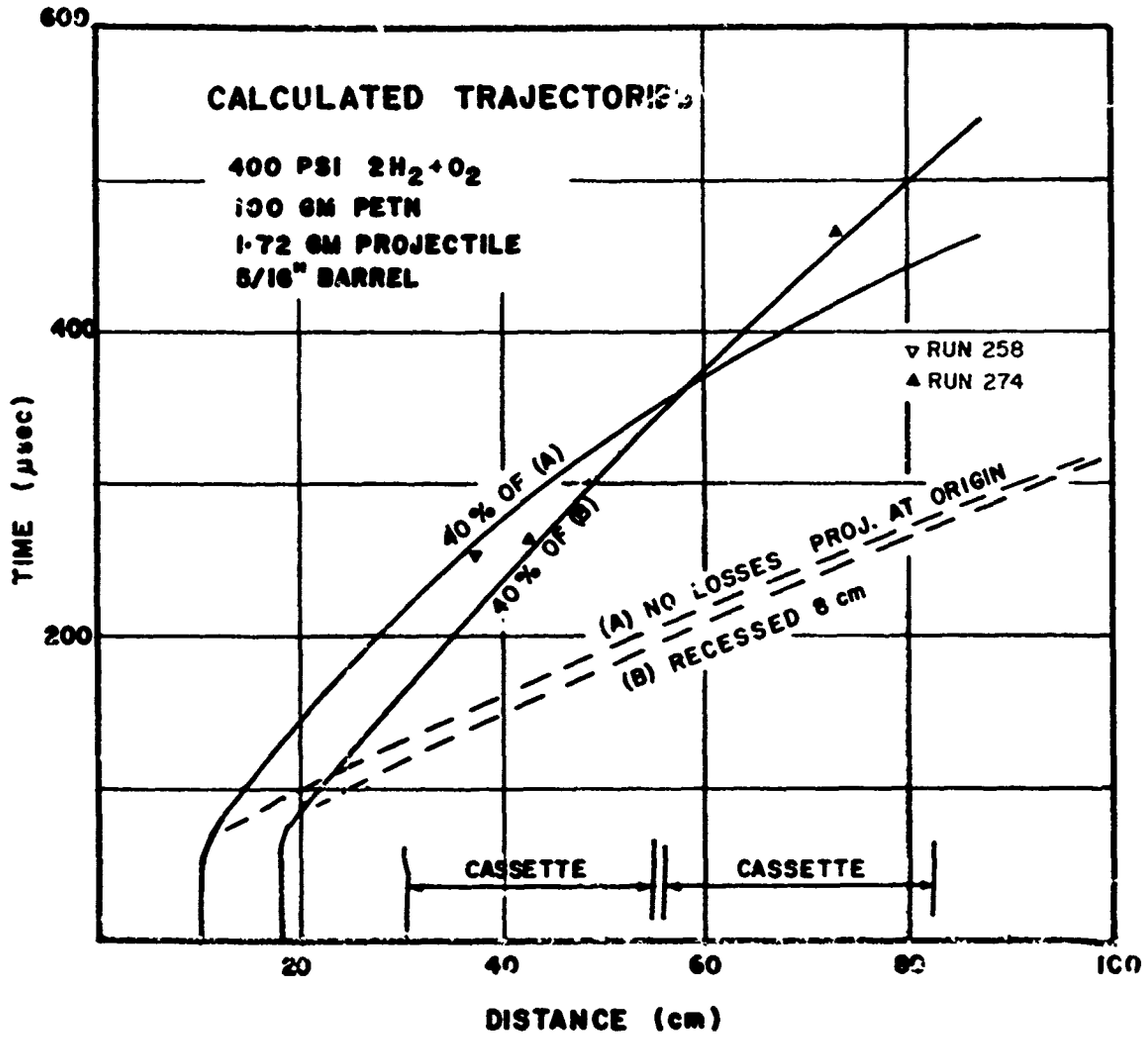

FIG. C.5.3 CALCULATED X-T PLOT OF PROJECTILE MOTION IN BARREL AND OBSERVED PROJECTILE LOCATIONS FROM X-RAY SHOTS

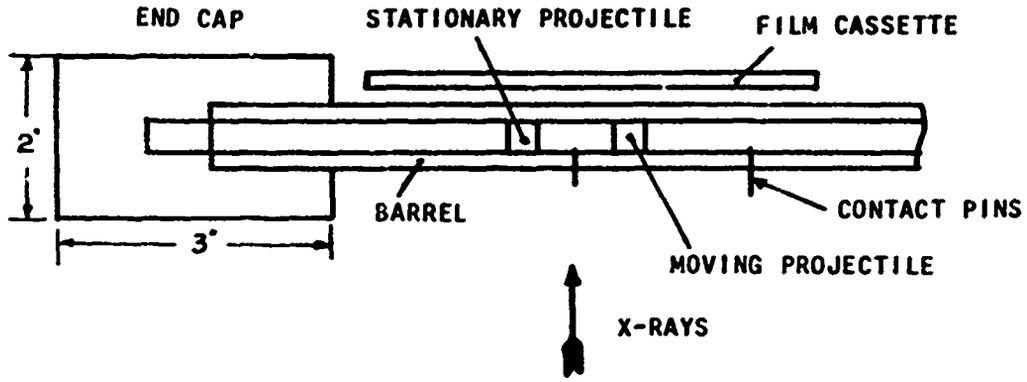

FIG. C.5.4 SCHEMATIC OF 'END CAP'

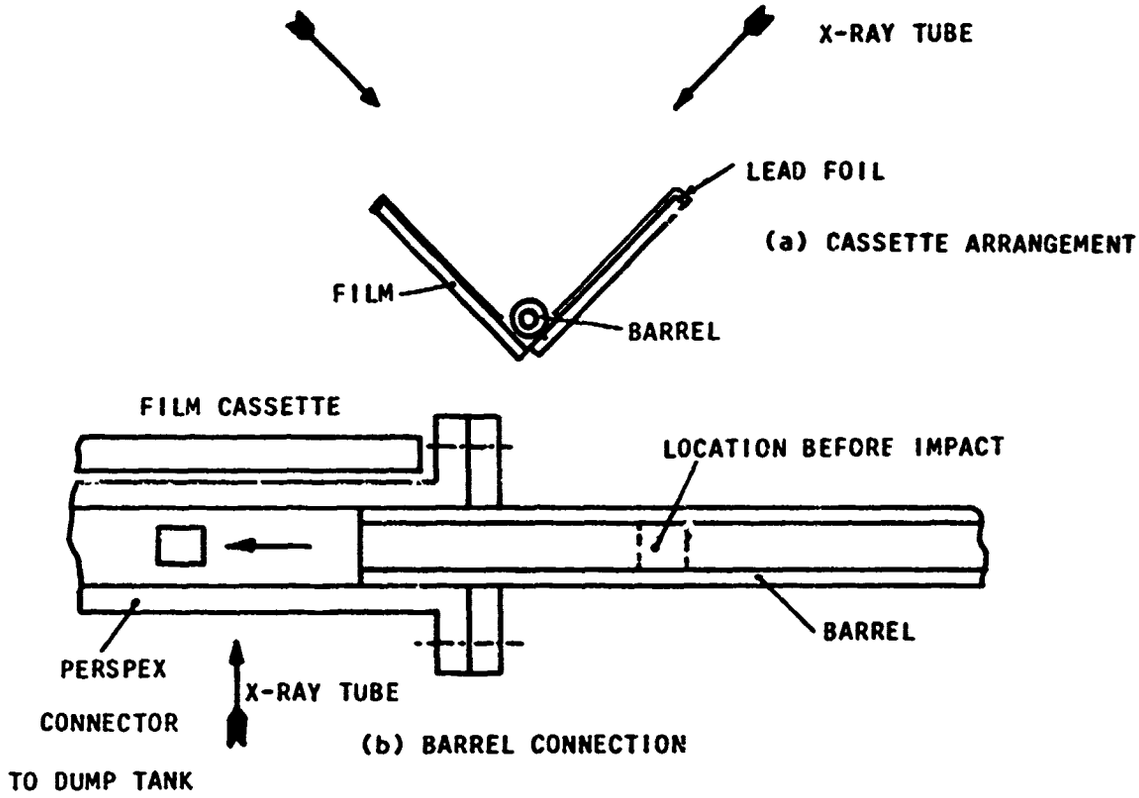

FIG. C.5.5 FREE FLIGHT X-RAY SHOTS

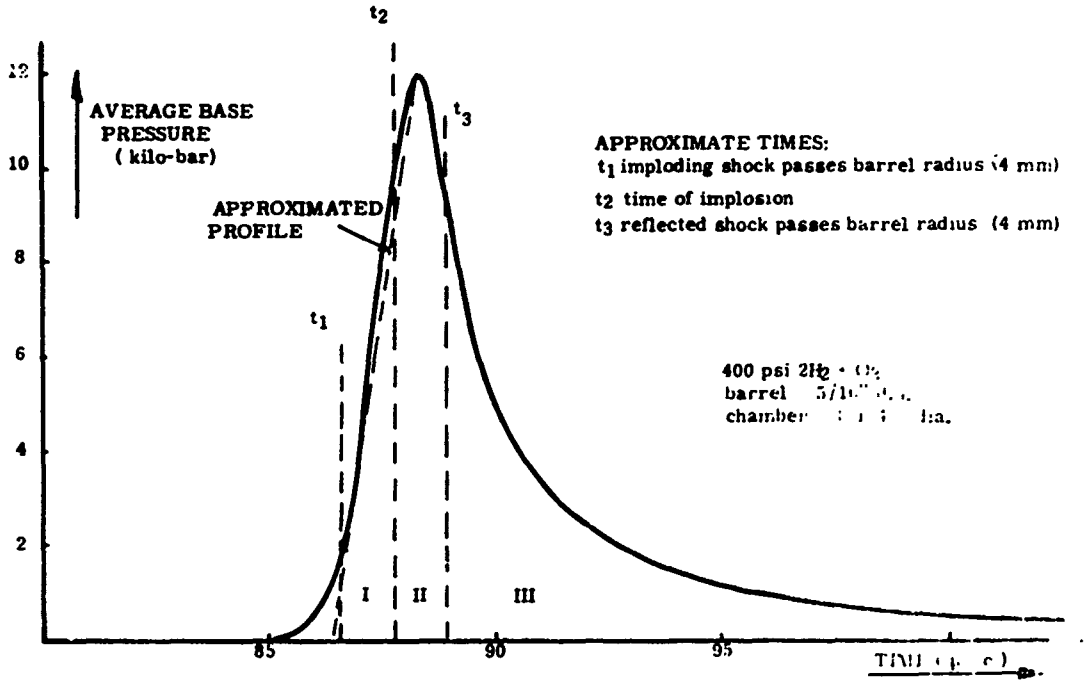

FIG. C.6.1 COMPUTED BASE PRESSURE ON PROJECTILE (REF. C.11)

FIG. C.6.2 PEAK TENSILE STRESSES IN ALUMINUM PROJECTILES AS A FUNCTION OF BASE PRESSURE

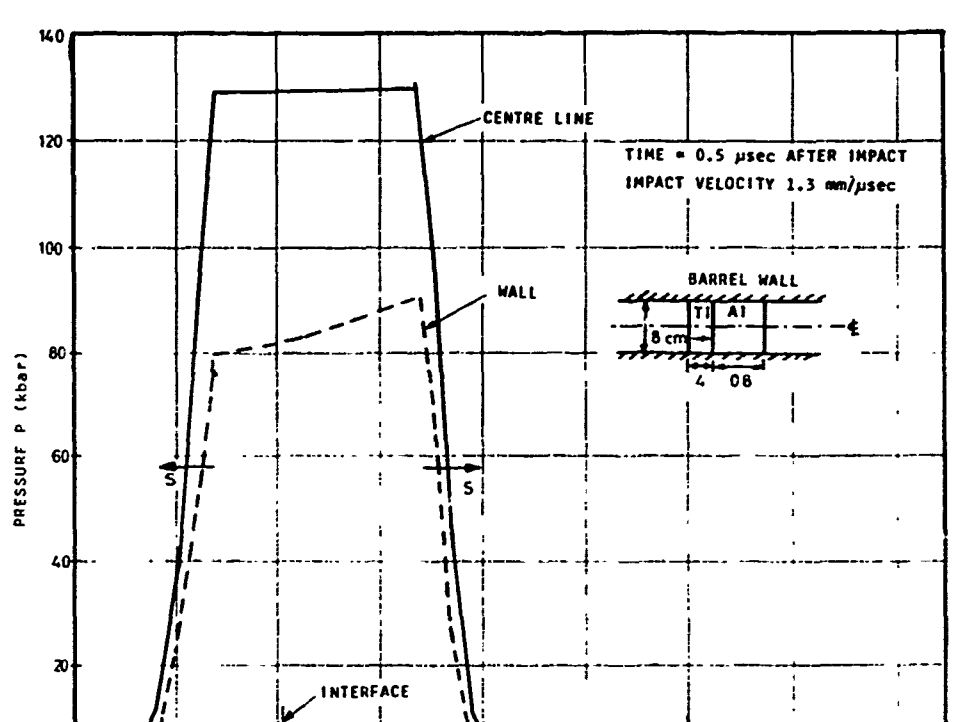

FIG. C.7.1(a) AXIAL PRESSURE PROFILES IN Ti - Al COLLISIONS IN A STEEL BARREL

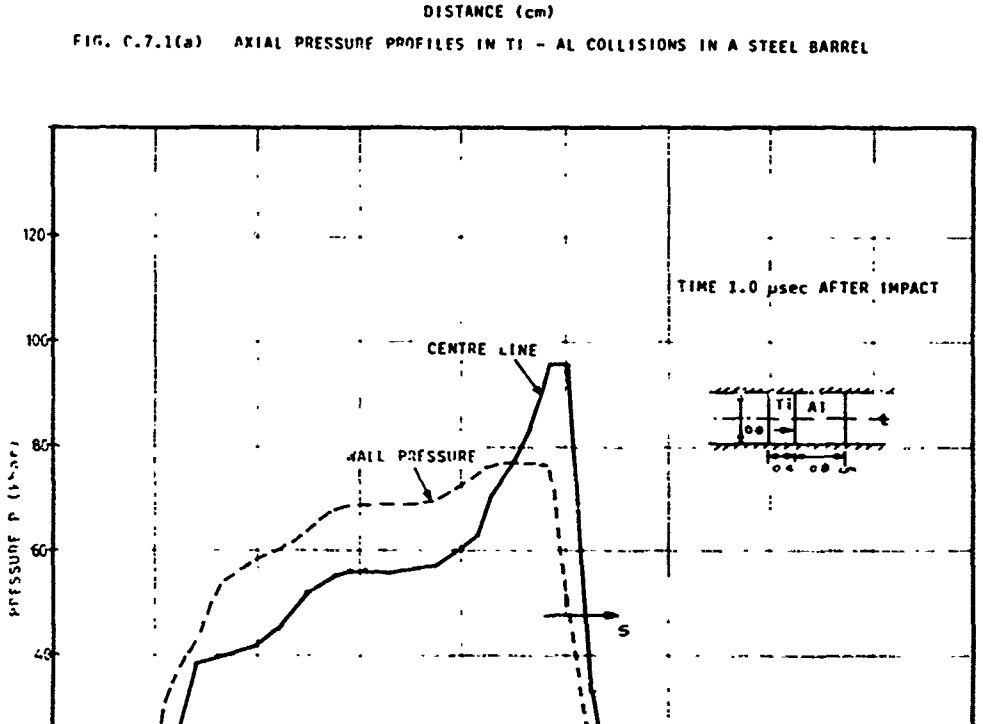

FIG. C.7.1(b) AXIAL PRESSURE PROFILE IN Ti-Al COLLISION IN A STEEL BARREL

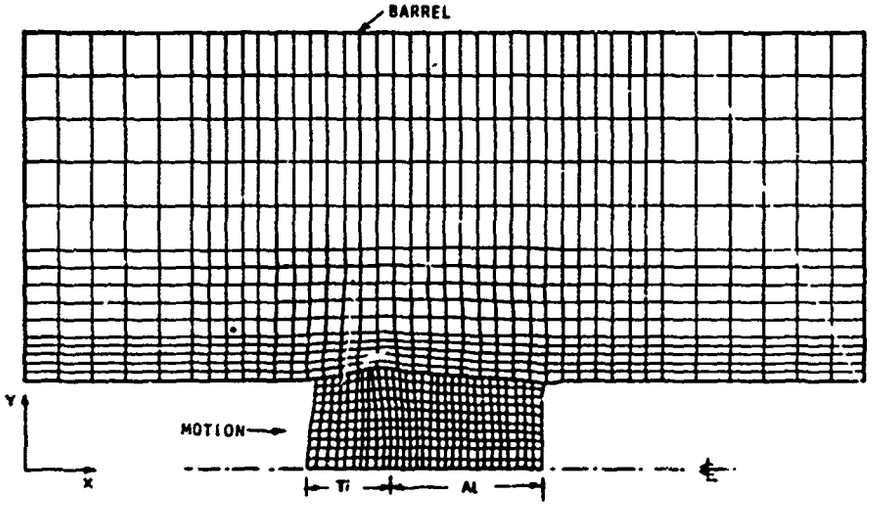

SCALE: 1 INCH = 0.4 CENTIMETER

FIG. C.7.2 X - Y COORDINATES 2.0 μsec AFTER IMPACT OF A TITANIUM PROJECTILE ON A STATIONARY ALUMINUM SLUG IN A STEEL BARREL

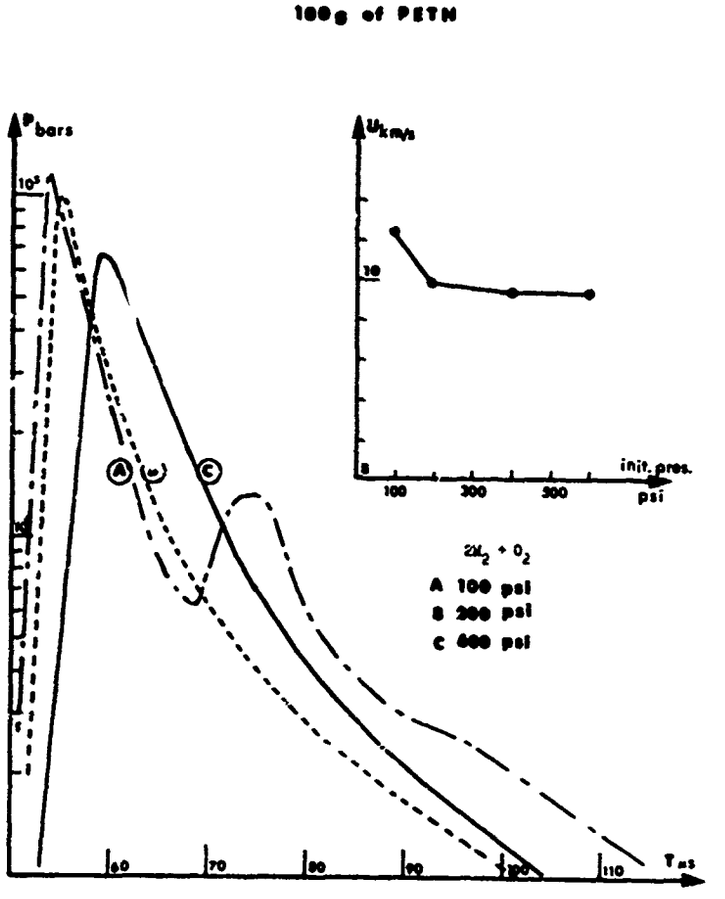

FIG. C.8.1 BASE PRESSURE PROFILES IN AN 8 INCH DIAMETER LAUNCHER (REF. C.16)

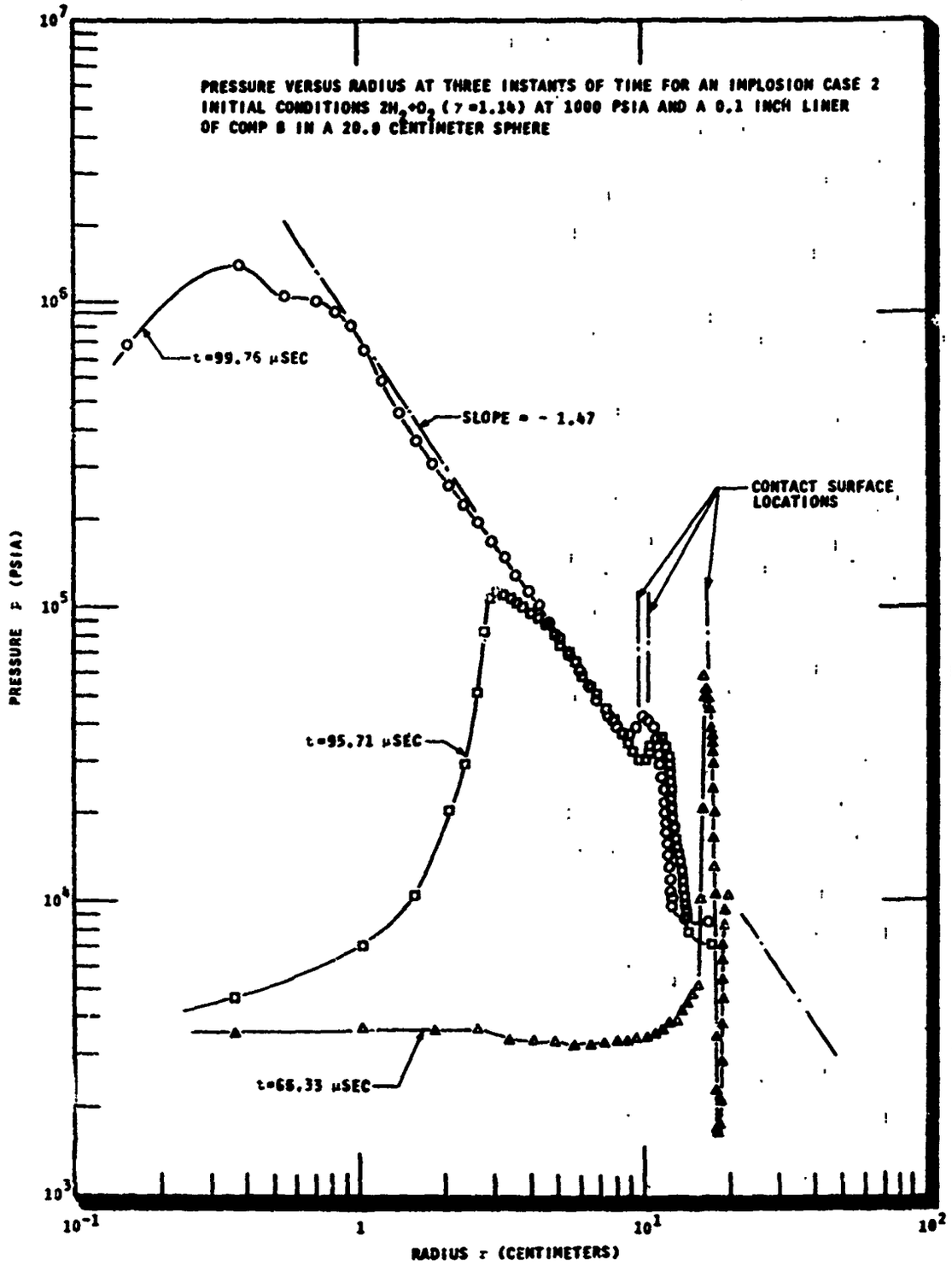

FIG. C.8.2 PRESSURE VS. RADIUS FOR $2H_2O + O_2$ at AT 1000 PSIA AND A 0.1 INCH LINER OF COMP B IN A 20 CENTIMETER SPHERE (REF. C.2)

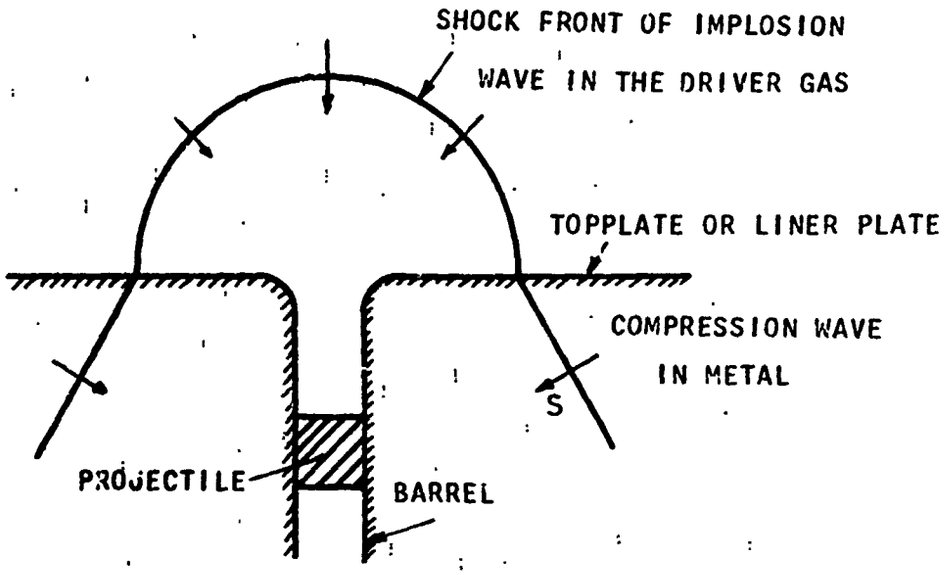

FIG. C.8.3 GENERAL WAVE PATTERN AROUND THE BARREL ENTRANCE DURING THE IMPLOSION PHASE

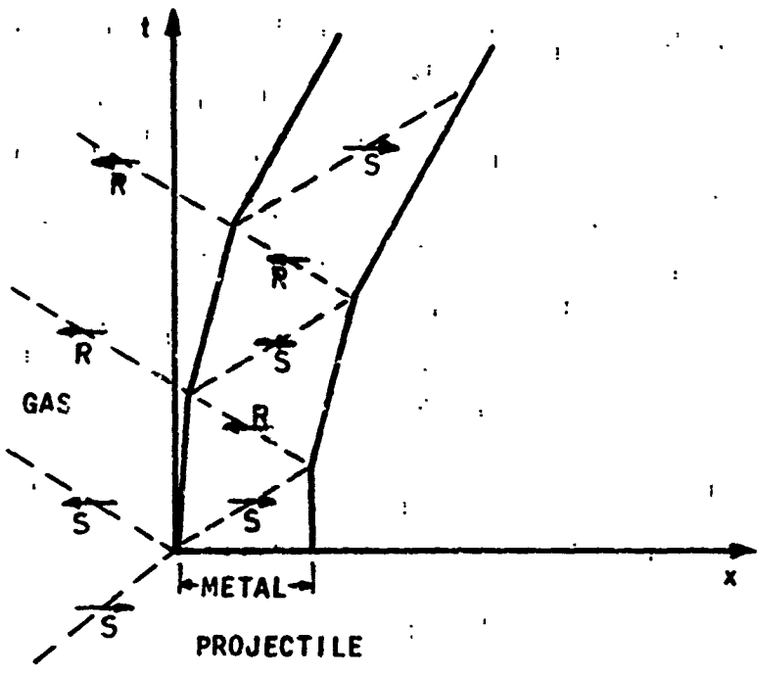

FIG. C.8.4 ACCELERATION OF A PROJECTILE BY A SHOCK WAVE

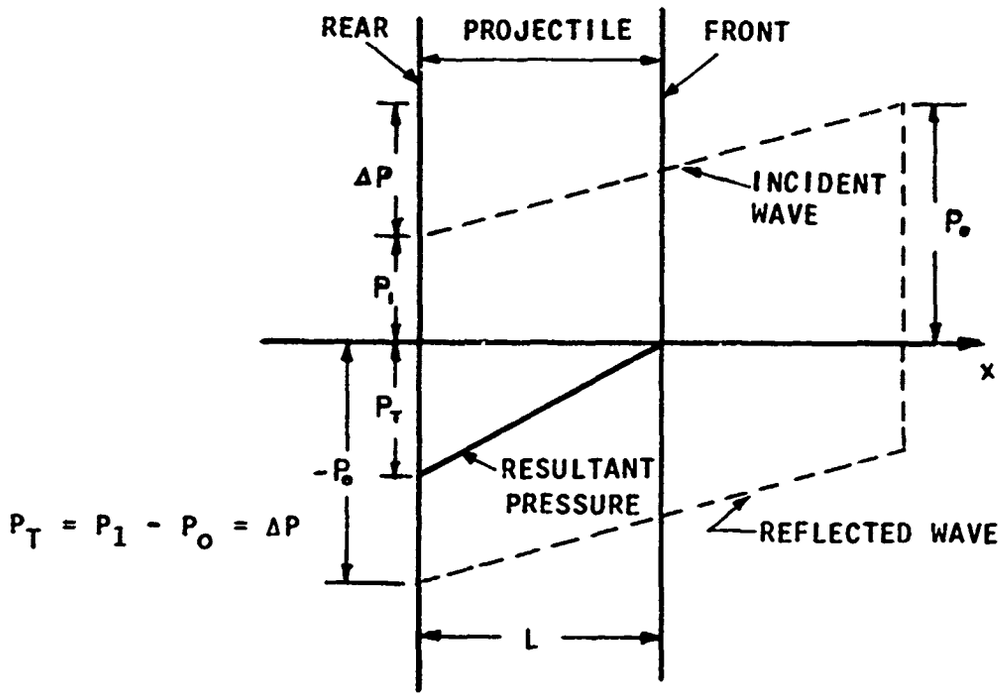

FIG. C.8.5 PRESSURE DISTRIBUTION IN A PROJECTILE WHEN A TRIANGULAR PRESSURE PULSE HAS REFLECTED BACK TO THE REAR SURFACE

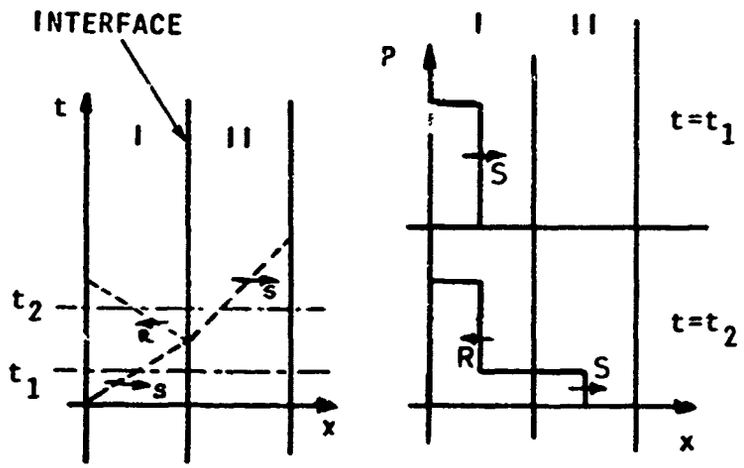

FIG. C.8.6
SHOCK REFLECTION AT AN INTERFACE WHERE $(\rho c)_I > (\rho c)_{II}$